NTNU

Norwegian University of
Science and Technology

Experimental and numerical investigations of loads on aquaculture net panels.

Mael Korentin Ivan Moreau

Abstract

Drag tests on aquaculture net panels were carried out in the towing tank Lilletanken (NTNU) for fifteen current velocities. The data were post-treated and discussed in order to characterize the dependency of the drag forces on several parameters, as the solidity ratio, the Reynold number, or the nets' material and size.
The behaviour of the turbulent flows around, and in the wake of the net panels has then been described.

Several experiments were also achieved in model-scale for wave conditions. The resulting loads were analyzed, and the influence of the wave periods and steepness on the loads were then investigated. The study has been extended to the force amplitude harmonics, significant for high steepness.

In parallel, CFD models were created in the open source software OpenFoam. They have been defined from the dimensions and properties of the experimental installation in order to produce comparable results. A convergence study was achieved to mesh 2D top and side views of the system.
The twines of the nets were too small to be meshed, and were modeled thanks to a pressure drop added in the Navier-Stokes equations.

The results revealed large differences between the numerical and experimental loads for high solidity ratios. The uncertainties linked to the experimental set-up have been discussed, focusing on the water elevation on the nets during the experiments, or the speed-up caused by the frames supporting the nets.

Preface

This Master Thesis has been written during spring 2017 at the Norwegian University of Science and Technology (NTNU, Norway) as the achievement of the 2-years international master *Marine Technology*, Hydrodynamics specialization. It is the continuation of the specialization project achieved during Autumn 2016.

The experiments performed in the towing tank Lilletanken, from the 9th of January to the 17th of February 2017, have been carried out in collaboration with Jialing Yu. The achievement of these tests, in addition to the post-treatment of the resulting data have been a very time consuming exercise, but also a very interesting and valuable experience.
All the non-referenced figures appearing in this report were produced during and for this thesis.

Acknowledgment

First, I would like to thank Torgeir Wahl, Terje Rosten, Trond Innset and the all team working in the lab for their great help in Lilletanken. They have always been available to explain us how the appliances worked, to provide us all the extra-equipment that we needed, or to fix the technical problems that we met during this period.
I would also like to thank Trygve Kristiansen for his guidance and his help all along the semester, Martin Søreide for giving me the opportunity of doing this Master Thesis, and Jialing Yu for her collaboration in performing the experiments and the constructive discussions that we had afterward.

Finally, I whish to thank Hao Chen and Tufan Aslan for their good advises in OpenFoam, and Céline Minh for always practicing her own unique humor and supporting me when we were writing our respective theses together.

Trondheim, 11.06.2017

Mael Korentin Ivan Moreau

Contents

Nomenclature

Abreviations

BC   Boundary Condition

CFD   Computational Fluid Dynamics

DNS   Direct Numerical Simulation

EDF   Experimental Fluid Dynamics

LES   Large Eddy Simulation

NaN   Not a Number

NSE   Navier-Stokes Equations

VIV   Vortex Induced Vibrations

WP   Wave Probe

Greek symbols

α Volume fraction of water

ϵ Porosity

ϵ_w Wave steepness

λ Wave length $[m]$

μ_x Mean of x [x]

ν_{air} Air kinematic viscosity $[m^2/s]$

ν_{water} Water kinematic viscosity $[m^2/s]$

ω Wave frequency [rad/s]

ω_e Encounter wave frequency [rad/s]

ρ_{air} Air density $[kg/m^3]$

ρ_{water} Water density $[kg/m^3]$

σ_x Standard deviation of x [x]

ζ Wave elevation [m]

Latin symbols

A Wave amplitude from rest to crest $[m]$

A_{Net} Frontal area of a net panel $[m^2]$

A_{twine} Projected area of one twine $[m^2]$

C_D Drag coefficient of a net

$C_{i,j}$ Fochheimer coefficient $[Nms^2/kg]$

d_w Twine diameter $[m]$

$D_{i,j}$ Darcy coefficient $[Ns^2/kg]$

f Wave frequency $[Hz]$

g Gravitational acceleration $[m/s^2]$

H Wave amplitude from crest to crest $[m]$

h Depth of the towing tank $[m]$

k Wave number $[rad/m]$

l Twine length $[m]$

N Length of discrete signals

p Pressure $[Pa]$

s Scale factor

S_i Dracy-Fochheimer force $[N/kg]$

S_N Solidity ratio

T Wave period $[s]$

t Time [s]

T_e Encounter wave period $[s]$

U_0 Mean incoming velocity $[m/s]$

u_i Velocity in the i-th direction $[m/s]$

V Volume of the porous media $[m^3]$

x_i Global coordinate in the i-th direction [m]

Introduction

From 2004 to 2014, the aquafarming production of fish has increased by more than 10%, and the trend predicts that this raise is not going to stop[1]. The part of marine aquaculture is also increasing, and the industry is determined to implant fish farms in places more and more exposed to extreme environmental conditions.
The currents met near the Norwegian coasts are among the strongest in Europe, and the littoral is directly exposed to the waves coming from the Atlantic Ocean. The improvement of aquaculture structures, and especially the aquaculture nets used in such farms, is therefore a technical challenge.

The loads acting on net panels provided by the net cage system supplier Aqualine were tested in the towing tank Lilletanken (NTNU) for several environmental conditions during this thesis. They have then been completed by numerical investigations.

Structure of the report

At first, the motivations and the main objectives of the project will be enunciated. A literature review will be hold, and the main concepts and theories used in the present work will be introduced.

Then, the set-up of the experiments will be described, followed by a deep presentation of the methodology used to analyze and post-treat the different types of experimental data recorded in Lilletanken.

The third section of this report will be dedicated to the numerical set-up, and to the description of the different models created in OpenFoam.

Finally, all the results of both the experiments and the computational simulations will be discussed and compared in the last section.

Computer equipment

Different software and numerical tools were used to achieve this project. They are presented below, together with a brief description of the use that have been made of them:

- Excel - Calibration of the wave probes.

- Matlab - Analysis of the experimental data.

- Maple - Solve complex analytic equations.

- OpenFoam - Run CFD simulations.

- ParaView - Visualization of the CFD results.

- Octave - Analysis and calculations of the CFD results in Linux.

- GIMP - Retouch photos.

1 | Background and motivations

1.1   Objectives

Several objectives were expressed when starting the work presented in this thesis. The main purposes were to:

- Carry out experiments in the towing tank Lilletanken to investigate the loads caused by steady currents on several aquaculture net panels provided by Aqualine.

- Extend this experimental work by generating regular waves in the towing tank, and test several wave periods and steepness.

- Post-treat the experimental data to analyse the resulting forces.

- Compare the results in order to bring out the influence of the different parameters: the incoming velocities, the wave periods and steepness, but also the properties of the nets themselves.

- Propose a numerical model in OpenFoam of the tests made in Lilletanken for steady current conditions, and compare the results.

- Characterize the main physical phenomena occurring during the drag tests, both numerical and experimental. For instance the wave elevations behind the nets, the side effects (the nets were provided with two width), or the influence of the frames supporting the nets.

1.2   Literature review

From aquaculture cages to net panels

The determination of the loads acting on circular net cages is an important issue for the aquaculture industry, which tends to look to implant aquaculture farms in sites exposed to more and more intense environmental conditions. Experimental studies were carried out in different works on this issue, most of the time completed and compared with CFD simulations.

Model-scale cages subjected to steady currents have been tested, e.g. in Kristiansen (2013) or in Lader and Enerhaug (2005). The first one points out the dependency of the drag forces in the Reynold number (defined in Equation 1.1 for a cylinder where D is the diameter and U_0 the incoming velocity), and discuss the scaling effects, while the second one emphasizes the importance of the hydro-elasticity, i.e. the inter-dependence between the deformation of the net cages and the forces acting on them.

Both of these works were compared to numerical results. Since the twines' diameter of aquaculture nets are too small to be included in the mesh, direct numerical resolutions
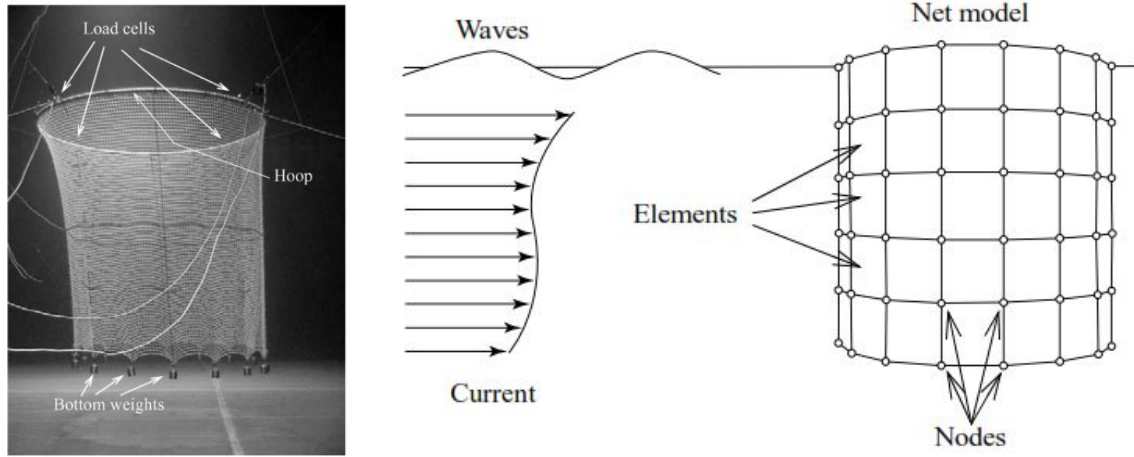
(a) Experimental set-up .   *(b) Decomposition of an aquaculture cage into net panels and nodes.*

Figure 1.1: *Illustration of experimental and numerical set-up on aquaculture net cages. Picture taken in the North Sea Center Flume Tank in Hirstskals (Denmark), from Lader and Enerhaug (2005). Schema from Lader et al. (2003).*

are not possible.

For instance, the nets used in the present thesis would require approximately between 45 and 50 millions of cells to integrate the twines into the rectilinear meshes considered, and to be solved directly (without considering turbulent phenomena), which is unrealistic for most of the current calculators.

Thus, the nets need to be modeled. Most commonly, the net cages are divided into net panels (or screens), on which the loads are calculated knowing a set of variables, including the inclination of the panels with respect to the incoming current. Such method is described in Lader et al. (2003): the cages are decomposed into many panels, the forces are calculated for each screen and then transmitted to the nodes connecting four panels to deduced the response of the whole structure (as illustrated in Figure 1.1). In Kristiansen (2012), a similar method is proposed, based on a more complex modeling of the cages: the circular aquaculture net is decomposed into trusses connected by nodes and delimiting four net panels. The forces of each panel are solved independently at each time step knowing their inclination and solidity ratio, these loads are then transmitted to the trusses (tension), and finally to the nodes which are responsible for the behaviour of the system.

$$Re = \frac{U_0 D}{\nu} \tag{1.1}$$

The solidity ratio of a net panel is by definition:

$$S_N = \frac{Effective\ solid\ area}{Total\ area} \tag{1.2}$$

Numerical models

The study of net panels have then been developed during the last decades. Several formulations of the drag and lift forces have been proposed to estimate the loads caused by steady currents on net screens.

In practice, the nets are numerically described as thin porous media, within which a resistance is added, i.e. inserted into the Navier-Stokes Equations (NSE) to take into account the pressure drop of the flows crossing the nets:

$$\frac{\Delta P}{\rho g} = K_1 u + K_2 u|u| \tag{1.3}$$

Where ΔP is the pressure drop in the porous media assuming a constant pressure gradient, ρ is the water density, g the gravity acceleration, u the velocity and K_1 ad K_2 are constants.

The first term, introduced by Darcy (1856), models the linear viscous effects occurring at low Reynolds numbers. For Darcy flows (Re<1), the second term is usually neglected, while for higher Re a non-linear term introduced by Forchheimer (1901) is considered. This inertial term, caused by the form drag, become predominant for fully turbulent flow regimes (Re>300). Most of the flows due to currents through net panels are fully turbulent, and so the Dracy's term is often neglected. It is the case for the present work: most of the computed flows verified Re>300, and only the Reynolds numbers for the lowest incoming velocity that have been considered ($U_0 = 0.1 m/s$) were slightly below 300.
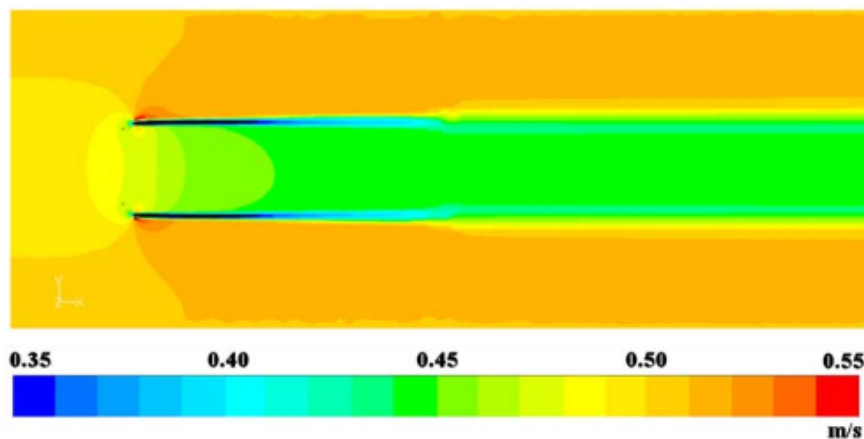
Figure 1.2: *Example of result presented in Patursson et al. (2010). The velocity magnitude in the flow is display for an horizontal section of a net panel, for an incoming velocity of 0.5m/s and an angle of attack of 0°.*

Experimental comparison

Different methods exist to estimate the coefficients K_1 and K_2, and most of them are based on finding the best fit between numerical and experimental results.

In Patursson (2008), the porous coefficients are obtained by minimizing the error between CFD and experimental results. Many numerical simulations were achieved for aquaculture net panels and cylindrical fish farming farms, both made in nylon. They are compared with experimental results for several angle of attack of the incoming flows. This method provided a good finding of both the Darcy and Forchheimer coefficients. Similar results are concluded in Zhao et al. (2013) where a a least square method is used to calibrate these coefficients.

In Patursson et al. (2010), CFD simulations and experiments on aquaculture net panels are also carried out for different incoming velocities and inclinations (cf. Figure 1.2). Several methods are investigated to find the best fit between numerical and experimental drag and lift coefficients. The porous coefficients are directly deduced from the experimental results, three methods are compared to calculate this "fitting": the least squared normalized error (LSNE), the least absolute error (LAE), the a least absolute normalized error (LANE). It turns out that the LANE formulation leads to the best results, with 10% of error on C_D and C_L, and 6.2% of error for the velocity in the wake.

Morison type and screen type loads
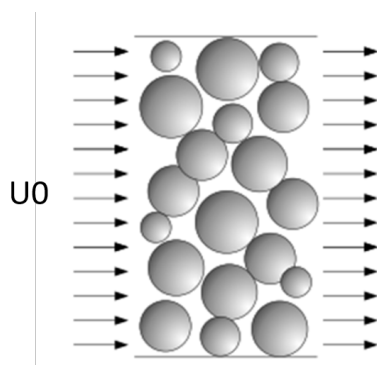
Figure 1.3: *Packed bed model .*

The Darcy-Forchheimer was initially conceived for packed bed flow, i.e. tubes filled with particles, as illustrated in Figure 1.3. Few empirical or analytic formulas have been proposed to determinate the Darcy and Forchheimer coefficients in order to generalize this equations.
Ergun (1952) expresses a first formulation of these coefficients, depending on the sizes of the particles d_w, and the porosity ($\epsilon = 1 - S_N$).

Since, other formulations have been proposed, and adapted for nets. One of the most widespread method is the Morison type load model. Based on the Morison force $F_x = \dfrac{1}{2}\rho A_{Net}U_0^2 C_{D,twine}$ for a circular cylinder, and summed over the number of twines. Chen and Christensen (2016) extended this approach by introducing empirical coefficients to take into account the interaction between the twines.

Løland (1991) introduced an other method based on a more global approach. This screen type load model expresses the drag force as a function of the solidity ratios of the nets, valid for $S_N \in [0.13 - 0.317]$. Kristiansen and Faltinsen (2012) extended this model for a larger number of solidity ratios, and integrated the dependency of the drag force on the Reynold number.

This two approaches are detailed below, they have been used in the present work and compared to the experiments carried out in Lilletanken.

Complex flows

The study of loads acting on aquaculture nets is wide, and integrates many complex physical phenomena occurring and interacting between each other. Few of these phenomena, that were not considered in detailed in this report, are presented below.

The behavior of the flow in the wake behind the screen is deeply related to the drag force. In Løland (1993), the velocity profile of the flow in the wake of a net panel is investigated, and a formulation of the drag force is proposed depending on the velocity reduction factor $r = 1 - \dfrac{u_{wake}}{U_0}$.

The shading effects are one of the main effects occurring when considering inclined or deformed nets. They are studied in Fredheim (2005), where the interference in the flow around several twines (cylinders) is characterized. It is emphasized how the forces acting on the twines in the wake of other twines are highly decreased. The importance of the elasticity of the nets is also discussed.
In Zhao et al. (2013), several panels are placed the one after the others, and the consequences on the velocity reduction factor are described. These investigations show that r is 4 times higher when five panels are installed.
In this present work, only perpendicular incoming flows are considered, and these shading effects are neglected. However, they should be discussed as soon as the panels are inclined.

The experimental set-up and external conditions are also an important issue to take into consideration. Thus, during the experiments carried out in Patursson (2008), the generation of waves behind the panels are avoided by positioning the net far below the free surface (Patursson et al. (2010) recommends to model the free-surface elevation

in CFD to investigate the influence on C_D).
Sobieski and Trykozko (2014) point out the role played by the temperature during the experimental studies carried out to determinate Forchheimer coefficients, especially since the water density and viscosity depend on it, as well as the transducers measuring the forces.

The geometry of the nets themselves is a key factor in the comprehension of the loads acting on them. The not-cylindrical shape of Nylon nets is discussed in Kristian and Faltinsen (2012), and Patursson (2008) concludes that a deeper study of the net designs is necessary in order to find a clear relationship between C_D and S_N.
Fredheim (2005) emphasizes the importance of the design of the knots in the resulting C_D. A new formulation adapted from the Morsion type load model and based on the decomposition of the drag coefficient into two terms is proposed: one coefficient for the cylindrical part of the twine, and a new term to include the drag of the knots ($C_D = C_{D,twines} + C_{D,knots}$).

Finally, different treatments of the turbulence have been made when simulating a flow through nets. Chen and Christensen (2016) did not implemented any turbulent models, while Patursson et al. (2010) and Zhao et al. (2013) uses a realizable $k - \epsilon$ turbulent model.
In Patursson (2008), common turbulent models based on an isotropic eddy viscosity were tested, leading to fast simulations. Nevertheless, the conclusion is that this simplified assumption could have led to inaccurate results. Thus, it is recommended to try to use higher order turbulent models (LES, Reynolds stress models, etc.).

Summary

The investigations of loads acting on net screens are widely spread to determine in a second time the drag force acting on whole aquaculture net cages. It has been shown that the drag coefficient obtained in such studies were very dependent on the properties of the nets, as the twine diameter, or the solidity ratio, but also on the Reynold number (and the inclination of the panels, not considered in the present work).
In CFD, the nets can not be integrated directly into the mesh because of the too small size of the twines. Thus, porous models based on the Darcy-Forchheimer equations, and either on the drag coefficients of the twines, or on empirical coefficients (or both) are used.

1.3   Theory

The main theories used in the different parts of this thesis are presented below. At first, the main equations of fluid mechanics that have been considered and solved in CFD are briefly described.

Then, a focus is done on the Dracy-Forchheimer equation, which has been used to model the net panels. The two main approaches used in the present work to determine the unknown coefficients are described.

Finally, the influence of the frames supporting the net panels on the flow velocity will be discussed. The speed-up of the flow near the cylindrical part of these frames will be estimated thanks to analytic formulas based on singularity methods (potential flow).

1.3.1   The main equations

The equations defining a flow through a net panel can be described by Equation 1.4, based on the incompressible Navier-Stokes Equations (NSE). $g_3 = -9.81 m/s^2$ is the gravitational acceleration, ρ the fluid density, and ν the kinematic viscosity of the fluid. S_i is the additional resistance acting in the porous media representing the net. This term - detailed below - is equal to $0 m/s^2$ outside the porous volume. The porous volume V is calculated from the wet area of the net panels and the twines' diameter (cf. Equation 1.5).

$$\begin{cases} \dfrac{\partial u_i}{\partial t} + u_j * \dfrac{\partial u_i}{\partial x_j} = -\dfrac{1}{\rho} * \dfrac{\partial p}{\partial x_i} + \nu * \dfrac{\partial}{\partial x_j}(\dfrac{\partial u_i}{dx_j} + \dfrac{\partial u_j}{\partial x_i}) + g_i + S_i \\ \dfrac{\partial u_j}{\partial x_j} = 0 \end{cases} \tag{1.4}$$

$$V = d_w \times A_{Net} \tag{1.5}$$

Turbulent model

The turbulent eddies formed in the flow crossing the net panels are far too small to be catch with the mesh created to model this system. Several simplified turbulent models exist to integrate the effects of turbulence in the NSE. The Large Eddy Simulation models which solve the NSE for the largest eddies, and model the smaller ones are very common, but their numerical resolution is also very time consuming. Thus the RANS Equations 1.7 were chosen in this study to be solved in OpenFoam.

They are obtained by averaging the NSE. The velocity and the pressure are decomposed in a time average term and a fluctuating term, as shown Equation 1.6 (Reynold decomposition).

$$\begin{cases} u_i(x,t) = \overline{u_i(x)} + u_i'(x,t) \\ p(x,t) = \overline{p(x)} + p'(x,t) \end{cases} \tag{1.6}$$

$$\begin{cases} \dfrac{\partial \overline{u_i}}{dt} + \overline{u_j} \times \dfrac{\partial \overline{u_i}}{\partial x_j} = -\dfrac{1}{\rho} * \dfrac{\partial \overline{p}}{\partial x_i} + \nu \times \dfrac{\partial \overline{u_i}^2}{\partial x_j^2} - \dfrac{\partial \overline{u_i' \times u_j'}}{\partial x_j} + g_i + S_i \\ \dfrac{\partial u_j}{\partial x_j} = 0 \end{cases} \tag{1.7}$$

The new term $-\rho \times \overline{u'_i * u'_j}$ that appears in the first equation is called Reynold stressed, and is expressed through the turbulent-viscosity hypothesis (Equation 1.8).

$$\overline{u'_i u'_j} = -\nu_T \times (\frac{d\overline{u_i}}{dx_j} + \frac{d\overline{u_j}}{dx_i}) - \frac{2}{3} \times k_t \times \delta_{i,j} \tag{1.8}$$

$k_t = \dfrac{1}{2} * \rho * \overline{u'_i u'_i}$ is the turbulent kinetic energy, and ν_t the turbulent viscosity.

Among the different turbulent models based on this hypothesis, the Shear Stress Transport $k - \omega$ model[2] has been retained. Its advantage is to automatically switch between the $k - \epsilon$ model, adapted for free-stream flows, and the $k - \omega$ model, often preferred near the boundaries. This model is also known to be performing for high pressure gradient.

The estimation of the turbulent parameters used to define the boundary conditions was achieved thanks to the following formulas[2]:

$$k_t = \frac{1}{2} u_t^2 \tag{1.9}$$

$$\epsilon = \frac{C_\mu^{0.75} k_t^{1/2}}{l_t} \tag{1.10}$$

$$\omega = \frac{\sqrt{k_t}}{l_t} \tag{1.11}$$

$$\widetilde{\nu}_t = \frac{C_\mu k_t^2}{\epsilon_t} \tag{1.12}$$

Where d_w is the twine diameter, and C_μ, u_t and l_t are defined as follow:

$$\begin{cases} C_\mu = 0.09 \\ u_t = 6\% U_0 \\ l_t = 6\% d_w \end{cases} \tag{1.13}$$

Multiphase flows

For the numerical simulations for which the free surface elevation were considered, the Equation 1.14 was also solved to determine the volume fraction of water α at each time step.

$$\frac{\partial \alpha}{\partial t} - \frac{\partial (\alpha u_j)}{\partial x_j} = 0 \tag{1.14}$$

The properties of the two fluid (air and water) used in the present work are given in Table 1.1.

Table 1.1: *Fluids' properties.*

	Water	**Air**
$\rho \; [kg/m^3]$	1000	1
$\nu \; [m^2/s]$	1e-6	1.48e-5

1.3.2   Porous media

The resistance term S_i representing the porous media in Equation 1.7 has been expressed through the **Darcy-Forchheimer equation**. This resistance is effective only inside the volume defined with the dimensions of the real net panels.

$$S_i = -[\nu D_{i,j} + \frac{1}{2}|u|C_{i,j}]u_j \tag{1.15}$$

$$|u| = \sqrt{u_1^2 + u_2^2 + u_3^2} \tag{1.16}$$

The first term of the Equation 1.15 corresponds to viscous effects, while the second term corresponds to inertial effects (non-linear). As discussed in Section 1.2 , the viscous term has been neglected because of its low order of magnitude compared to the quadratic term. Furthermore, in the particular case where the incoming flow is perpendicular to the panels, the unknown matrix $D_{i,j}$ and $C_{i,j}$ are diagonal. It leads then to:

$$S_i = \frac{1}{2}|u|C_{i,j}u_j \tag{1.17}$$

The unidirectional Forchheimer coefficient C proposed by the Ergun formula (cf. Equation 1.18) has been used for the set-up of the CFD study, its determination is straightforward since it does not depends on Re, but only on the twine diameter d_w and the porosity of the net panels ($\epsilon = 1 - S_N$).

$$C = \frac{1.75(1 - \epsilon)}{d_w \epsilon^3} \tag{1.18}$$

The two approaches introduced in the literature review and presented below have been implemented in OpenFoam in order to compare the computational results with the experimental ones.

The drag coefficient of a cylinder (i.e. of one twine) is used in both methods. As in Kristiansen and Faltinsen (2012), the empirical formula proposed by Goldstein (1965) has been adopted to calculate this coefficient dependently of the incoming flow's Reynold number:

$$\begin{aligned}
C_D^{cylinder} &= -78.46675 + 254.73873\,log_{10}(Re) \\
&-327.8864\,(log_{10}(Re))^2 + 223.64577\,(log_{10}(Re))^3 \\
&-87.92234\,(log_{10}(Re))^4 + 20.00769\,(log_{10}(Re))^5 \\
&-2.44894\,(log_{10}(Re))^6 + 0.12479\,(log_{10}(Re))^7;
\end{aligned} \tag{1.19}$$

The Reynold numbers have been determined with the increased incoming velocity $u = \dfrac{U_0}{1 - S_N}$, which is subjected to a speed-up when crossing the meshes of the nets.

$$Re = \frac{d_W \, U_0}{\nu \, (1 - S_N)} \tag{1.20}$$

Morison type loads

The principles and formulas of this part present the theory developed in Chen and Christensen (2016).
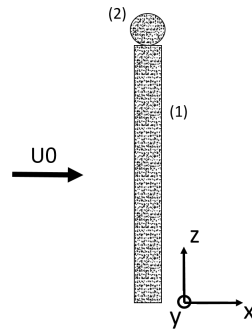
Figure 1.4: *Vertical (1) and horizontal (2) twines subjected to a perpendicular incoming flow U_0.*

The Morsion loads $F_{cylinder} = \dfrac{1}{2}\rho A U_0^2 C_D^{cylinder}$ acting on the horizontal and vertical twines constituting the nets (cf. Figure 1.4) are first summed over the total number of twines to obtain the load acting on the whole panel. Then the resulting load is equalized with the porous resistance (cf. Equation 1.17) to determine the expression of the Forchheimer coefficients C_i.

Finally, empirical coefficients a and b have been added to the model to take into account the interactions between the twines, leading to the following coefficients:

$$\begin{cases} C1 = \dfrac{1}{V}\, a\, C_{D,twine}\,(S1 + S2) \\[3mm] C2 = \dfrac{1}{V} b C_{D,twine} S2 \\[3mm] C3 = \dfrac{1}{V} b C_{D,twine} S1 \end{cases} \tag{1.21}$$

Where S1, respectively S2, is the summation of the projected areas of the vertical (1) twines, respectively horizontal (2), constituting the full net panel. S1 and S2 are not equal if the nets are inclined, but here the y and z directions are assumed to be symmetric, and $S1 = S2$. This quantity has then been obtained as shown in Equation 1.22.

$$\begin{cases} S1 = \sum_{i=1}^{N_{twine}^{(1)}} A_{ith\,twine}^{(1)} = S_N \times \dfrac{A_{Net}}{2} \\[6mm] S2 = \sum_{i=1}^{N_{twine}^{(2)}} A_{ith\,twine}^{(2)} = S1 \end{cases} \tag{1.22}$$

The empirical coefficients a and b are based on the Reynold number, and can be expressed as follow:

$$a = \begin{cases} 2.3484 S_N + 1 & if\ \ 0 < S_N \leqslant 0.13 \\ 1.3128 S_N + 1.1346 & if\ \ 0.13 < S_N \leqslant 0.243 \\ 5.3094 S_N + 10.1634 & if\ \ 0.243 < S_N \leqslant 0.317 \end{cases} \tag{1.23}$$

$$b = \begin{cases} 0.9241 & if\ \ 0 < S_N \leqslant 0.13 \\ -0.6310 S_N + 1.0061 & if\ \ 0.13 < S_N \leqslant 0.243 \\ 8.7581 S_N & if\ \ 0.243 < S_N \leqslant 0.317 \end{cases} \tag{1.24}$$

Screen type loads

O.M Faltinsen and T.Kristiansen (2012) proposes the following expression to estimate the forces caused by a current U_0 crossing a net characterized by its solidity ratio S_N:

$$F_x = \frac{1}{2}\,\rho\,A\,U_0^2\,\frac{S_N(2-S_N)}{2(1-S_N)^2}\,C_D^{cylinder} \tag{1.25}$$

Where A is the frontal area of the panel. The term $\dfrac{U_0^2}{(1-S_N)^2}$ comes from the speed-up of the flow crossing the meshes, while the numerator $S_N(2-S_N)$ was chosen such a way that the interaction of the twines vanish (and the Morison load is found) if S_N approaches 0 (cf. Condition 1.26).

$$\frac{S_N(2-S_N)}{2(1-S_N)^2}A \xrightarrow[S_N \to 0]{} S_N A \tag{1.26}$$

This force was used directly, as expressed in Equation 1.25, to obtain analytic results comparable to the experimental ones.

In addition, it was also used to estimate the Forchheimer coefficients called in the numerical simulations. Equalized with the porous resistance (Equation 1.17), it led to:

$$C_1 = \frac{S_N(2-S_N)}{2d_w(1-S_N)^2}C_D^{cylinder} \tag{1.27}$$

1.3.3   Singularity methods- Speed-up

Singularity methods[3] based on potential flow theory were used in this thesis to estimate the speed-up of the flow caused by the cylindrical parts of the frame on which the net panels were stretched. Indeed, the frames were not taking into account

in the CFD simulations, and this acceleration of the flow during the experimental investigations needed to be characterized in order to compare and understand the final results. More details about the geometry of the frames will be presented in Section 2.1.2 .

At first, the theoretical path from the general equations to the particular case of interest (i.e. the speed-up of the flow on the net panels) is studied. Then the application of the resulting formula is described.

Flow around a cylinder

$$\vec{U} = \overrightarrow{grad}\Phi \tag{1.28}$$
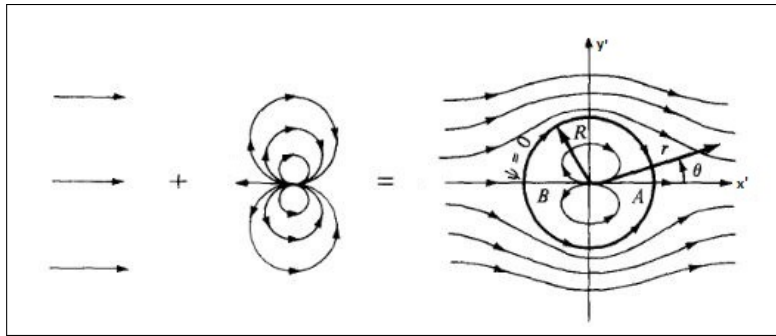
Figure 1.5: *Illustration of an incoming flow around a cylinder (potential flow theory). Picture taken from "Fundamentals of Aerodynamics" of John D. Anderson.*

In this theory, the velocity flow is derived from a potential Φ, as expressed in Equation 1.28. The flow around a cylinder is then expressed as the sum of a uniform flow U_0 and a dipole:

$$\Phi = U_0 r cos(\theta) - \frac{\kappa cos(\theta - \chi)}{2\pi r} \tag{1.29}$$

Where the notations and coordinates in both the cartesian and cylindrical frames are presented in Figure 1.5. The relationship between both coordinate systems is specified below:

$$\begin{cases} x' = r cos(\theta) \\ y' = r sin(\theta) \end{cases} \tag{1.30}$$

The orientation of the dipole χ is here equal to 0° since the incoming flow is parallel to the x axis. The velocity becomes then:

$$\begin{cases} U_r = \dfrac{\partial \Phi}{\partial r} = -U_0 cos(\theta) + \dfrac{\kappa cos(\theta)}{2\pi r^2} \\\\ U_\theta = \dfrac{1}{r}\dfrac{\partial \Phi}{r} = -U_0 sin(\theta) + \dfrac{\kappa sin(\theta)}{2\pi r^2} \end{cases} \tag{1.31}$$

Considering a vector $\vec{n}$ on the surface of the cylinder, perpendicular to it, the boundary condition along the body is expressed as follow:

$$\vec{U} \cdot \vec{n} = 0 \longrightarrow U_r(r = R) = 0 \tag{1.32}$$

Where R is the radius of the cylinder. Replaced in Equation 1.31, it leads to the following condition:
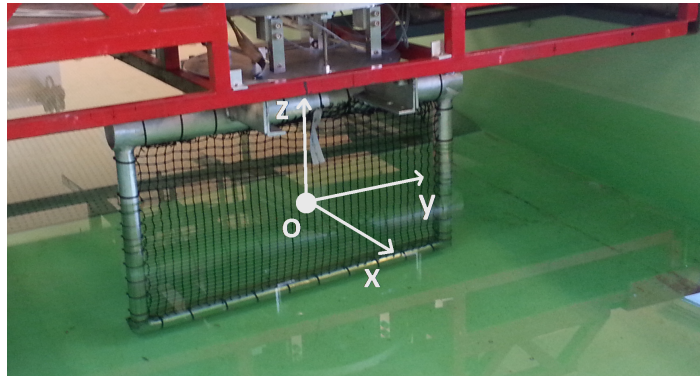
$$\kappa = -2\pi U_0 R^2 \tag{1.33}$$

The final expression of the velocity is then:

$$
\begin{cases}
U_r = U_0(1 - \dfrac{R^2}{r^2})cos(\theta) \\[4mm]
U_\theta = U_0(1 + \dfrac{R^2}{r^2})sin(\theta)
\end{cases}
\tag{1.34}
$$

The cylinder represents here the front part of the frame, and the net is stretched in the plan (x'Oy'), characterized by $\theta = \dfrac{\pi}{2}$. The velocity in this plan is express as:

$$
\begin{cases}
U_r = 0 \\[4mm]
U_\theta = U_{x'} = U_0(1 + \dfrac{R^2}{y'^2})
\end{cases}
\tag{1.35}
$$

Application to the speed-up of the frames

Figure 1.6: *Coordinate system used by the control computer when recording data.*

The global coordinates of the system used by the control computer recording the data during the experiments are presented in Figure 1.6. This system is used all along the present work, assuming that both the incoming flow and the drag force are expressed relatively to the negative x axis to avoid to work with negative loads (the carriage runs in the direction x>0).

Thus, the drag force acting on the net, which depends now on the real velocity U(y,z), can be writen as follow:

$$dF_{Theoretical} = \frac{1}{2}\rho U^2(y, z)\frac{S_N(1 - S_N)}{2(1 - S_N)^2}C_{D,twine}dydz \tag{1.36}$$

The velocity expressed in Equation 1.35 includes the incoming flow and the speed-up caused by one side of the frame. The speed-up caused by the other side and the bottom

part of the frame are included similarly, leading to:

$$U(y,z) = U_0(1 + \frac{R^2}{(R + \frac{B_N}{2} + y)^2} + \frac{R^2}{(R + \frac{B_N}{2} - y)^2} + \frac{R^2}{(R + \frac{H}{2} + z)^2}) \qquad (1.37)$$

Where B_N is the width of the $1m \times 1m$ net panel, H the height of the immersed part of the net, and R the radius of the cylindrical part of the frame. The analytic forces acting on the small net panels are then:

$$F_{Theoretical} = \frac{1}{2}\rho\frac{S_N(1 - S_N)}{2(1 - S_N)^2}C_{D,twine}\int_{\frac{B_N}{2}}^{-\frac{B_N}{2}}\int_{\frac{H_N}{2}}^{-\frac{H_N}{2}} U(y,z)dydz \qquad (1.38)$$

The analytic loads acting on the $2.5m \times 1m$ net panels are obtained similarly by "cutting" the net in two identical parts (each one treated as a small net) :

$$F_{Theoretical} = \rho\frac{S_N(1 - S_N)}{2(1 - S_N)^2}C_{D,twine}\int_{\frac{B_N}{4}}^{-\frac{B_N}{4}}\int_{\frac{H_N}{2}}^{-\frac{H_N}{2}} U(y,z)dydz \qquad (1.39)$$

2 | Experiments

2.1   Set-up

This section presents the set-up of the experiments carried out in Lilletanken from January to February 2017. The towing tank is 25m long, 2.8m wide, and the water level was measured at 0.945m. It is equipped with a damping ramp.

The main measure recorded and analysed during these tests was the drag force F_x, measured from the transducers which were fixed under the carriage.

In addition to the instrumentation used and presented below, few videos were taken directly from under the carriage during the runs in order to have a good visualization of the whole wake of the net panels.

2.1.1   Instrumentation and calibration

Strain gauges

Transducers have been used to measure the forces acting on the net panels. These strain gauges, composed with a Wheatstone bridge circuit, measure the material elongation thanks to a variation of electric resistance (cf. Figure 2.1)
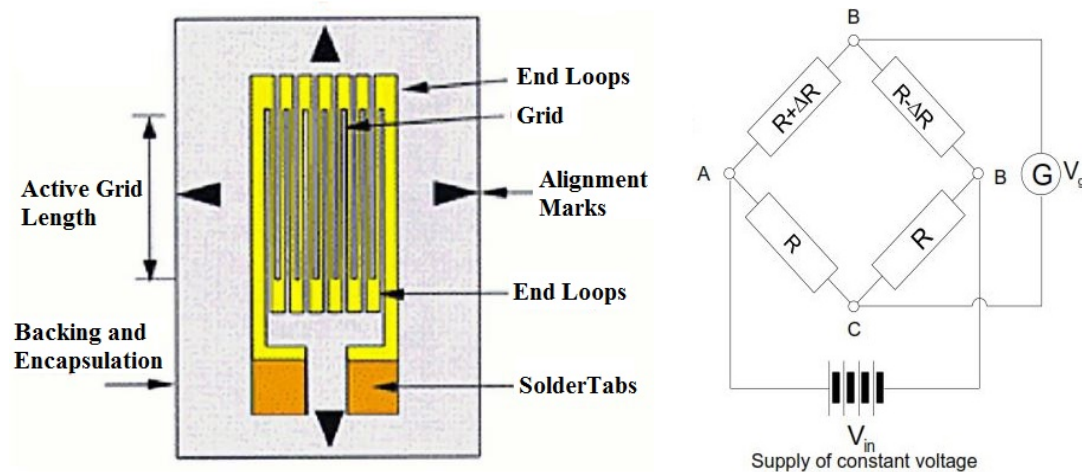
(a) Schema of a strain gauge[4].

(b) Wheatstone bridge. V_g is the signal, R (resistances in the amplifiers) and V_in (constant voltage source) are known, ΔR is variation of resistance due to the elongation of the strain gauge.[4]

***Figure 2.1:** Schematic description of a strain gauge.*

Torgeir Wahl and Terje Rosten did most of the set-up before our arrival. A platform containing 2 strain gauges in each direction was installed in the carriage before the beginning of the experiments. This system had been subjected to different (known)

loads in different directions in order to determine the calibration matrix, i.e. the conversion factors used to transform the measured voltages in forces and moments in the three directions of space. The platform was not perfectly symmetric and coupling had to be considered between the three directions, leading to a calibration matrix with non-null diagonal coefficients.

Wave probes

A wave probe consists in two parallel conductive wires half-immersed in the towing tank and subjected to an electric current. The water shorts-circuit this system, and the resulting resistance of the wires is then measured, and converted into a $^\pm 10V$ DC signal by the wave probes' amplifier.
6 probes have been used to record the wave elevation behind the net panels in order to characterize the physical behavior of the wake, the influence of the frames, of the side effects, but also to be compared to the computational results.

The calibration has been done with the help of Terje Rosten. Each probe has been immersed step by step in the water, the corresponding voltage and the water level were measured at each step. Plotted in the same graphic, the linear relationships between meter and voltage have been determined thanks to a linear regression on the data (done in Excel).
The results of this calibration work are presented in Figure A.2 in Appendix A.1 .

Data acquisition
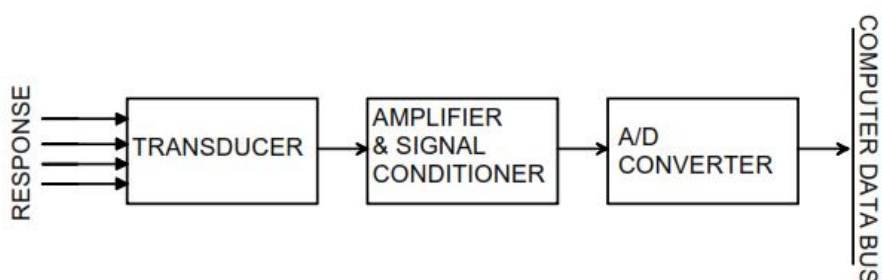
*Figure 2.2:* *Data acquisition from the strain gauges - Schema[4].*

The response electric current delivered by the sensors (e.g. the strain gauges, typically in micro-volts) is amplified to the range $^\pm 10V$ (DC signal) and most of the noise at high frequencies is removed thanks to low pass analog filters. The analog signal is then converted in a digital signal, and recorded from the control computer with the software CATMAN which converted this input into the corresponding physical units thanks to the calibration factors.
The offset of all the signals was set to zero in CATMAN before every experiments.

However, it will be seen later that both the offset and some noise remained in the signals and needed to be re-treated.

2.1.2   The frames
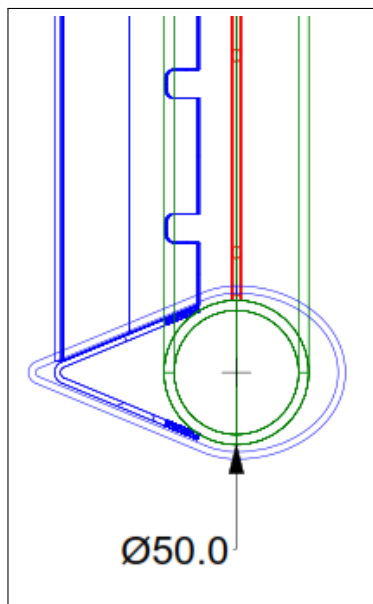
(a) *Profile of the frames, with a cylindrical part ahead, and "V" part behind. Designed by Trond innset.*

(b) *Strip clips placed behind the $1m \times 1m$ frames. Lilletanken, February 2017.*

Figure 2.3: *Schema and picture of the frame used in Lilletanken. The shape is illustrated from a top view, and the strips fixing the nets are presented.*

Two sizes of aluminum frame ($1m \times 1m$ and $2.5m \times 1m$) have been have been conceived by Trond Innset and built in the laboratory. The front part is cylindrical to improve the circulation of the incoming flow, and so to reduce the drag force due to the frame. The "V" part behind was added to avoid (or at least reduce) the VIV of this structure.

The net were stretched and fixed thanks to strips. Depending on the elasticity of the nets, different numbers of strips were needed and attached to the frames.

The dimensions of the frames are presented in details in Appendix A.2 .

2.1.3   Installation and test procedure

Installation of the wave probes

Six wave probes have been installed under the carriage to measure the wave elevation in the wake of the nets, but also to measure the wave amplitudes of the incoming waves in front of net. Their disposition is displayed in Figure 2.4, and have been chosen as follow:

- The first wave probe (WP1) was placed in front of the net to measure the incoming waves.

- WP5 and WP2 were aligned along the x-axis in the wake of the nets.

- WP3 was just behind the bar of the frame when testing $1m \times 1m$ panels.

- WP4 was in the wake, very close to the net.

- WP6 was placed between the frame and the side of the tank to observe the transverse waves created by the $1m \times 1m$ frame.
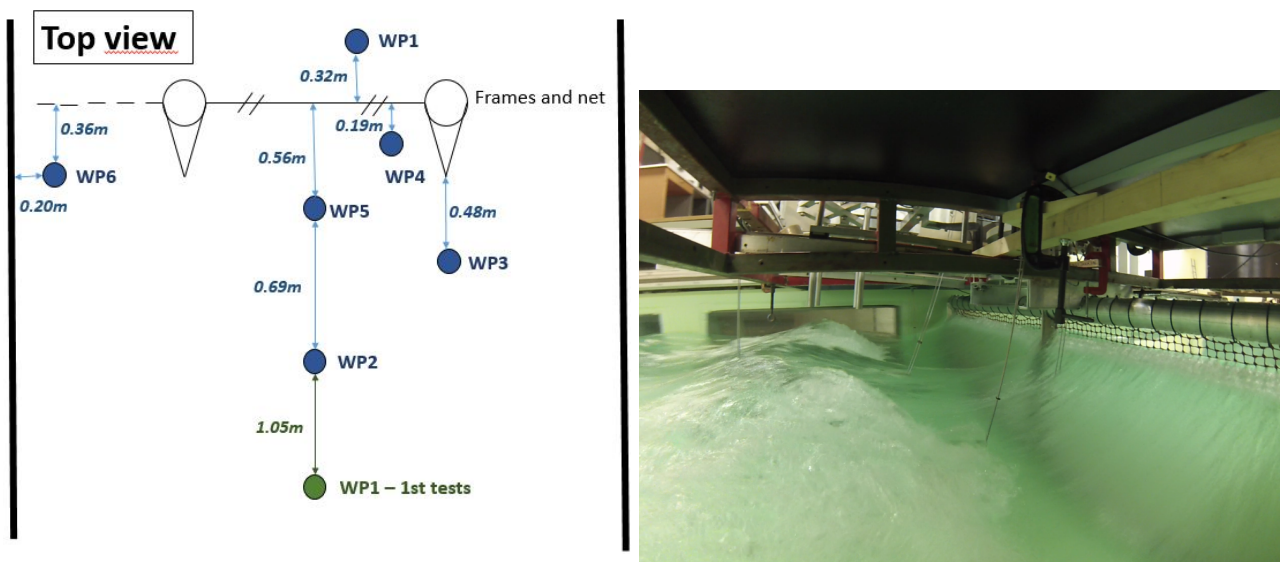

(a) *Distances of the wave probes relatively to the net panels.*

(b) *Wave probes behind the net for a current condition. Lilletanken, 25 January 2017*

Figure 2.4: *Schema and photography of the wave probes' disposition. The installation is identical for the 1m×1m and the 2.5m×1m net panels.*

Procedure of test

The following procedure has been followed to test each net panel:

- The net panel has been cut to fit the dimensions of the corresponding frame (1m×1m or 2.5m×1m).

- The net has been stretched the most has possible manually and attached to the frames with strips.

- The strips were cut the shortest as possible, and positioned such a way that their attachments were hidden behind the frames in order to interfere as little as possible with the incoming flow.

- Then the frame with the net has been transported under the carriage, and fixed with four screws to the platform.

- At the end of the test, the frame was carried out of the water. Then all the strips were cut, and the procedure was repeated.
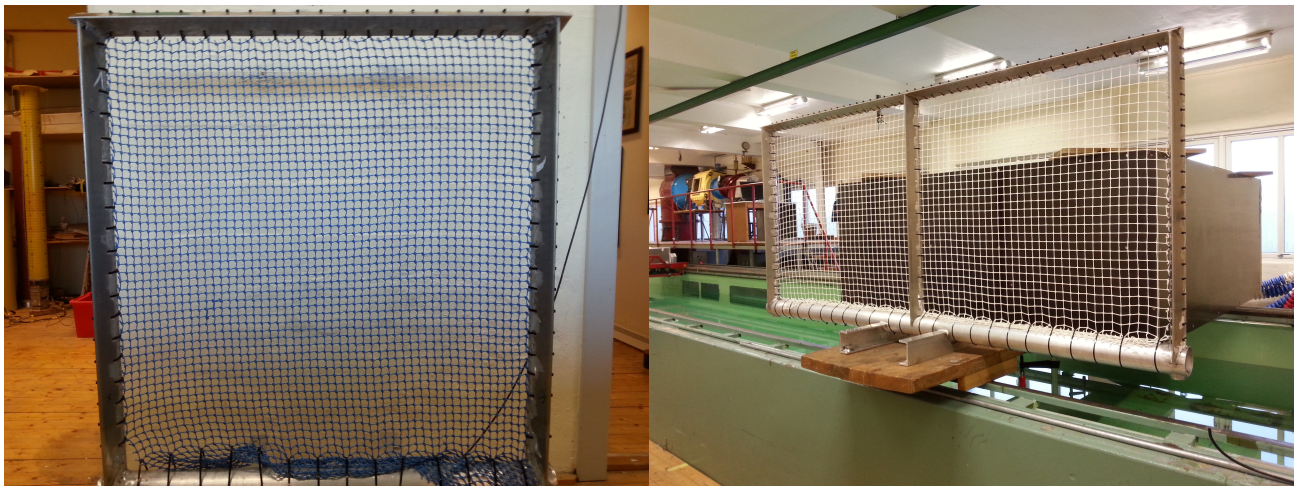
(a) $1m \times 1m$ net (S9).

(b) $2.5m \times 1m$ net (L5).

Figure 2.5: *Pictures of the nets just after that they have been stretched on the frames (upside down on the photos).*

Remarks

The wave maker was dysfunctional for some tests, and finally broke in the middle of the experiments. The water was emptied, the wave maker totally repaired thanks to the team working in the laboratory, and the tank was finally refilled (the water depth was then around 2/3cm higher).

Others (and less important) problems occurred, as a wrong handling of the forces' offset in CATMAN, dysfunctioning wave probes, etc. These technical problems led to missing data in the results presented in the last section of the present work.

2.2 Net panels' properties

2.2.1 Nets' properties
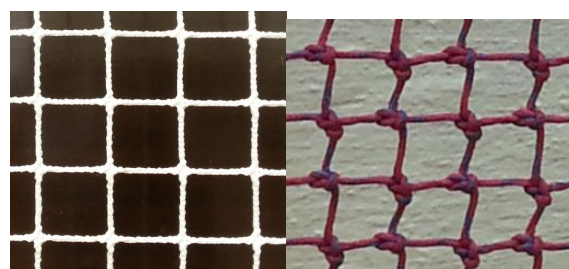
(a) Knot-less nylon net.

(b) HDPE net with knots.

Figure 2.6: *Two types of net panels. Pictures of the nets S2 (Nylon) and L6 (HDPE).*

Each net was provided with two sizes, a large one intended to be fixed to the 2.5m×1m frame, and a smaller one for the 1m×1m frame. Among them, two main types of net can be distinguished: HDPE (High-Density Poly-Ethylene) nets with knots at the

intersection of two twines, and knot-less Nylon net panels (cf. Figure 2.6).
The HDPE nets were more rigid, and harder to stretch on the frames (the blue ones were a little more flexible). On the contrary, Nylon nets were easier to stretch but also faster loosened after few experiments.

Three main parameters on which depend the drag coefficients were measured or estimated to characterize the net panels:

- The twine diameter d_w.

- The half mesh l (defined in Figure 2.7).

- The solidity ratio S_N. Most commonly between 0.2 and 0.35, lower values were considered to emphasize the dependency of C_D in this parameter.

Because the laboratory was available only for a limited period of time, it has been decided initially to test 6 small net panels and the corresponding 6 large net panels in Lilletanken during this master thesis: 3 made of HDPE and 3 of Nylon, chosen for their large variety of solidity ratios and twines' diameter. Finally 4 additional 1m×1m net panels have also been tested. The properties of all the small net panels, respectively the large net panels, are presented in Table 2.1, respectively Table 2.2. The characteristics of the nets used all along this thesis come from these tables, the small net panels (1m×1m) as numbered from S1 to S10, and the large ones (1m×1m) from L1 to L6. The correspondence between the 1m×1m and the 2.5m×1m net panels is indicated Table A.3, and generally more information about the nets can be found in Appendix A.5 .
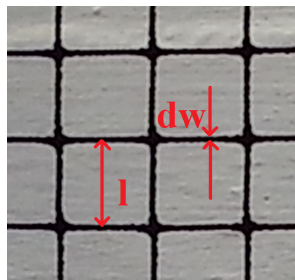
Figure 2.7: *Notations - Twine diameter d_w and half mesh l. Net S10.*

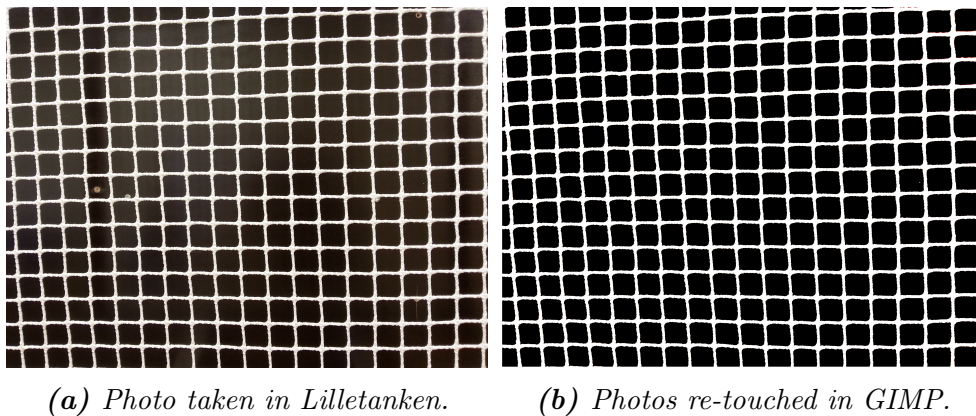## 2.2.2   Estimation of the solidity ratios

The solidity ratio is a crucial parameter characterizing the nets and the way with which a flow crosses it. The forces are very depend on this number, it should therefore be determined with as much accuracy as possible. Two methods, providing two S_N, have been tried and compared.

One way to estimate it was to calculate it from the twins' diameters and lengths (as defined Figure 2.7), that have been previously measured on the net panels, thanks to the following formula[5]:
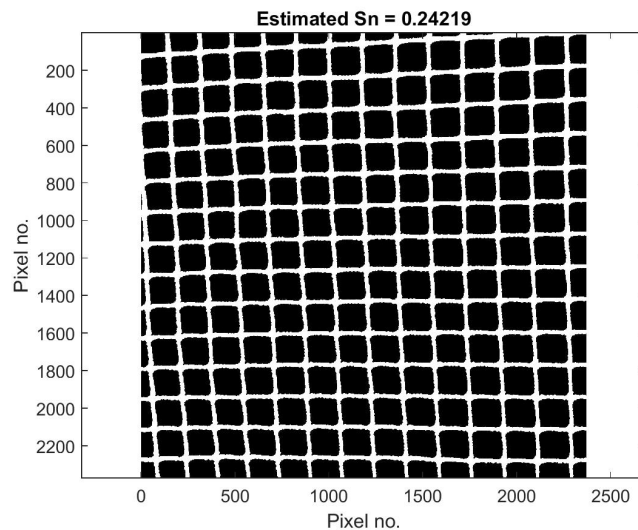
$$S_N = \frac{2\,d_w}{l} - (\frac{d_w}{l})^2 \tag{2.1}$$

However the nodes at the intersections of two perpendicular twins, as well as the irregularity caused by a non-uniform stretching of the net panels are not taken into account by this simple method, which can lead to inaccurate results.

(a) *Photo taken in Lilletanken.*   **(b)** *Photos re-touched in GIMP.*

(c) *Calculation of S_N in Matlab.*

Figure 2.8: *Photo of the net S10, re-touched with GIMP and post-treated in Matlab. The solidity ratio is here the number of "white"" pixels divided by the total number of pixels.*

Another method consisted in photographing the net after being stretched to the frames in front of a contrasted background: a white background for the dark nets (i.e. red, blue, or black nets), and a black background for the white nets. Then, the photos have been retouched with GIMP to eliminate the spurious tasks (disparity of the wall behind, shadows, etc.), improve the luminosity and increase the contrast.
Figure 2.8a shows typical results of this work: on the picture, the luminosity is high to the top right, and low to the bottom. Furthermore, some white holes can be seen in the background to the left side.
Finally the solidity ratios have been estimated from these images thanks to a Matlab

program provided by Trygve Kristiansen and calculating S_N as a ratio of pixels, i.e. as the ratio of black or white pixels, depending on the net's color, over the total number of pixels.
The rendering of the Matlab plots corresponding to the pictures of every net are presented in Appendix A.4 .

Some uncertainties are expected about the resulting S_N. The stretching was probably the most important issue for both methods. It was not equal all along the panel (especially true for the $2.5m \times 1m$ net panels), and S_N seemed then locally higher near the frame than in the middle. It is observed in Figure 2.8a: near the bottom left, the twines are a little closer the ones to the others.
The sizes of the sampled pictures, their inclinations and the uniformity of the background were also among the main concerns.

These uncertainties could explain the large differences of S_N between the two methods. The results, presented in Table 2.1 and 2.2 show that the solidity ratios obtained from the pictures are higher than those calculated from Equation 2.1 (up to 30% higher for S3), even if few values match very well, as for S2 for which the two S_N are equal.
These results will be discussed when looking at the drag forces.

Table 2.1: *Characteristics of the small net panels.*

Net	d_w (mm)	l (mm)	S_N (cf. photos)	S_N (cf. Equation 2.1)	Material - Color
$S1$	2.2	21	0.164	0.199	Nylon - Black
$S2$	1.9	17,8	0.202	0.202	Nylon - Black
$S3$	2.5	23.5	0.286	0.201	HDPE - Red
$S4$	2.1	32	0.173	0.127	Nylon - White
$S5$	2.4	14.5	0.257	0.303	Nylon - Black
$S6$	3	68.7	0.075	0.085	HDPE - Red
$S7$	3	17.4	0.252	0.315	HDPE - Red
$S8$	1.7	27.9	0.154	0.118	Nylon - Black
$S9$	2	16.5	0.288	0.228	HDPE - Blue
$S10$	2.4	23.9	0.242	0.191	Nylon - White

Table 2.2: *Characteristics of the large net panels.*

Net	d_w (mm)	l (mm)	S_N (cf. photos)	S_N (cf. Equation 2.1)	Material - Color
L1	3	68.7	0.075	0.085	HDPE - Red
L2	2.1	23.5	0.240	0.171	Nylon - White
L3	1.9	15.9	0.2304	0.225	Nylon - Black
L4	2	18	0.260	0.210	HDPE - Blue
L5	2.4	31.4	0.176	0.147	Nylon - White
L6	2.6	21.5	0.249	0.227	HDPE - Red

2.3   Modal tests

(a) *1m*1m frames - Fx.*

(b) *1m*1m frames - Fy.*
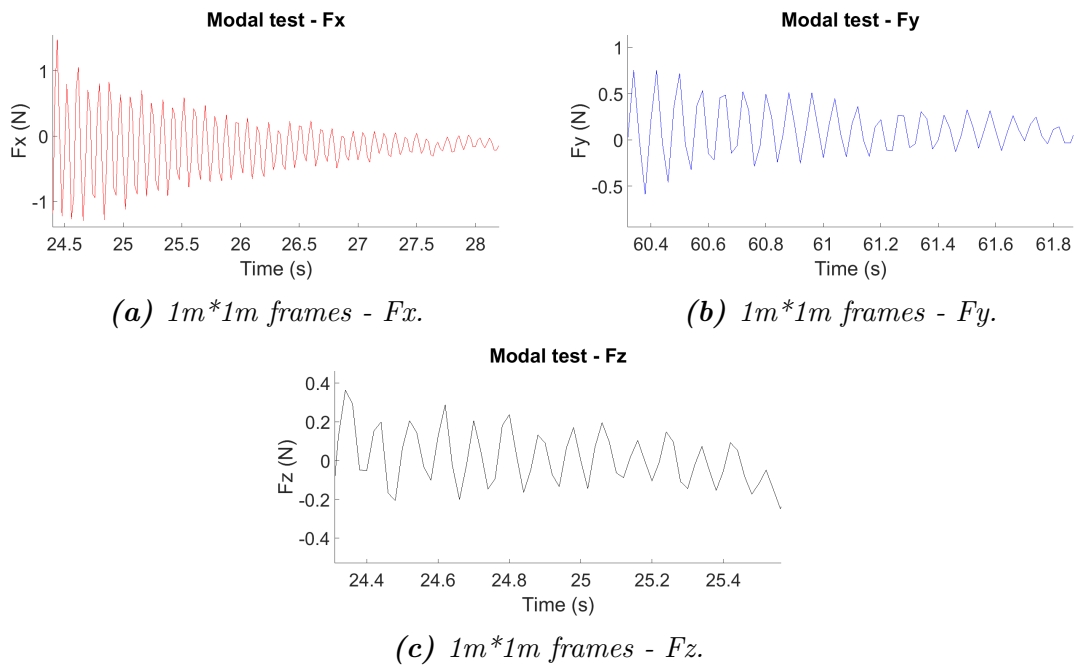
(c) *1m*1m frames - Fz.*

Figure 2.9: *Modal tests of the 1m*1m frames - Time series of the forces just after the hit.*

Modal tests have been submitted to the two sizes of (empty) frame in order to characterize the noise created by the vibrations of the frames while the carriage was running. The principle is simple: the frames have been fixed to the carriage, itself fixed to the towing tank, and hit with a hammer in the three directions x, y and z. The damped vibrations of the frames have been recorded through the time series of the forces Fx, Fy, and Fz (cf. Figures 2.9 for the small frame).

A spectral analysis of these three signals provided the natural frequencies of the frames (cf. Figure 2.10 for the small frame), they are presented Table 2.3. The time series and spectrum obtained for the $2.5m \times 1m$ empty frame can be found in Appendix A.3 .
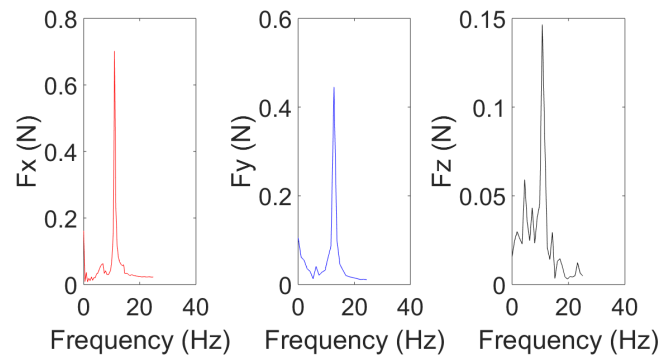
Figure 2.10: *Fourier transform (spectral analysis) of the forces' time series. Modal test achieved on the $1m \times 1m$ empty frame without strips.*

Some uncertainties are expected on these frequencies. For instance, the hits were not done exactly in the desired direction. Besides, the oscillations were quickly damped, leading to wide spectra (especially in z).

Table 2.3: *Natural frequencies - Modal tests.*

(a) 1m*1m frames.
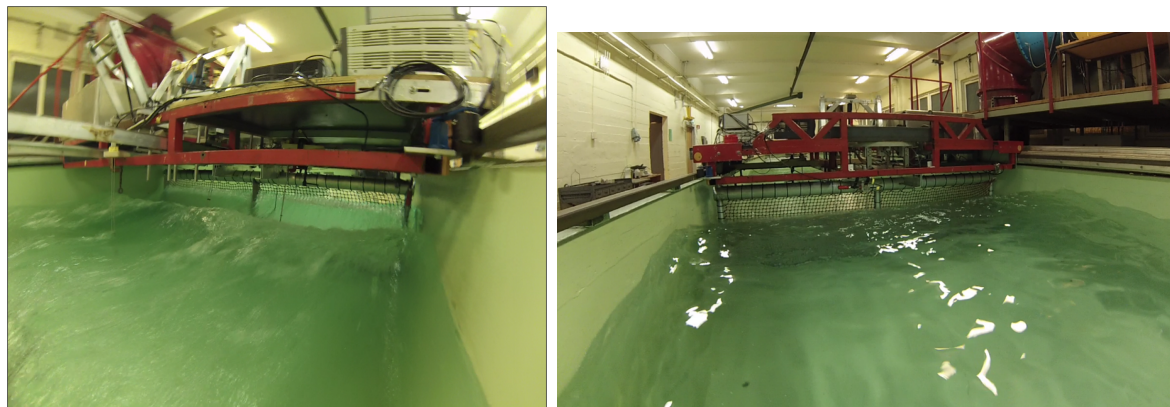
x direction (Hz)	y direction (Hz)	z direction (Hz)
11.04	13.01	11.40

(b) 1m*2.5m frames.

x direction (Hz)	y direction (Hz)	z direction (Hz)
6.56	8.51	13.11

2.4   Environmental conditions

(a) *The carriage is running at $U_0 = 1.5m/s$.*

(b) *The carriage is fixed in the middle of the towing tank, and subjected to incoming waves ($T = 2s$, $\epsilon_w = \dfrac{1}{20}$)*

Figure 2.11: *Pictures taken in the towing tank during experiments achieved on $2.5m \times 1m$ net panels. Lilletanken, January 2017.*

The environmental conditions tested in Lilletanken from January to February 2017 are presented in this section. Different conditions of waves and currents have been imposed. The goal was to generate external conditions met by real aquaculture farms in sea thanks to the facilities available in the laboratory.

- Several velocities of currents have been simulated by running the carriage along the towing tank.

- Several regular waves have been generated by the wave maker while the carriage supporting the frames was fixed to the towing tank by imposing a 0 m/s velocity from the carriage control computer.

- Conditions of waves and currents together have been simulated by running the carriage while generating waves, fewer wave periods were then considered.

Only frontal waves and currents (i.e. coming perpendicularly to the net panels) have been considered in this thesis.

Because of the large number of tests and the limited time available in the towing tank, Matlab scripts provided by Trygve Kristiansen, and modified for our needs, have been used to generate automatic tests from the control computers. Thus, all the velocities (or wave periods) were tested the one after the other for each net, with a mean duration of one hour per set of tests. This task automation allowed us to the stretch the next net to be tested without controlling and launching permanently the experiments.

The two terms "currents' velocities" and "carriage's speeds" are interchangeable in this report.

Current conditions

The determination of the forces due to incoming currents on the nets has been the preponderant part of this thesis. Indeed the net panels, built in full scale, have been conceived for these tests, and only current conditions have been modelled and studied in CFD.

Fifteen velocities of currents from 0.1 m/s to 1.5 m/s have been subjected to each net panel. These velocities have been proposed by Aqualine and correspond to real scale currents encountered by aquaculture farms.
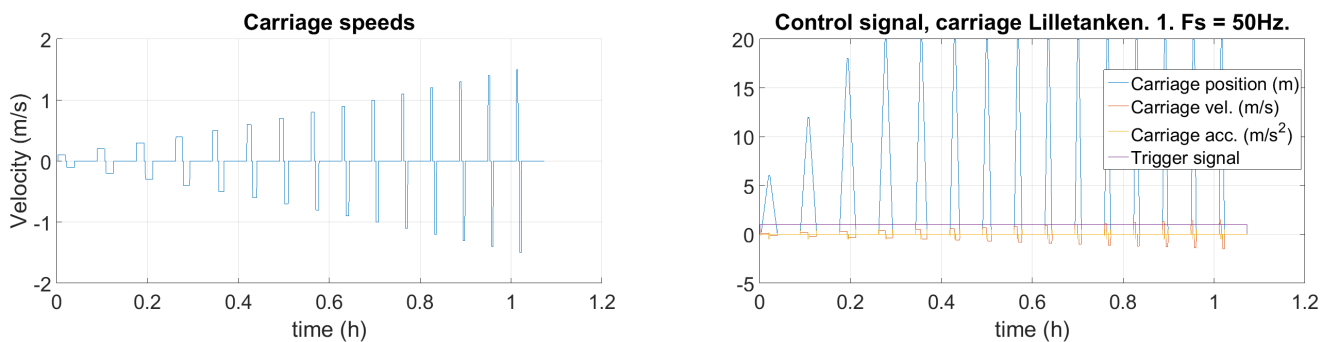
(a) *Visualization of the carriage speeds.*   *(b)* *Carriage position, velocity, and acceleration.*

Figure 2.12: *Tests in currents. To the left, the desired carriage velocities are plotted in Matlab. To the right, the carriage position is displayed in blue as defined in the control computer, as well as the carriage position and acceleration. The trigger signal is 1 as long as the script runs.*

The length of the towing tank is 25m. For security measures, the carriage was always stopped before 20m.
The duration of the tests was set to 60s by default, but for the highest velocities (from $U_0 = 0.4m/s$) the carriage was traveling the 20m faster than this time, and so it was stopped and the experiment was much shortened (about 13s for $U_0 = 1.5m/s$).
This is illustrated in Figure 2.12, showing the times series of the carriage speed and position as generated in Matlab. The tests with high velocities are shorter as soon as the position of the carriage reach the 20m.

Furthermore, the acceleration was fixed manually to $800m/s^2$ for each test, but in reality the phase of acceleration of the carriage was longer because of the high forces acting on the nets (the consequences of this are described in Section 2.5).

Wave conditions

Contrary to the currents which were in full-scale, the tests in waves have been achieved in model-scale to create "realistic" regular waves in the towing tank. A scale factor **s=36** was considered for all the waves generated in Lilletanken in order to create wave

periods from 4.8 to 12s (full-scale) which represents typical T near the locations of aquaculture farms, often a little sheltered from the biggest waves.

The results were then expected to be a little inaccurate because the full-scaled net panels (i.e. with full-scaled d_w, l) have been subjected to model-scaled waves. Due to the lack of time, and also because of the technical problems met with the wave maker, fewer nets were tested in waves.
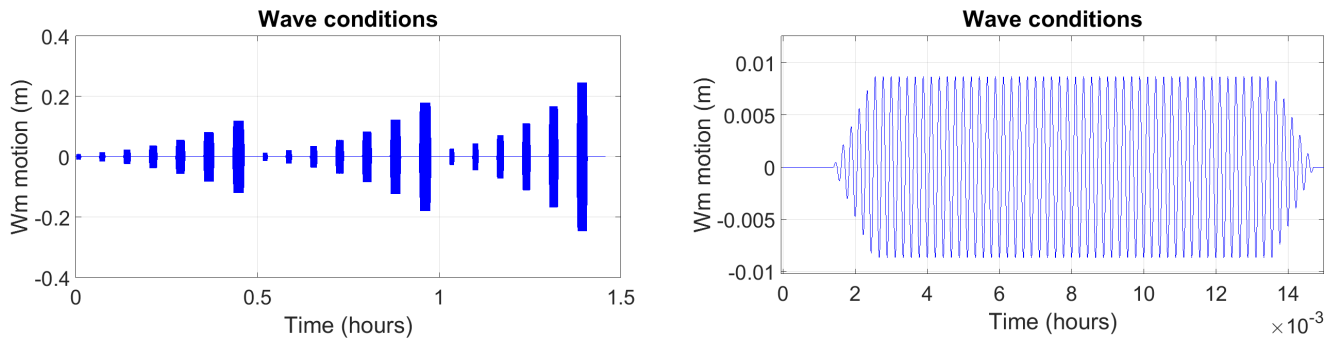
(a) *All the wave tests gather in one time series.*   **(b)** *Focus on the first test.*

Figure 2.13: *Tests in waves as defined in Matlab for the control computer. Wave amplitudes, generated by the wave maker.*

Each regular wave have been tested for a duration equal to 60 periods, including two ramps defined over 5 periods (cf. Figure 2.13b). All the waves have been tested in once thanks to an automatic script imposing a break of 180 seconds between two tests to start each new test with the water at rest.

The waves have been defined by their periods, and their steepness, which is defined Equation 2.2 where H is the wave amplitude (crest to crest) and λ the wave length.

$$\epsilon_w = \frac{H}{\lambda} \tag{2.2}$$

Table 2.4 presents the regular wave periods considered in this report, defined by their periods and steepness. $T = 2s$ for the highest steepness could not be tested because the corresponding wave amplitude was higher than the limitation imposed by the control computer of the wave generator (due to security measures).

Finite water depth

The dispersion relationship, written in Equation 2.3, can often be reduced to Equation 2.4 (and Equation 2.6) assuming that the water depth is high compared to the wave length.

For the highest period T=2s considered in these experiments, it leads to $\lambda = 6.24m$. The water depth of the towing tank has been measured to $h = 0.95m$, $g = 9.81m/s$, leading to $\dfrac{\lambda}{h} = 6.57 \gg \dfrac{1}{2}$, which is contradictory with the deep water assumption.

Thus, the calculations of the theoretical wave amplitudes from ϵ_w and T (defining the waves) have been done considering finite water depth (i.e. using the general dispersion relationship).

$$\omega^2 = g\,k\,tanh(k\,h) \tag{2.3}$$

Table 2.4: *All the wave periods tested for each steepness.*

(a) *Periods (s) - Model scale.*

$\epsilon_w = \dfrac{1}{60}$	$\epsilon_w = \dfrac{1}{40}$	$\epsilon_w = \dfrac{1}{20}$
0.8	0.8	0.8
1.0	1.0	1.0
1.2	1.2	1.2
1.4	1.4	1.4
1.6	1.6	1.6
1.8	1.8	1.8
2.0	2.0	\

(b) *Periods (s) - Full scale.*

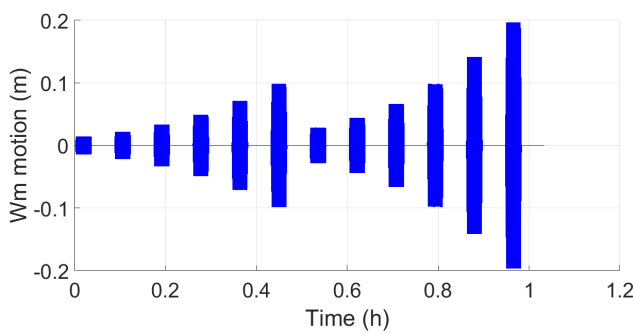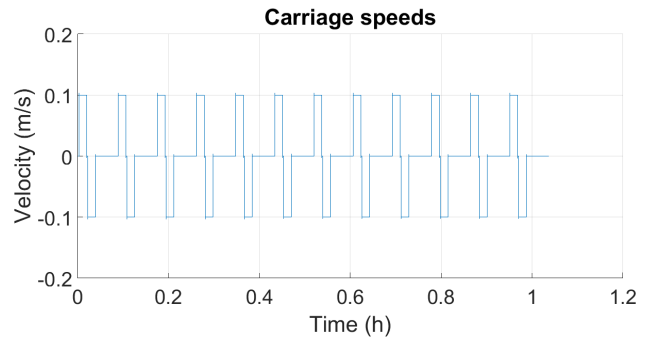| $\epsilon_w = \dfrac{1}{60}$	$\epsilon_w = \dfrac{1}{40}$	$\epsilon_w = \dfrac{1}{20}$
4.8	4.8	4.8
6.0	6.0	6.0
7.2	7.2	7.2
8.4	8.4	8.4
9.6	9.6	8.4
10.8	10.8	10.8
12.0	12.0	\

$$\omega^2 = g\,k \qquad (2.4)$$

$$\begin{cases} \omega = \dfrac{2\pi}{T} \\ k = \dfrac{2\pi}{\lambda} \end{cases} \qquad (2.5)$$

$$\lambda = \frac{g}{2\pi}\,T^2 \qquad (2.6)$$

Wave and current conditions

The same scale $s = 36$ has been conserved for both current and wave conditions.

(a) *Wave conditions as defined in Matlab.*

(b) *Carriage speeds for the 12 tests, $U_0 = 0.1 m/s$).*

Figure 2.14: *Wave and current conditions are defined separately in Matlab. The scripts are then launch simultaneously from the two control computers managing respectively the wave maker and the carriage.*

Wave and current conditions were defined separately in Matlab. The scripts were then launch simultaneously (but independently) from the two control computers managing respectively the wave maker and the carriage. Figure 2.14 presents the theoretical signals created in Matlab.

Figure 2.15 shows a signal recorded from a test, showing both the carriage speed and

the wave amplitude measured in front of the net panel (WP1). It is observed that the carriage first starts at $t = 40s$, then the incoming waves generated at the other end of the towing tank meet the net around $t = 50s$. the carriage stops at $t = 100s$, and comes back to its inital position until $t = 175s$. Too much waves are generated to avoid de-synchronization between waves and currents (the scripts are independent, and all the periods are tested all along the same script), but the waves stop as soon as the carriage is back, and a resting period of $180s$ is imposed before the next test.
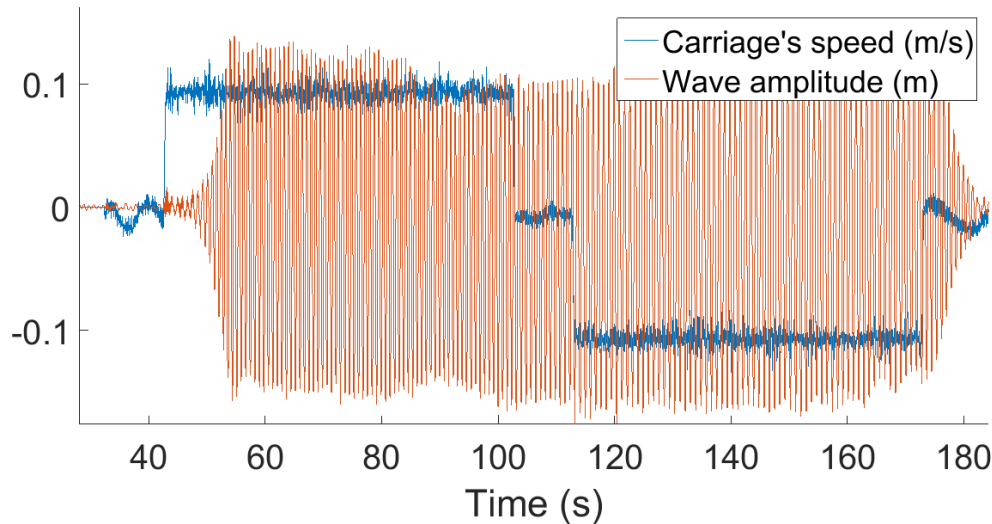
Figure 2.15: *Recorded carriage speed and wave amplitude. Focus on the first wave period.*

Encounter periods

$$\omega_e = \omega + k \times U_0 \tag{2.7}$$

For these tests, the wave frequencies encountered at the net panel were higher than the wave frequencies created by the wave maker because of the velocity of the carriage. The relationship between the encounter wave frequency ω_e, the wave frequency ω, and the wave number k is presented Equation 2.7. Considering the dispersion relationship (Equation 2.3), it is then possible to determine the encounter period $T_e = \dfrac{2\pi}{\omega_e}$ from the wave period T.

Fewer wave periods and steepness have been considered when adding currents: the 6 periods presented Table 2.5 have been tested for two steepness, $\epsilon_w = 1/20$ and $\epsilon_w = 1/40$, using an automatic script for each net. The process has been repeated for both speeds $U_0 = 0.1$ and $U_0 = 0.2m/s$.

Table 2.5: *Wave periods generated by the wave maker.*

Model scale (s)	Full scale (s)
0.83	5
1.0	6
1.17	7
1.33	8
1.5	9
1.67	10

Table 2.6: *Encounter wave periods measured in front of the Net. These periods are given for the two carriage speeds, in both model and full scales.*

(a) *First current velocity.*

Te (s) - Model scale	Te (s) - Full scale
$U_0 = 0.1 m/s$	$U_0 = 0.6 m/s$
0.77	4.64
0.94	5.64
1.11	6.64
1.27	7.63
1.44	8.63
1.61	9.63

(b) *Second current velocity.*

Te (s) - Model scale	Te (s) - Full scale
$U_0 = 0.2 m/s$	$U_0 = 1.2 m/s$
0.72	4.33
0.89	5.32
1.05	6.31
1.22	7.30
1.38	8.29
1.54	9.29

2.5   Data analysis - Methodology

This section presents the methodology applied to extract the results from the raw data obtained from the experiments performed at Lilletanken. The post-treatment of more than 1000 individual tests has been achieved with Matlab. The binary files saved from the control computer were loaded in Matlab thanks to the provided function *catmanread.m*. Automatic procedures have been used, but each of them included a visual control of the results (both for the time series and the spectra for each test, and then for the resulting forces). The small and large net panels have been post-treated in the same way.

A general description about how the data have been cleaned, and the noise recorded on the signals filtered will be first described. Then the post-treatment of the data for the three types of imposed conditions (currents, waves, and waves plus currents, cf. Section 2.4) is presented, focusing on how the results presented in Section 4   were deduced from the raw data recorded in Lilletanken.

2.5.1   Filtering and cleaning

All the data were cleaned and filtered thanks to the process explained below. Filtering the data was especially important for the tests with waves, for which the spectra of the forces were studied in detail.

Cleaning

Several data have been recorded with few erroneous values during the experiments (e.g. with infinite values, or NaN returns). These problematic values had to be removed before post-treating the signals. This has been done using the *clean_data* Matlab function provided by Valentin Chabaud within the course *Experimental Methods in Marine Hydrodynamics* at NTNU.

This function takes in inputs the discrete signal, for example F_x, of length N, and two parameters CrtSTD and CrtCONV. Then the values are controlled one by one as follow: if at least one of the three conditions defined Equation 2.8 is verified, then the value is removed and replaced by a linear interpolation of the nearest valid points.
Once the signal has been "cleaned", the mean value μ_{F_x} and the standard deviation σ_{F_x} of the signal are re-calculated, and the same operation is repeated n times until the standard deviation converges according the criterion presented Equation 2.9.

Thus the values abnormally high are removed thanks to the *Conditions 1* and *2*, as well as the values abnormally low with the *Condition 3*.
The parameters CrtSTD and CrtCONV have been adapted to each test (by trying

different values until it gave reasonable results). Hence, CrtSTD has been taken higher for wave conditions in order to not cut the crest of the response to the waves.

$$
i \in [1:N], \begin{cases} Condition1: \ |F_x(i) - \mu_{F_x}| \geq CrtSTD * \sigma_{F_x} \\[2ex] Condition2: \ |\dot{F}_x(i)| \geq CrtSTD * \sigma_{\dot{F}_x} \\[2ex] Condition3: \ |\dot{F}_x(i)| \leq \dfrac{\sigma_{\dot{F}_x}}{10 * CrtSTD} \end{cases} \tag{2.8}
$$

$$
\frac{|\sigma_{F_x,n} - \sigma_{F_x,n-1}|}{\sigma_{F_x,n-1}} \leq CrtCONV \tag{2.9}
$$
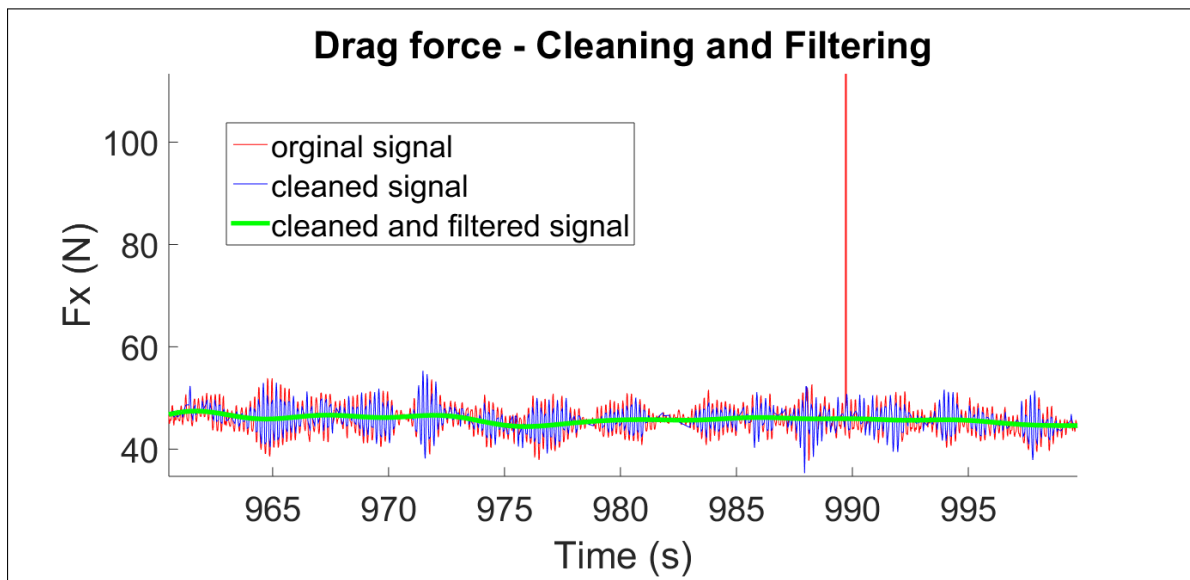
Figure 2.16: *Example of cleaning and filtering - Net S7 in currents, $U_0 = 0.4m/s$.*

An example of cleaned data is given in Figure 2.16: it can be seen that the nonphysical peak met at 990s is removed.

Filtering of the noise

The signals contained a lot of noise, especially when the carriage was running. It was a real problem to calculate the amplitude of the force oscillations in response to waves, and this noise had to be removed.
This noise could come from many sources: the vibration of the installation (the carriage, the frames, and the electronic installation with them), the amplifier, etc.

(a) *Before filtering.*   **(b)** *After filtering.*
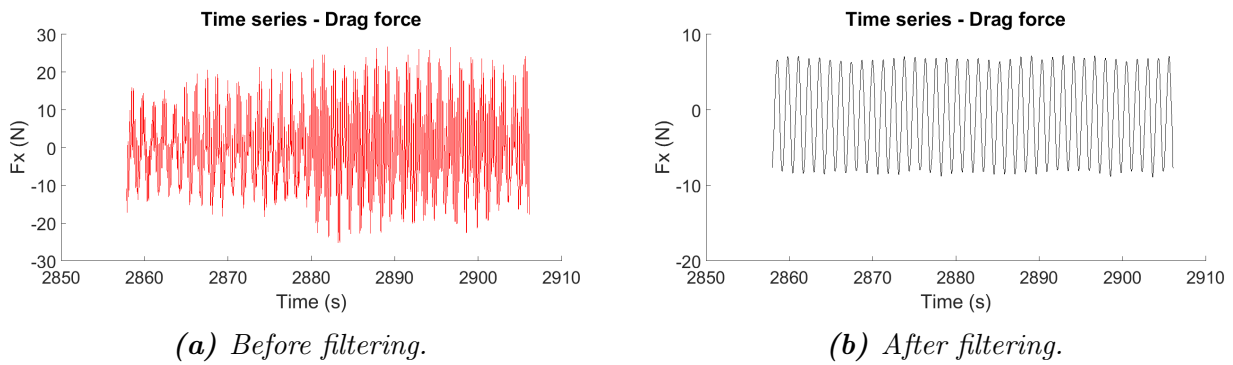
Figure 2.17: *Time series of F_x, example of filtering. The empty $1m \times 1m$ frame is dragged at $U_0 = 0.1m/s$ and subjected to incoming waves defined by $T_e = 1.27s$ and $\epsilon_w = \dfrac{1}{20}$.*

Figure 2.17a shows an example of drag force's time series (raw data) for the $1m \times 1m$ empty frame when it is subjected to waves and that the carriage is running at $U_0 = 0.1m/s$. The noise is preponderant and the oscillation of the loads at the wave frequency are not observed.

Figure 2.18 presents a Fourier transform made with the *fft* Matlab function (based on *the Fast Fourier Transform* algorithm) and a normalization $2/N$ (N is length of the discrete signal) for the same net panel and for $U_0 = 1m/s$. This graphic shows the decomposition of the noise corresponding to all the frequencies above zero. Two frequencies can especially be pointed out: the natural frequency of the frame, around 11Hz for the $1m \times 1m$ frames in the x direction, and the frequency around 5Hz that appeared for all the velocities (and also for the large frame). This last one is suspected to be the natural frequency of the platform supporting the transducers, it could also come from the vibration of the all carriage during the runs, but the spectra of the wave elevations obtained from the wave probes fixed to the carriage do not show this noise at 5Hz.

Most of the noise has been removed using a low-pass filter (with the Matlab functions *butter* and *filtfilt*). The cut frequency has been adapted and fixed between 2.5Hz to 4Hz according the tests. For the highest wave frequency ($f = 1.25Hz$), the peak in $2f$ was always hidden into the noise, so the load responses could not be studied.

A result of this filtering is presented in Figure 2.17b: the force F_x oscillates now at the same period as the incoming waves (an other example can be found in Appendix A.6). Since most of the energy was focused in the noise, the amplitude of the signal decreases from about 20N to 8N after filtering. It was essential to achieve correctly this operation, that is why the results were always controlled "visually".
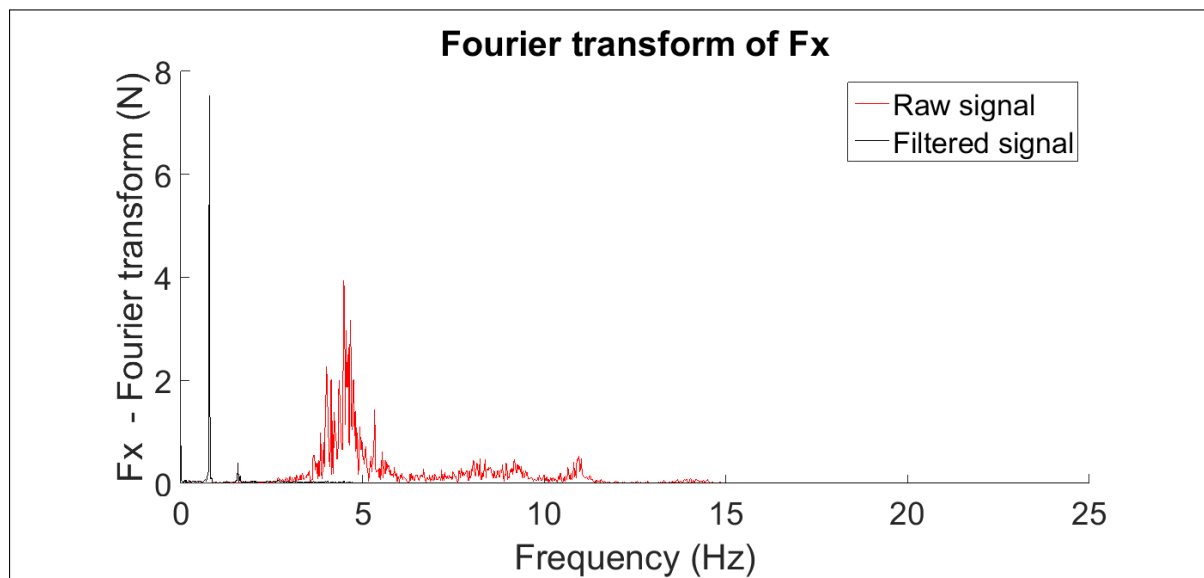
Figure 2.18: *Spectrum of F_x.*

2.5.2   Currents

Offset

An offset has first been calculated at the beginning of every time series, before that the first experiment starts, as the mean value of this part of the signal. This operation has been done for all the nets, and all the signals (forces, speed, wave probes, etc.). Then this offset has been subtracted to the corresponding time series.

As the recorded signals was composed by a set of tests (i.e. 15 velocities), this method was fast but not very accurate. Indeed the transducer depends on external conditions, like the temperature, and in reality the offset was not constant over the all signals. Sometimes, "large variations" of the forces (about 1N) were even observed during one unique resting periods. Example of these phenomena are shown in Figure A.13 and A.12 in Appendix A.6 .
The offset could have been re-calculated before each individual test, but since the accuracy for our experiments was not expected to be smaller than 1N, the method adopted here was considered to be satisfying.

Mean forces

The mean forces and the mean speed were then calculated. First, a time window corresponding to the desired velocity was selected, i.e. after the acceleration of the carriage, and before it starts to stop.
For low speeds the acceleration was quasi-instantaneous and the "constant-speed" phases above 50s. However, as soon as U_0 increased the acceleration was longer. For these high velocities, the speed was never constant, and a little lower than expected (typically 0.05m/s lower) because of the high forces acting on the nets.

(a) $U_0 = 0.2m/s$.   *(b)* $U_0 = 1.5m/s$.
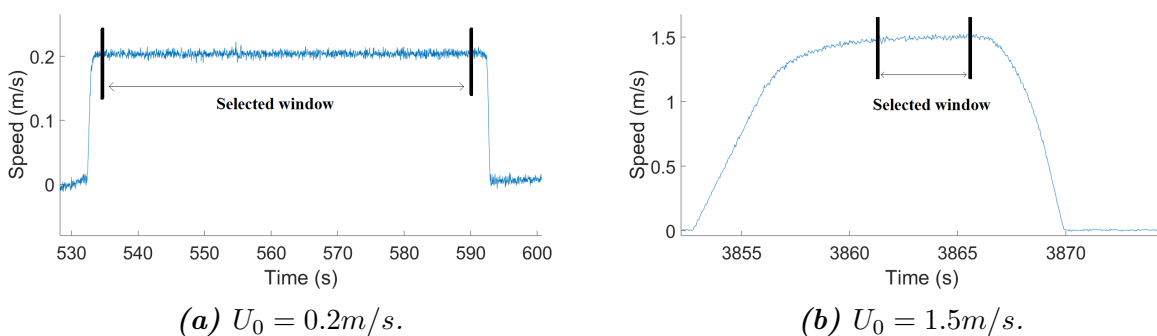
Figure 2.19: *Example of time series for the carriage speed - Net S6. A time window is selected from the time series of the carriage velocity to calculate the mean speed, and then the mean force over the same period.*

Generally, the forces have been observed to be higher during the acceleration, so these phases were avoid carefully by selecting the "constant-speed" periods manually. However, the limit between these acceleration and "constant-speed" phases was often

blurred for the highest velocities. Two examples of such intervals are shown in Figure 2.19 for both a low and high velocities and from the same time series, recorded for the net S6 (Nylon, $S_N = 0.075$).

The mean speed and forces were finally calculated over these selected intervals.

Drag coefficients

$$C_D = \frac{(1 - S_N)^2 F_x}{\frac{1}{2}\rho U_0^2 A_{Net}} \tag{2.10}$$

$$C_L = \frac{(1 - S_N)^2 F_z}{\frac{1}{2}\rho U_0^2 A_{Net}} \tag{2.11}$$

The drag coefficients were then calculated as in Equation 2.10, where A_{Net} is the wet frontal area of the nets (calculated from the measures taken in Lilletanken). The loads on the empty frames were subtracted to the total forces in order to conserve uniquely the loads acting on the net panels. Since the velocities of the carriage were not exactly the same for all the tests - especially for the nets with high S_N, where the velocity was between 0.05 and 0.1 m/s lower than expected - the values obtained for the empty frames were interpolated to match. Thus, this subtraction was done at the exact same speeds.

Lift coefficients have been obtained similarly (cf Equation 2.11). Reynolds numbers were also calculated from the measured velocities and the properties of the net panels, as expressed previously in Equation 1.20.

2.5.3 Waves

Selection of the time window

The offset of each signal has been removed following the same procedure as for the current conditions. The time interval studied for each test has been chosen by looking at the time series of the first wave probes (WP1), placed in front of the nets and measuring the "undisturbed" incoming waves.

For these experiments, the carriage was fixed in the middle of the towing tank. Thus, it was possible to record a large number of wave periods before that the reflexive waves at the end of the towing tank interfere with the incoming waves. The selection of the time periods over which the amplitude of the forces' oscillations and their mean values have been calculated was chosen after the ramp (a transition of 5 waves, as described previously), and before that the reflection interfere. Furthermore, a whole number of periods was considered for the spectral analysis.

The time spent by the first wave arriving on the net to be reflected and come back on the carriage has been estimated from the position of the carriage in the towing tank

and the wave velocity, expressed in Equation 2.12 using the deep water assumption. Hence, between 11 and 29 waves were considered for each test, from the lowest period ($T = 0.8s$, $C_g = 0.62m/s$, 29 waves) to the highest ($T = 2s$, $C_g = 1.56m/s$, 11 waves).

$$C_g = \frac{\partial \omega}{\partial k} = \frac{g}{2\omega} \qquad (2.12)$$

Force harmonics in ω, 2ω and 3ω

The mean forces were first calculated. Then the loads' response to the wave frequency, as well as the harmonic in 2 and 3ω, have been studied as follow:

1. The signal has been cut around the frequency of interest using a pass-band filter (still with the Matlab functions *butter* and *filtfilt*).

2. The spectra of the wave amplitude and the loads were compared before and after filtering to control the operation.

3. The amplitude crest-to-crest of the loads were then measured from the time series of the filtered signals. The results were then divided by 2 to conserve the rest-to-crest amplitudes.

4. The resulting loads have been plotted against the theoretical wave periods (it turned out that they matched quite well to the measured ones).

(a) *Spectrum of the wave amplitude.*   *(b)* *Spectrum of F_x.*
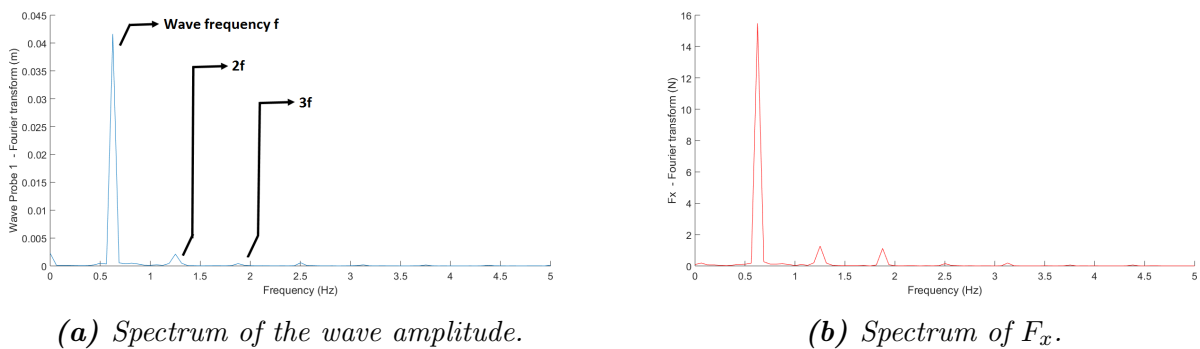
Figure 2.20: *Spectrum of the wave amplitude measured in front of the net, and spectrum of the resulting drag force. Net L6, $T = 1.6s$ and $\epsilon_w = \dfrac{1}{40}$.*

Figure 2.20 shows an example of both the wave and the F_x spectra. The fundamental harmonic f=0.625, as well as the second and third harmonics are observed before applying any pass-band filter.

Verification of the wave periods and wave amplitudes

The wave periods measured by WP1 during the experiments, and obtained in Matlab thanks to the wave spectra, have been compared to the expected ones. It has also been done for the 2 and 3ω components. The objective was to detect the technical problems (often coming from the wave maker before it was repaired) in order to understand the resulting loads.

The wave amplitudes measured from the wave probe 1 have also been compared to the expected ones.

$$\zeta = A * sin(\omega t - kx) \tag{2.13}$$

The wave amplitude ($A = \dfrac{H}{2}$), introduced in Equation 2.13 for a regular wave, and where ζ is free surface elevation, was deduced from the wave steepness (cf. Equation 2.2) and from the dispersion relationship. Both finite water depth and deep water assumption have been compared.

The wave amplitudes in 2 and 3ω have also been confronted to the theoretical ones, which were calculated as follow[6]:

$$
\begin{cases}
A_{2\omega} = k \times A^2 \times \dfrac{3 - \sigma^2}{4\sigma^3} \\[3mm]
A_{3\omega} = k^2 \times A^3 * \dfrac{27 - 9\sigma^2 + 9\sigma^4 + 3\sigma^6}{64\sigma^6} \\[3mm]
\sigma = tanh(kh)
\end{cases}
\tag{2.14}
$$

2.5.4 Waves and currents

The treatment made on these tests were comparable to the previous case (i.e. with only waves). However, the selection of an appropriate time window has been done by looking both at the time series of WP1 (i.e. the waves amplitudes measured from the carriage), and at the carriage speed. Furthermore, the carriage had to start from the beginning of the towing tank (compared to previously where it was fixed in the middle of the tank), and its velocity was relatively low compared to the velocity of the wave propagation. Thus, the reflection was inevitable and a probable source of error on the measured wave amplitudes (and the resulting forces).

The final loads have been plotted against the encounter wave periods to be discussed.

During these tests, a lot of noise was observed in the signals, probably caused by the vibrations of the different parts of the installation. Hence, it was never possible to study the third harmonic of the forces, nor the second harmonic for the lowest wave periods, because they were both hidden in the noise which was seen from 2.5Hz (for the "noisiest" data) to higher frequencies.

Seiching

Observed in the time series for all the environmental conditions tested in the towing tank, the seiching was particularly strong for wave and current conditions, especially for high wave steepness.

The seiching is a standing wave whose wavelength is twice longer than the length of the towing tank (here $\lambda_{seiching} \simeq 50m$). The seiching period can be estimated as follow[4]:

$$T_{seiching} = \frac{2L_{tank}}{\sqrt{gh}} \tag{2.15}$$

Where h is the water depth and g the gravitational acceleration. In Lilletanken, $T_{seiching} \simeq 16.3s$ (but the encounter period could be shorter due to the velocity of the carriage).
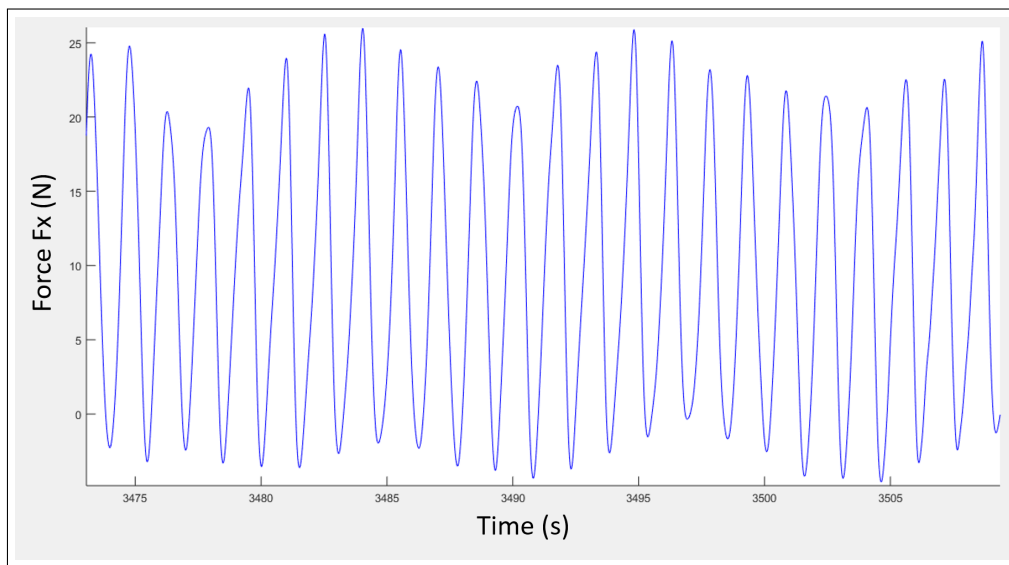
Figure 2.21: *Time series of drag force in waves ($T_e = 1.61s$ and $\epsilon_w = \dfrac{1}{20}$) and subjected to current ($U_0 = 0.1m/s$). Illustration of Seiching (extreme case). The signal was cleaned and filtered at 2.5HZ.*

An example of seiching occurring in the drag force's time series is presented in Figure 2.21: the loads oscillate both at the wave period and at the seiching period (much larger).

The errors on the force amplitudes caused by this phenomenon could be minimized when using the pass-band filter around the wave frequency. However, the seiching frequency was so small ($f_{seiching} \simeq 0.06Hz$) that is was almost impossible to filter it when calculating mean values, and so the mean forces could have been affected.

3 | CFD simulations

3.1 Introduction and objectives

Introduction to CFD

The CFD is a branch of Fluid Mechanics developed since the middle of the 20th century which uses numerical supports to solve the Navier-Stokes equations governing fluid flows. The increase of computational speed and memory over the last ten years helped CFD to become a valuable tool, at the same level as EDF.
The computational work can be decomposed in three main steps:

- **Pre-processing:** the geometry, the domain, the mesh, the boundary conditions, as well as the fluid properties have to be defined properly.

- **Processing:** the NSE are solved to determine the velocity and pressure at every time steps, and every points of the discretized domain.

- **Post-processing:** the results can then be post-treated (e.g. calculating the forces from the pressures) and visualized with appropriate tools.

OpenFoam

OpenFoam® is an open source CFD software based on C++ libraries and applications. First released in 2004 on Linux, series of solvers and utilities have been created and developed to handle the different steps of the computational work (from the mesh generation to the visualization of the results), and to solve a large number of fluid mechanic problems.

The latest version 4.1 has been used in the present study, and run in Linux Mint 17 through a virtual box. The models presented in Section 3.2 have been created with the OpenFoam's mesh generator *blockMesh*, and the quality of the mesh have been controlled with the help of the command *checkMesh*, which indicates all the main characteristics of the current discretization.

3.2 The numerical models

(a) *Model 1 - Top view.*

(b) *Model 2 - Side view.*

(c) *Model 3 - Side view with free surface.*
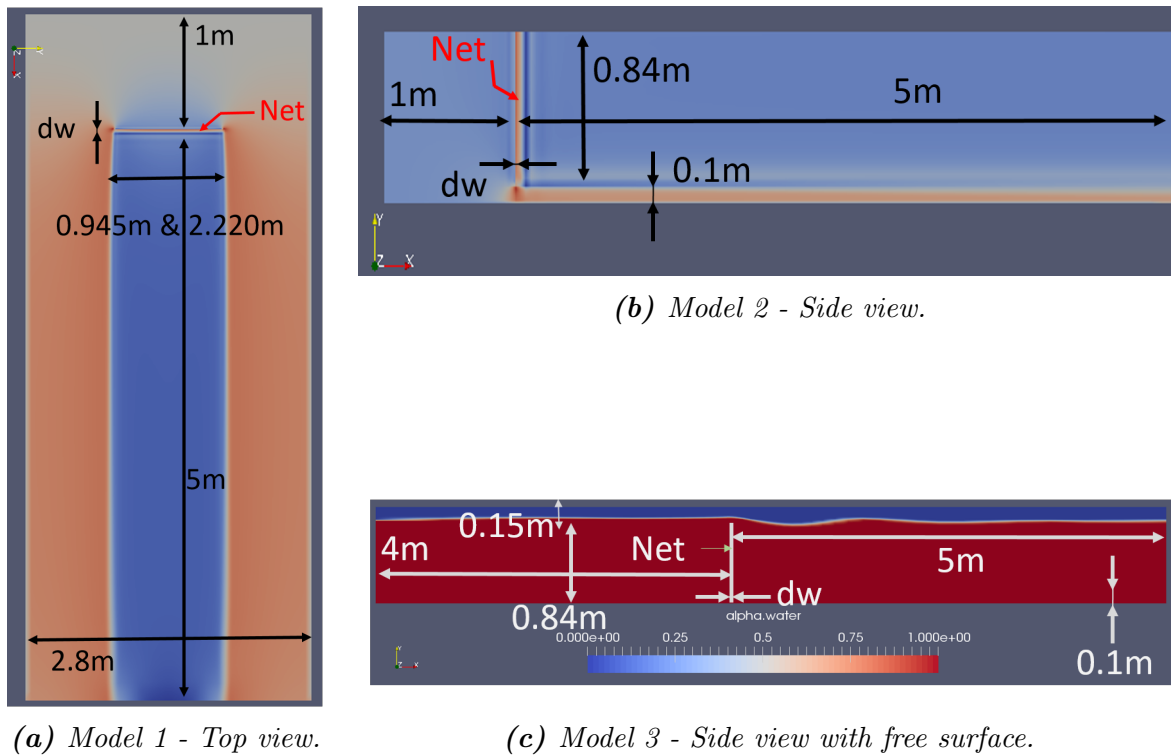
Figure 3.1: *Presentation of the numerical models with their main dimensions. the top view shows a* $1m \times 1m$ *net, but large panels have also been considered.*

The three 2D-models presented Figure 3.1 have been run for the the same cases (i.e. the same nets) in order to characterize the dependency of the different physical phenomena occurring on the drag forces:

- Model 1 is a top view of the towing tank, the flow between the net and the side of the tank can be observed.

- Model 2 is side view of the installation without considering the free surface elevation. This configuration allows the study of the flow between the net and the bottom of the tank.

- Model 3 is also a side view of the net, including the free surface to study the waves propagating behind the net.

Dimensions of the domains

The width and the water depth of the towing tank correspond to those measured during the experiments, however the length (originally at 25m) has been reduce in order to lighten the calculations (these dimensions are indicated in Figure 3.1. The distance in front of the net for the third model has been increased compared to Model 2 after few tries, because of strange phenomena occurring at the inlet boundary (i.e. elevations of the free surface at the boundary).

The widths and heights of the nets (both sizes) have also been fixed to the ones measured during the tests, as presented in Section 2.1.2 .
The thickness of the mesh defining the porous volume corresponds to the twine diameter of each net.

Only the submerged part of the net was considered and meshed in Model 3 to simplify the model. The height of the air domain was chosen according the largest wave elevation measured behind the panels in Lilletanken during tests in currents.

Finally, the thickness of these 2D models (0.1m by default) were defined in accordance with the experimental dimensions (cf. Figure A.3 in Appendix A) when post-treating the forces in Octave, i.e. by multiplying these forces by the water depth (Model 1), or by the net's width (Model 2 and 3).

The specific coordinate systems of each models observed in Figure 3.1 were used to define the cases (mesh, BCs, incoming flow, etc.). However, the notations and axis defined at the beginning of this thesis were conserved (cf. Figure 1.6 in Section 1) to analyse and compare the results with the experimental loads.

Boundary conditions (BC)

The meshes were created in 3D, and turned into 2D models by setting *empty* boundary conditions in the direction perpendicular to the considered 2D plane.

For the Models 1 and 2, the inlet boundary was defined by imposing a fluid velocity and a *zeroGradient* condition to the pressure. The outlet boundary was defined by setting $p = 0\,Pa$ and a *zeroGradient* condition to u.
Model 3 was run was a multiphase solver (*interFoam*) and only worked with the dynamic pressure $p_{dynamic} = p - \rho g h$ (contrary to the two other cases). For this case, an *inletOutlet* BC for the velocity coupled with *zeroGradient* BC for the pressure (respectively *outletInlet* BC for u and *fixedFluxPressure* BC for P) was imposed at the inlet boundary (respectively outlet boundary). This way, the velocity was imposed in the direction of the flow (x>0) at the two ends of the mesh, but free to come in or out in x<0 (e.g. the flow can reflect on the net and go out of the domain at the inlet boundary).

During the experiments, the carriage was running and the water in front of the net had no velocity. It is the opposite for the CFD simulations: the net is observed "from the carriage", fixed, and the all tank is moving around (with the water) at the same speed U_0. Thus, a fixed velocity boundary condition ($u = U_0$) was imposed in the walls on each side of the tank (e.g. left and right sides in Model 1).

Since the nets were not meshed (but represented as porous media), the effects of the real twines on the turbulence could not be simulated. That is why the turbulent coefficients have been fixed uniformly at the inlet boundary (i.e. in the incoming flow) thanks to the formula defined in Section 1.3.1 . These coefficients depend on the properties of

the nets used in Lilletanken.

Solvers

The *pimpleFoam* solver, based and the PIMPLE algorithm, has been used to solve the monophase problems (i.e. Model 1 and 2). It is a merger between the PISO algorithm (developed for unsteady incompressible flows), and the SIMPLE algorithm (more adapted for steady flows). The pressure, and then the velocity are solved at each time step.

The multiphase flow considered in the Model 3 has been treated with the solver *interFoam*. This solver integrate the equation of α (Equation 1.14, presented in Section 1.3.1), which is completed with a corrective term assuring the boundness of the volume fraction of water (and solved thanks to the MULES solver).
The inital volume of water (Model 3) was defined in a *setFields* based on the cells' definition made in the *blockMeshDict* file.

Porous media were modeled thanks to the *fvOptions* OpenFoam utility, in which the porous coefficients of the Dracy Forchheimer equation were defined. The porous volume was defined separately (*sellCellDict* file).

Courant number

The stability of the explicit numerical schemes used by openFoam to solve the RANS equations is dependent on the Courant number. This parameter translates the fact that the flow should not go faster than $\dfrac{\Delta x}{\Delta t}$ where Δx is the mesh size and Δt the time step, otherwise information will be lost.
Thus the maximum value reached by this number should not be higher than 1:

$$Co_{max} = \frac{u_{max}\Delta t}{\Delta x} \tag{3.1}$$

Adjustable time steps calculated from this number were used to reduce the computational time.
The condition $Co_{max} < 0.7$ was imposed for the Model 3 in order to catch the free surface elevation with more accuracy.

Numerical wave probes

Numerical wave probes were created in a *sampleDict* file for Model 3 to compare the experimental and numerical wave elevations. Five vertical lines were placed at the same distances of the net as the experimental wave probes (WP1 to WP5, cf. Figure 2.4 in Section 2). 100 points have been defined on each probe, and the value of α was

recorded for every of these points.

A short C++ code was then written to interpolate (at the 1st order) the free surface from these values. Since this surface was observed to be quite smooth in paraView, no significant errors are expected from these calculations, but they could be improved by increasing the number of recorded points, or the order of the interpolation.

3.3   Mesh convergence study

The objectives of this study were to find the mesh leading to the best compromise between accurate results and reasonable computational times. Thus the drag forces have been calculated for the three models, and compared for different sizes of meshes. All the simulations have been performed on my personal computer when no other program was running, the duration of the simulations have been recorded through the OpenFoam variable *clocktime*.

The conditions of the tests made on the net S2 have been taking account to define the dimensions of the net. The Ergun formulation has been used to calculate quickly the Fochheimer coefficients (acting in the porous media) from the measured solidity ratio ($S_N = 0.202$). The velocity has been fixed to $1\,m/s$ for every simulations.

3.3.1   Meshing

The three meshes constituted in rectilinear grids, not uniformly distributed. The meshes have been chosen thinner near the net, and more cells have been defined in the block behind the porous panel, where the wake was formed.
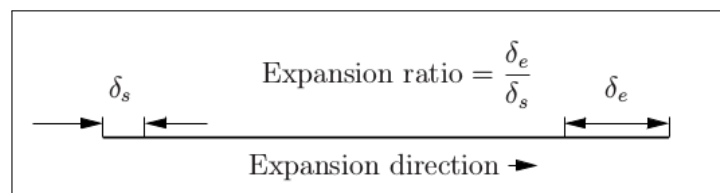
Figure 3.2: *Expansion ratio definition, OpenFoam UserGuide 2016. δ_s: start cell, δ_e: last cell of the same block in the same direction.*

Thus 2 expansion ratios, as defined Figure 3.2, have been imposed in both directions to increase the number of cells around the net, and in the wake, where the flow is more turbulent and needs to be solved more precisely.

An example of the importance of this work is given Figure 3.3: the images 3.3a and 3.3b show the exact same mesh, respectively without and with an expansion ratio.

It can be seen on the first picture that an undesired turbulent wake appears near the net's edges because the cells are too large to catch the flow, leading to oscillating time series of forces. On the contrary, defining appropriate expansion ratios leads to a more realistic flow, as shown on the second picture. Hence this third picture (3.3c) has even a lower total number of cells (reducing the computational time), but a bigger number of cells in the areas of interest, leading to better results than 3.3a.
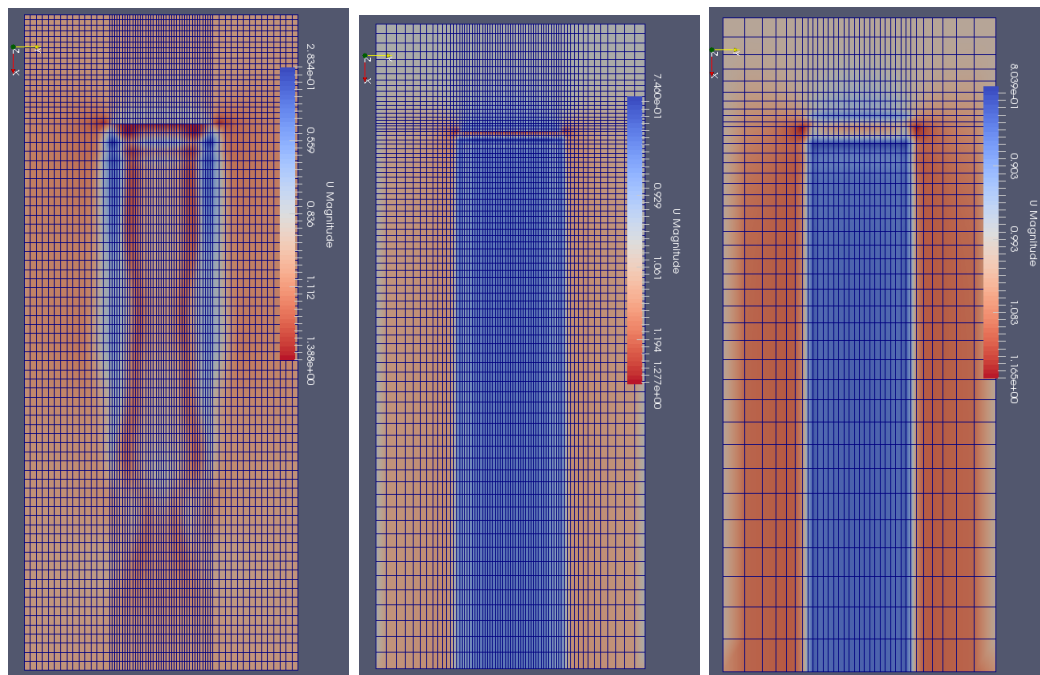
(a) $dx = 8.3cm$ without cell expansions   **(b)** $dx = 8.3cm$ **(c)** $dx = 16.7cm$

Figure 3.3: *Model 1 on ParaView - Defining appropriate expansion ratios.*

To achieve this convergence study, the total number of cells have been gradually increased, but their disposition has not been changed, i.e. the distribution of cells in the domain has not been modified proportionally to the total number of cells. More details about the meshes can be found in Appendix B.1 .

In order to have an estimation of their different refinements, they have been characterized in this report by the mean size of cell dx in the wake in the x-direction.

Five sizes of mesh have been studied for each models presented Section 3.2 , except for Model 3 for which 4 sizes were tested. The results are presented below.

The net thickness was very small compared to the dimensions of the domain (few millimetres against few meters), and has been much more discretized, with 1 cell in the x-direction for the coarsest mesh, 12 cells for the thinnest one.

3.3.2   Results

Time series of the drag forces can be found in Appendix B.1 . It can be seen that the forces are all decreasing drastically from t=0s, and start to converge just before t=1s. The velocity of the flow was put to $1\,m/s$ in the whole domain at t=0s, this transient phase corresponds to the time needed by the flow to reach its steady state form. Since it has been observed that the curves were in fact slightly decreasing until t=3s, the mean forces have been calculated from t=3s to t=6s (end of the simulation).

(a) *Porous drag force.*   **(b)** *Computational time.*
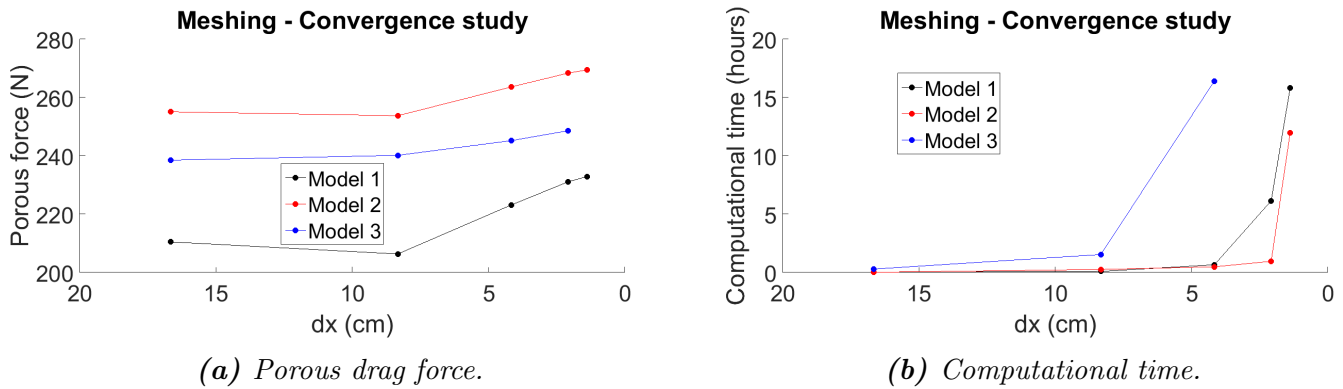
Figure 3.4:   *Results of the mesh convergence study for the three models.*

Figure 3.4 shows the results of the mesh convergence study. For the model 1 and 2, the two thinnest meshes led to very high computational times (from 1 to 17 hours). Therefore, the third size tested has be retained ($dx = 4.2cm$). The convergence is not reached for this mesh, leading for Model 1 to approximately 4.3% of errors compared to the values obtained for the thinnest discretization ($dx = 1.4cm$).

The time series of the third model (including the free surface) were much longer to converge, and have been run over 60s. The loads oscillate strongly at the beginning of the time series, and slightly from t=25s. The mean values of F_x were then calculated over the last 20s.
The simulation of the thinnest mesh of the third model was stopped after running during 25 hours, and is not plotted in the graphic. The coarsest mesh has been chosen for this model ($dx = 16.7cm$), with approximately 4.1% of errors compared to the thinnest discretization ($dx = 2.1cm$).

Comment

The experimental values corresponding to the loads found during this convergence study was around 170N. All these simulations, based on the Ergun porous model, led to forces about 50% higher. Because of these unrealistic results (also confirmed in Figure B.5 and B.6 in Appendix B.1), the Ergun porous model has not been studied in more details.

4 | Results

The results of both the experiments and CFD simulations are presented in this section. The drag forces F_x are analyzed for the different environmental conditions imposed in Lilletanken.
The totality of the experimental results can be found in Appendix C.

This presentation has been divided as follow for greater clarity:

1. At first the behaviour of the flow around, and in the wake, of the panels will described for steady currents. Few pictures will be shown to understand the physical phenomena met during the experiments.

2. Then, the experimental results of the tests achieved for steady currents will be presented. They are the main outcome of this work, so several aspects will be discussed, as forces acting on the frames, or the uncertainties met when doing repetitive tests. The drag loads will then be analysed by focusing on the solidity ratio.

3. The numerical drag forces obtained from the CFD simulations for steady currents will then been compared to the analytic and experimental loads.

4. The experimental loads and their harmonics will be described for the wave periods tested when the carriage was fixed.

5. Finally, the experimental drag forces will be considered for the tests in waves and currents, i.e. when the carriage was running in front of incoming waves.

All the loads (3 forces and 3 moments) were recorded during the tests achieved in Lilletanken. Most of them (as F_y, M_x and M_z) did not presented any peculiarity, and stayed close to 0N (0N.m for the moments) because of the symmetry of the experimental installation.
Furthermore, all the data could not be treated because of the technical problems met during the experiments (too strong VIV of the wave probes, defective wave maker, etc.), which led to erroneous records (or no records at all).

This section will be concluded by a discussion on the errors and uncertainties encountered during this thesis.

4.1 Wave elevation in steady currents

Few photos and videos were taken from under the carriage during the tests in steady currents to characterize the phenomena occurring in the wake, like the waves created behind the nets. In addition, the wave elevation was measured from the wave probes at different location (cf Figure 2.4).

The main observations resulting from these data will be enunciated in this section. A focus will be done on the consequences of the water elevation on the net panels.

4.1.1 Main observations

The wake's profile was very dependent on the current velocity, as shown in Figure 4.3. The flow was strongly accelerated when crossing the net, and an hydraulic jump[7] was observed behind the net, from few centimeters (low U_0) to few dozens of centimeters behind (high U_0). The wake was fully turbulent, and large eddies could be seen.

An example of wave elevation measured from the wave probes (both numerical and experimental) is given in Figure 4.1 for $U_0 = 1.5 m/s$. It is observed that:

- The water rises in front of the net. Both experimental and numerical WPs recorded a approximately 2cm elevation at 30cm of the panel.

- The values are positive or negative whether the probe was in the trough or crest of the wave.

- Numerical and experimental values have the same order of magnitude in amplitude. WP3 is an exception: this probe was placed behind the frame (which is not included in the CFD model).

4.1.2 Water elevation on the panels

The level of water on the net was rising during the tests as shown in Figure 4.2 and 4.3. This level seemed to depend on the width of the panels, but also their solidity ratio. It has an direct impact on the loads since the wet area on which the forces were acting increased.
For the net presented in Figure 4.2, the height of the water elevation has been estimated roughly to 11cm by counting the number of meshes on the picture. It represents then a raise of 12.7% of the wet area for this velocity ($U_0 = 1.2 m/s$).
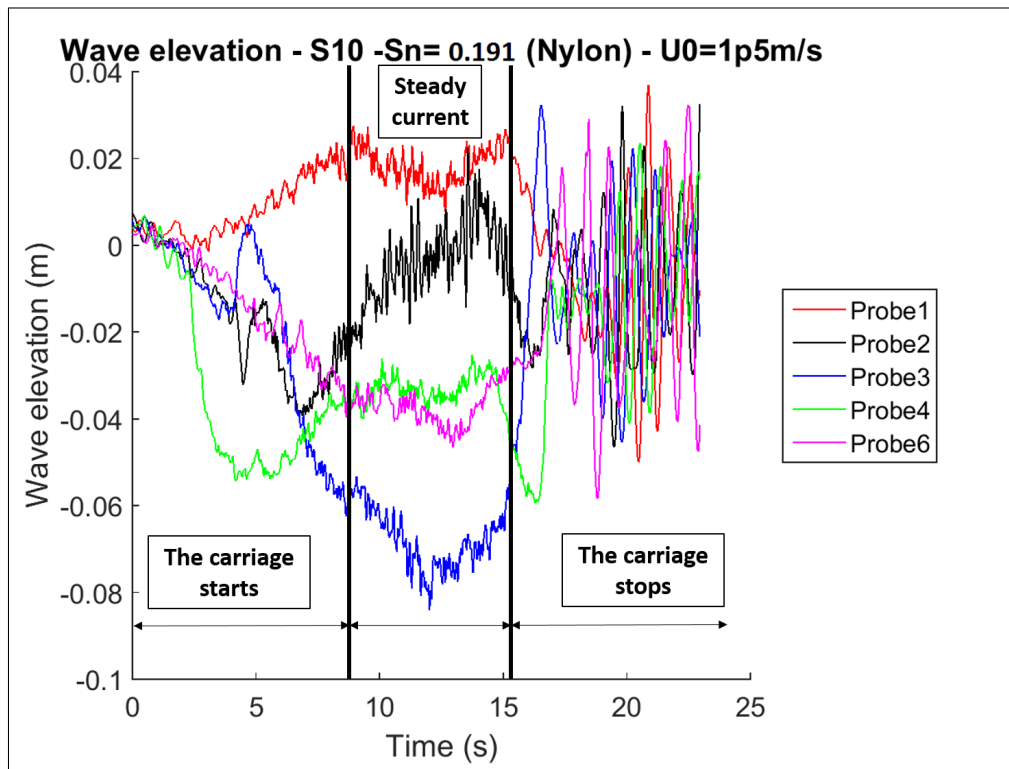
(a) *Measured wave amplitudes. Net S10 (Nylon, $S_N = 0.191$), $U_0 = 1.5m/s$.*
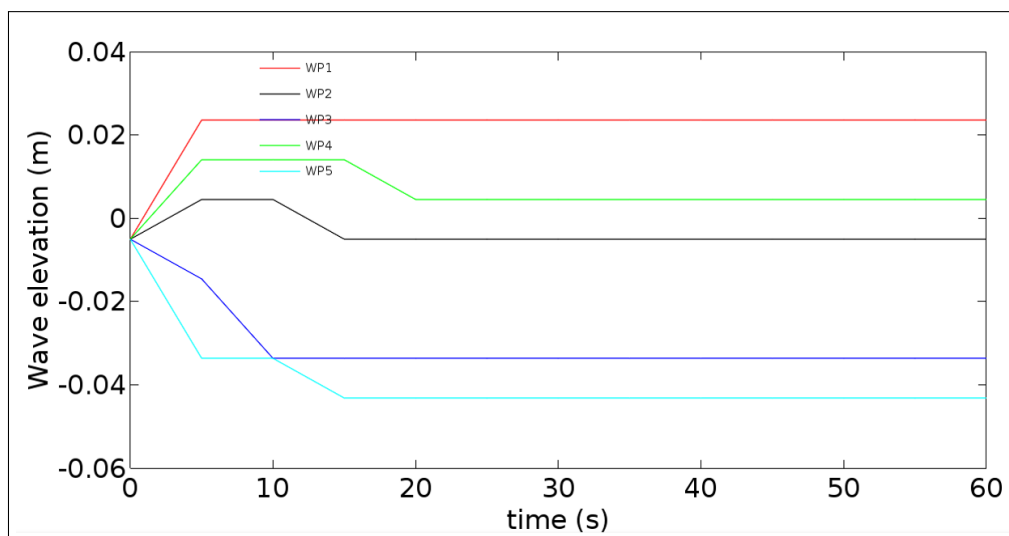
(b) *Numerical wave amplitudes. $S_N = 0.202$ and $U_0 = 1.5m/s$.*

Figure 4.1: *Experimental and numerical wave elevations. To the left: experimental measurments taken fom the wave probe in front of the panels (WP1). To the right: numerical recording of waves in the same conditions (Model 3).*

(a) *At rest.*

(b) $U_0 = 1.2m/s$.

Figure 4.2: *Free surface elevation. Pictures taken on the net L6 (HDPE), $S_N = 0.227$. Lilletanken, February 2017.*
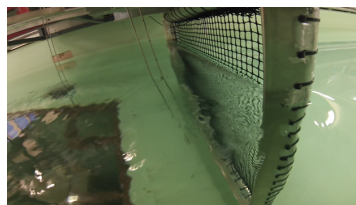
(a) $U_0 = 0.3m/s$.   **(b)** $U_0 = 0.4m/s$.   **(c)** $U_0 = 0.5m/s$.
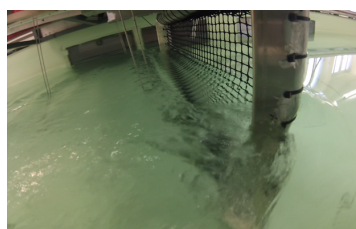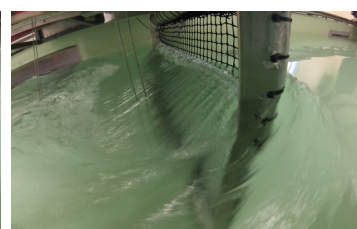
(d) $U_0 = 0.6m/s$.   **(e)** $U_0 = 0.8m/s$.   **(f)** $U_0 = 1.0m/s$.

(g) $U_0 = 1.2m/s$.   **(h)** $U_0 = 1.4m/s$.   **(i)** $U_0 = 1.5m/s$.

Figure 4.3: *Pictures taken during the experiments on the same net S2 ($S_N = 0.202$, $d_w = 1.9$) for different velocities and from different views. Lilletanken, January 2017.*

4.2 Experimental results - Currents

The experimental results of the tests made over several carriage velocities (without any waves) are presented first in this section. Several phenomena will be successively discussed:

1. The loads acting on the empty frame. They were always measured in addition of the loads acting on the nets, and needed to be determined the most accurately as possible.

2. The variations of the forces applied on one net panel over many repetitive tests. They have been studied to characterize the uncertainty of the measurements.

3. Typical results, emphasizing on the influence of the solidity ratio. They will be discussed through representative examples.

4. The vertical loads acting on the nets subjected to currents. A brief discussion about the forces in the other directions.

5. The comparison between the drag coefficients obtained for the $1m \times 1m$ and the corresponding $2.5m \times 1m$ net panels.

The totality of the results can be found in Appendix C.1 .

4.2.1 Forces acting on the empty frames

For all the different tests achieved in Lilletanken with the net panels, the same tests have been made for the empty frames (both sizes) in view to subtract the forces acting on the frames alone from the loads measured on the net panels fixed with strips on these frames.

For the $1m \times 1m$ empty frame, two sets of tests have been carried out:

- without the strips.

- with the maximal number of strips that it was possible to attach.

The objective was to characterize the influence of the strips.

The results are presented in Figure 4.4. The presence of the strips lower the loads acting on the empty frame, until a maximum difference of 13.9% between the two curves for the highest carriage velocity ($U_0 = 1.5m/s$).

The strips probably caused turbulent boundary layers along the frame. Considering an horizontal cross-section of the frame, the separation of the flow, and especially its
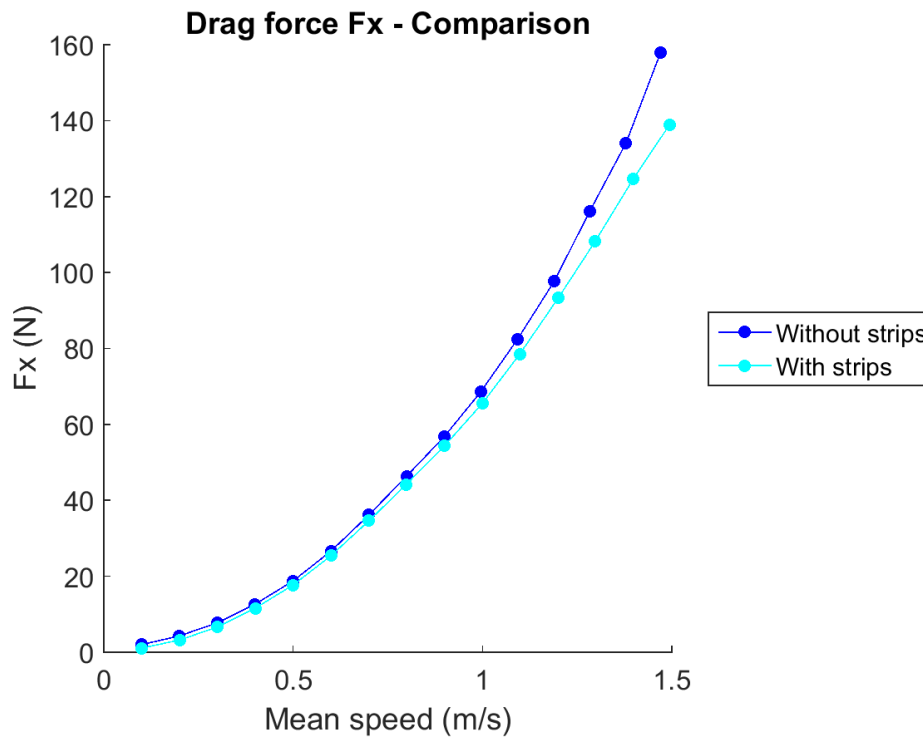
Figure 4.4: *Drag force acting on the 1m×1m frames.*

reattachment to the body (due to the turbulence) appeared then more upstream on the profile. The pressure behind the frame caused by this "soon" reattachment of the flow led to lower forces in the direction of the incoming flow. An example of this phenomenom is shown for a sphere (with and without a trip wire) in Figure A.14, in Appendix A.6 .

For the highest velocity, and considering an horizontal cross-section of the frame (without the "V" profile), the Reynolds number can be approximated as $Re = \dfrac{D\,U_0}{\nu} = \dfrac{0.025 \times 1.5}{10^{-6}} = 3.75 \times 10^4$. D is here the diameter of the cylindrical part of the frame (cf Figure A.2 in Appendix A.4). It is near the range of Re for which a drop of C_D is observed experimentally for cylindrical cross-sections, as showed in Figure 4.5 (it can be noticed that after this drop, the drag forces increase again).
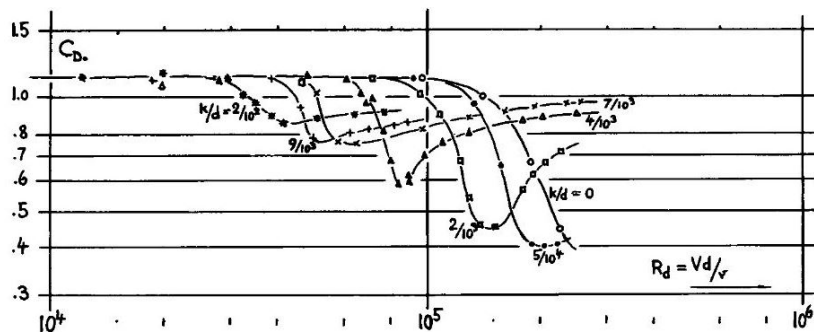
Figure 4.5: *Drag coefficient of cylinder for different surface roughness from Hoerner (1965). "k": sand-grain size, "d": diameter of the cylinders.*

The number of strips used to fix the nets was not the same for all the nets. It is also

expected that the presence of the nets themselves influence the forces on the frames. It probably led to errors when subtracting the loads obtained with the empty frames to the total forces measured in the towing tank.

4.2.2   Repetitive tests

All the velocities have been applied 6 times on the net S2 ($1m \times 1m$ net panel in nylon, $S_N = 0.202$ and $d_w = 1.9$mm). these nets are numbered from 1 to 6:

- Test 1: the net was stretched to the maximum.

- Test 2 and 3: performed one day after test 1, the nets were fully relaxed (from visual observations).

- Test 4, 5 and 6: the net has been re-stretch for these three tests. The three tests were carried out the same day, the ones after the others.

(a) *Drag coefficient C_D.*   **(b)** *Drag force F_x.*
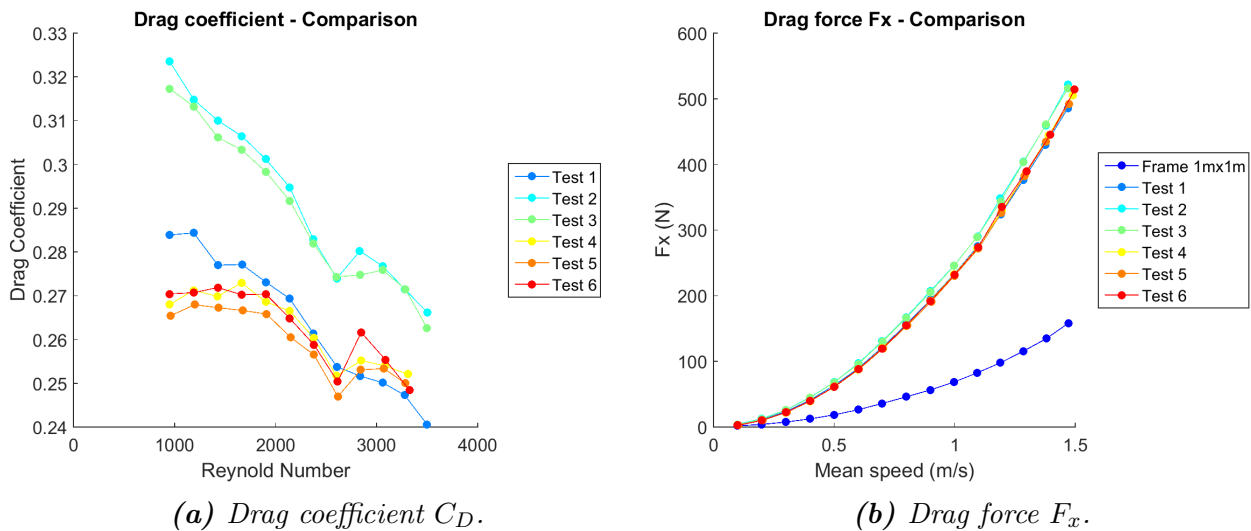
Figure 4.6: *Repetitive tests, net S2.*

The graphics observed in Figure 4.6 show that the loads measured for the tests 4, 5 and 6 do not vary more than few newtons over all the velocities. It is not true for $U_0 = 1.5m/s$ (where the gap is around 15N), but for this velocity, the selection of the time window in which the calculation of the mean force was made from the time series could have caused this variation.

The first test provides comparable results with the tests 4, 5 and 6. This could be explained by a similar stretching of the net. Indeed, before both test 1 and 4, the net was stretched by hand, the most as possible.

On the contrary, the two tests for which the net was relaxed (tests 2 and 3) present higher loads, around 5% higher in average (with a maximum of 11%) when subtracting the force of the empty frame (cf. Figure C.5 in Appendix C.1). This gap is also observed for the drag coefficient, which is in average 0.03 higher (but until 0.06 in maximum for low Re) for the relaxed net.

Thus, these repetitive tests point out the uncertainties in the measurements met when performing the drag tests in the towing tank. The post-treatment of the data may have participated to these uncertainties, but most of the variations observed in the loads (i.e. in the "raw" time series, cf. Figure 4.7) seemed mainly due to the stretching of the net, and dependent on the velocities. Indeed if the relative differences between the tests are higher for high velocities when looking at the drag forces, they are more important for low Re (corresponding to the low velocities) when looking the drag coefficient (the variation in force are then "amplified" by the division by U_0).
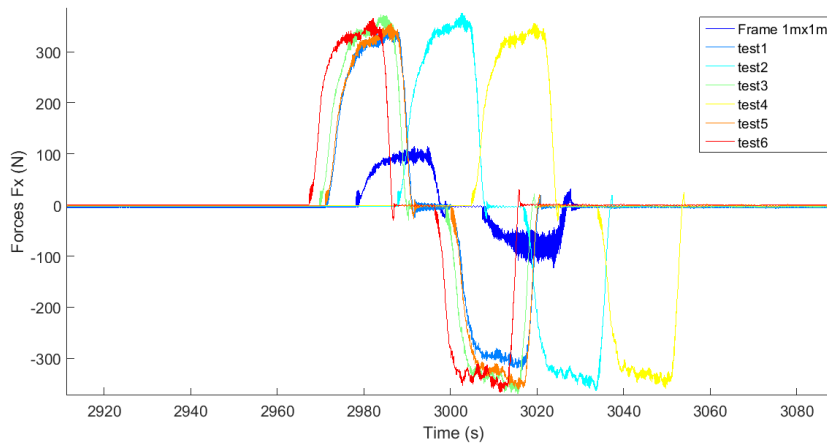
Figure 4.7: *Time series of the drag forces acting on the net S2 for the carriage velocity $U_0 = 1.2m/s$ (repetitive tests).*

4.2.3   Drag force - Main results

The drag force of the $2.5m \times 1m$ panels are described in this section. The results are presented with the solidity ratios obtained from both the photos and the Equation 2.1 to compare the two methods.

Analog results were found for the $1m \times 1m$ net panels, they are presented in Appendix C.1 .

The total drag forces measured for the large nets, including the frame, are presented in Figure 4.8. The results for the first S_N (i.e. from the photos) are surprising: some nets present higher loads than others even if they have a lower solidity ratio. It is all the more unexpected that it happens for comparable net panels, like L6 and L4 (HDPE), or L2 and L3 (Nylon).

On the contrary, the curves obtained with the second S_N are more easily understandable: higher solidity ratios leading to higher loads. L4 seems to be an exception: even if its solidity ratio is lower than for L3, the drag forces are slightly higher. It could be explained by the difference of material (HDPE for L4, Nylon for L3).

Thus, it seems that the S_N determined on Matlab from the pictures are not as accurate as the calculated ones. The fact that they are in average higher than the calculated ones could come from the impurities and shadows on the walls behind which the nets were photographed.

(a) F_X - S_N from photos.

(b) F_X - S_N from Equation 2.1.
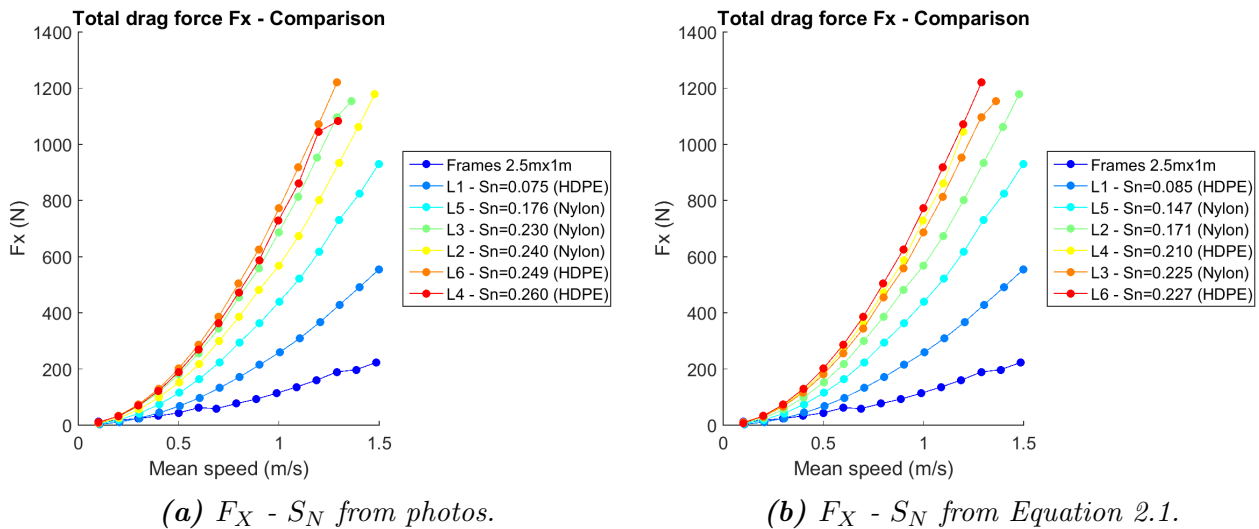
Figure 4.8: *Total drag force - 2.5m×1m net panels.*

(a) C_D - S_N from photos.

(b) C_D - S_N from Equation 2.1.
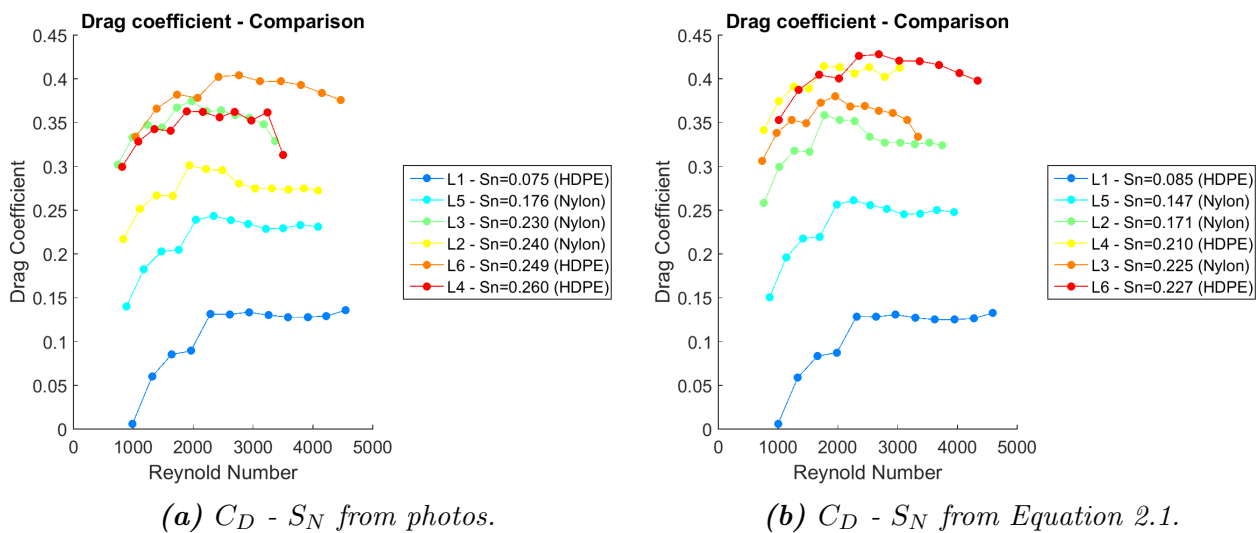
Figure 4.9: *Drag coefficients - 2.5m×1m net panels.*

The drag coefficients shown in Figure 4.9 seem to confirm that the second S_N provide better results: HDPE nets leading to slightly higher C_D than nylon nets, and generally, higher S_N leading to higher drag coefficients.

For low velocities, the errors are higher relatively to the force magnitudes, and are amplified when dividing by U_0^2 in the calculation of C_D. It could explain why some values seem abnormally low, it is then difficult to conclude about these values.
From $Re = 2300$, the drag coefficients stay approximately constant, slightly decreasing, and cover a large range of values over all the nets, from 0.14 for the extremely low $S_N = 0.085$ to 0.44 for the highest S_N of the HDPE net.

4.2.4 Discussion of forces in other directions

In addition to the drag forces in the x-direction presented above, the forces and moments along the other axis were recorded during the experiments (as defined in

Figure 1.6, Section 1.3.3). Few of them were post-treated (similarly to Fx) and are discussed below.

(a) *Vertical force F_z.*

(b) *Moment M_y around the transverse axis y.*
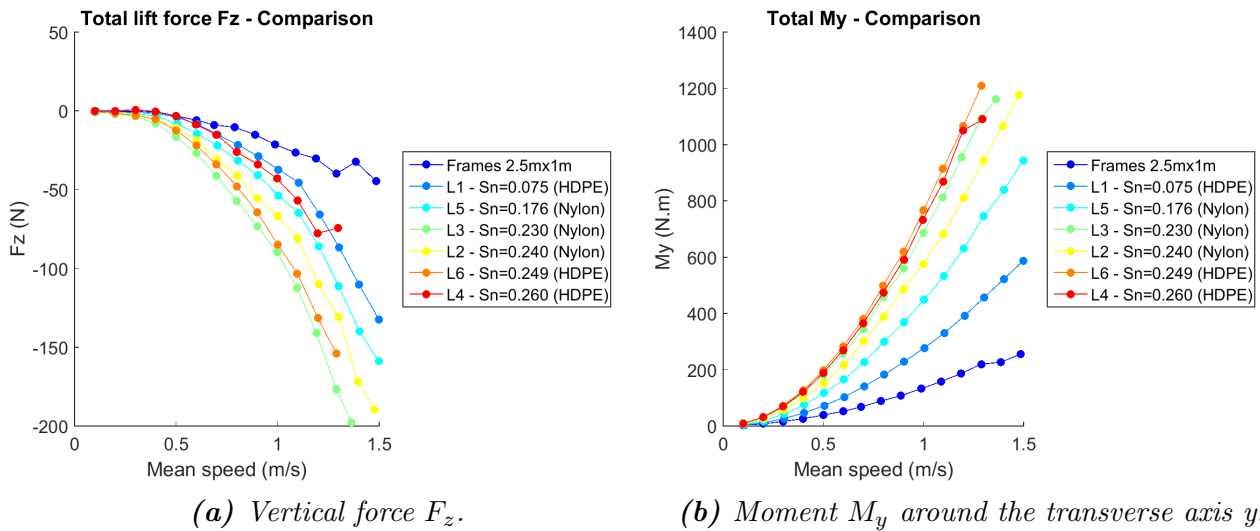
Figure 4.10: F_z and M_y for the $2.5m \times 1m$ net panels, where S_N comes from the Equation 2.1.

The vertical forces acting on the large net panels shown in Figure 4.10a are negative, and decrease with U_0. It could be explained by the fact that the flow can circulate under the bottom bar of the frame, but is "blocked" by the net above. Thus, the pressure should be higher above this bar, and the vertical force oriented downward. This phenomenon could be accentuated by the speed-up of the flow below the bottom bar, caused by the small distance between the frame and the bottom of the towing tank (around 10cm).

Lift coefficients have been calculated (presented in Appendix). They present strange behavior for low velocities (as for C_D), and are globally very low: $|C_L|$ stay below 0.06 as soon as Re exceeds 2000 for all the nets.

The F_y force should be equal to 0N due to the symmetry of the installation relatively to the plan (xOz). It was not the case in reality (cf. Figure C.4 in Appendix C.1): the values tended to be negative (reaching 35N for $U_0 = 1.5m/s$), maybe because of an inaccurate positioning of the panels along the y-axis when fixing them to the carriage.

The moments M_y around the transverse axis y are presented in Figure 4.10b. These moments are significant because the forces were measured from the carriage, i.e. from the top of the frame, while the drag forces acted in the bottom part of the frames. Thus, the comparison to the different solidity ratios lead to the same conclusion as for the drag forces: higher S_N seem to provide higher M_y, and for equivalent solidity ratios, HDPE nets tend to provide higher moments than nylon nets.

4.2.5 Influence of the panel widths on the drag coefficient

Is this section, the influence of the width of the panels has been investigated. The drag coefficients of the same nets are compared for two sizes ($1m \times 1m$ and $2.5m \times 1m$) in Figure 4.11.
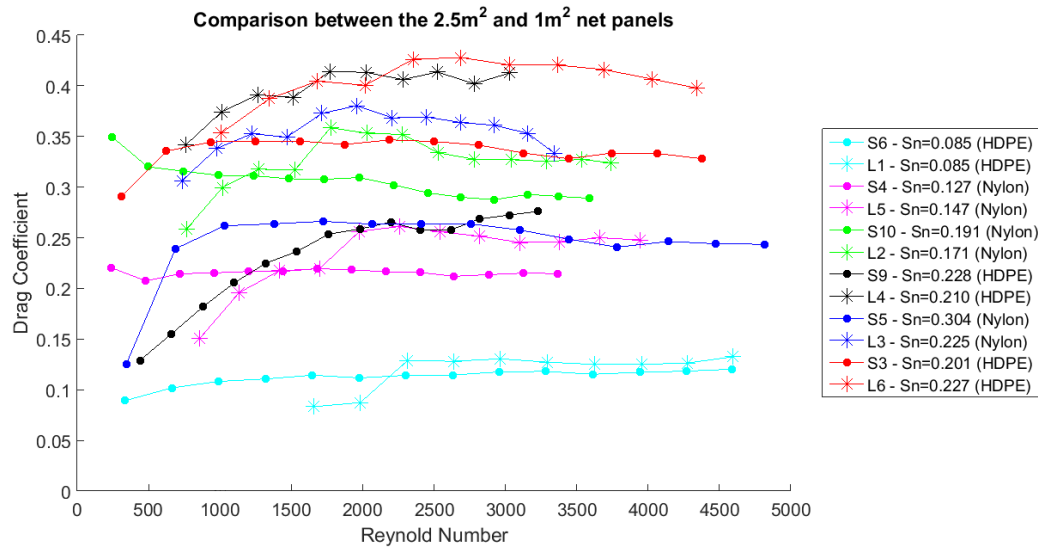
Figure 4.11: *Drag coefficients of the corresponding* $1m \times 1m$ *and* $2.5m \times 1m$ *net panels.*

It turns out that the large net panels provided higher C_D than the $1m \times 1m$ nets. Some curves are matching well (as L6 nd S3), but other presents very large variations (as S9 and L4). Several effects could have cause these differences. At first, the stretching of the nets, done manually, and not identical for the small and large versions of the same nets.
Secondly, it clearly emphasizes the importance of the set-up:

- The speed-up of the flow between the $2.5m \times 1m$ frame and the side walls was probably higher than for the small frames. Furthermore, the acceleration of the flow caused by the bar in the middle probably participated to increase the loads.

- The water elevation just in front of the nets seemed to be higher for the large nets, leading to an erroneous wet area, and errors when calculating C_D.

4.3 Analytic and numerical results

Numerical simulations were run for steady currents. They are discussed in this section, and compared to the analytic and experimental results.
The theoretical (or analytic) forces refer to the direct calculations of the loads made from the Equation 1.38 saw previously.

4.3.1 Discussion on the numerical porous models

Several numerical models were tested for the same cases (i.e. same nets and current velocities). They have been created to discuss both the physical phenomena occurring in the numerical towing tank and the porous modeling methods used to represent the nets in OpenFoam.
Thus, two porous models were compared:

- A Morison type load model, based on the expression of the porous coefficients proposed by Chen and Christensen (2016).

- A screen type load model, based on the formula used in Kristiansen and Faltinsen (2012).

as well as three different views of the system:

- Model 1: a top view.

- Model 2: a side view of the immersed part of the panels.

- Model 3: a side view which includes the free surface elevation.

(a) *Drag force F_x.*

(b) *Drag coefficient C_D.*
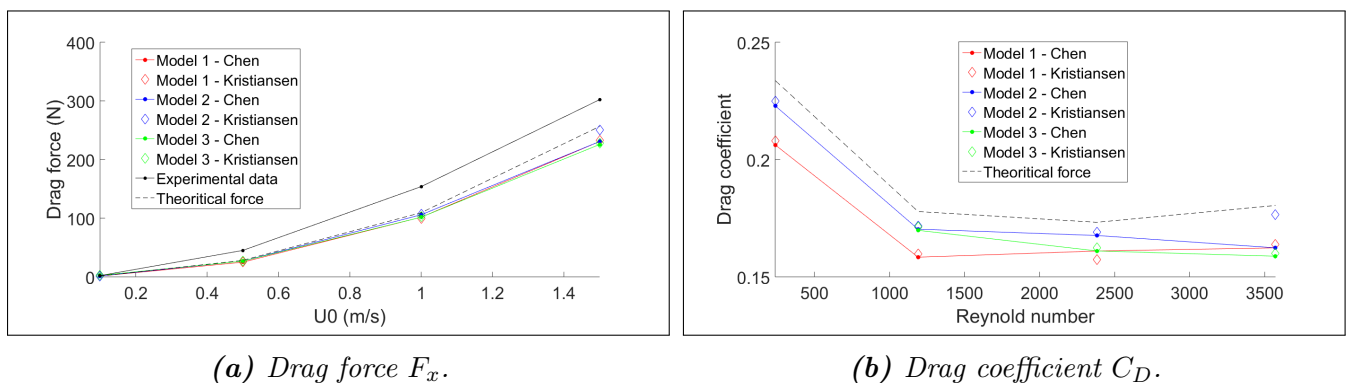
Figure 4.12: *Comparison of the porous models with the analytic and experimental forces.*
$S_N = 0.202$

Figure 4.12a compares drag loads on the same net obtained with different methods. The numerical and analytic loads are very close, and lower than the experimental ones. Figure 4.12a focus on the numerical and analytic drag coefficients in order to compare the different models. It seems that Model 3 over-predict the loads for low velocities, but tend to lower them for high Re, maybe because the high forces met in the bottom of the panels are avoided by the circulation of the flow above the nets (i.e. by the

creation of a wave). Globally, the screen type load models seem to give slightly higher loads. The Model 2 simulated with this porous model provides results very close to the theoretical ones.

Figure 4.13 shows a top view (Model 1) of the velocity magnitudes in the flow for two S_N, and for a small and large net panels. For the $1m \times 1m$ nets (low S_N), the flow can circulate freely, and the maximum velocity is much lower (1.03m/s against 1.12m/s). When S_N increases, this maximum increases of 0.25m/s for the $2.5m \times 1m$ to reach up to 1.37m/s (against 1.08m/s for the small screen).

Figure 4.14 shows the pressure in the flow (Model 3) and the velocity magnitude for a side view. The dynamic pressure observed ahead of the nets is relatively high and "push" the flow above, or below the panels. In the same case as for the top view, the maximum velocity magnitude reached up to 1.41m/s (against 1.37m/s for Model 1). When adding the free surface, the velocities reached between the net and the bottom wall are much lower (because the flow circulate above). It turned out that the length of the wave in the wake created for Model 3 were matching well with theoretical values (cf. Appendix B.3).

Conclusion

The results of the porous model proposed by Kristiansen and Faltinsen (2012) are closer to the experimental ones than the results obtained with the porous coefficients calculated from Chen and Christensen (2016). The flow circulation at the bottom of the tank and the panel seems to be predominating in the determination of the loads (cf. Model 2). The side effects caused by the different widths of the net play also an important role in the circulation of the flow.

The model which includes a free surface elevation gives similar results to the two other models, but should probably integrate the part of the net in the air to obtain a more realistic pressure profile to the top of the panels.

4.3.2 Numerical drag forces

The frames have not been modeled in OpenFoam. However, their influence on the drag force appeared to be consequent.

The speed-up of the flow along the bars of the frames was evaluated analytically. Theoretical loads calculated in Matlab are first presented below with and without this speed-up, and compared to the experimental forces.
Then CFD results will be compared to the experimental ones for two different solidity ratios.
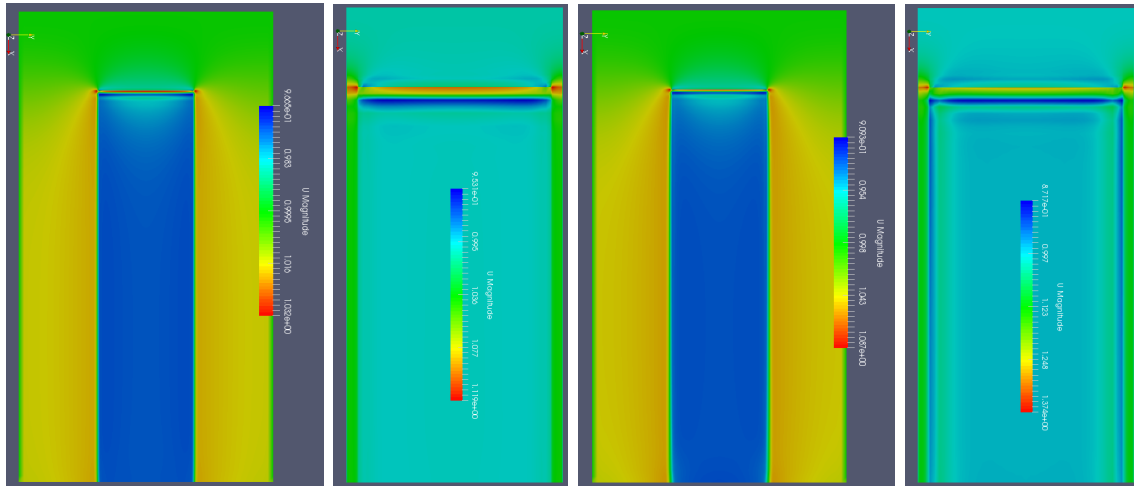
(a) $1m \times 1m$ net, $S_N = $ 0.085. **(b)** $2.5m \times 1m$ net, $S_N = 0.085$. **(c)** $1m \times 1m$ net, $S_N = $ 0.201. **(d)** $2.5m \times 1m$ net, $S_N = 0.227$.

Figure 4.13: *Model 1 (top view), comparison between two widths for a low and high solidity ratios.* $U_0 = 1m/s$
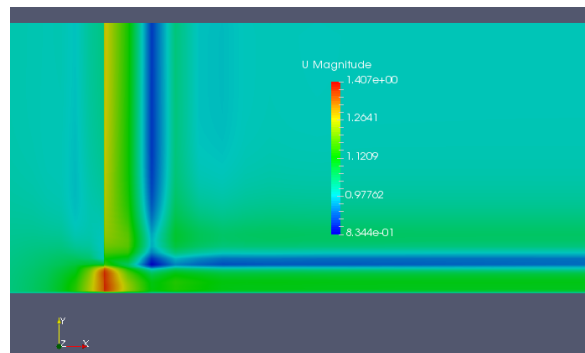
(a) *Model 2 (side view) - Velocity magnitude,* $U_0 = 1m/s$.
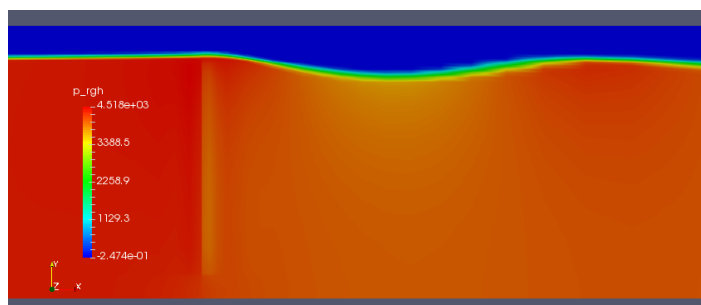
(b) *Model 3 (side view with free surface) - Dynamic pressure,* $U_0 = 1.5m/s$.

Figure 4.14: *Side view with and without free surface, observation of the velocity magnitude and the dynamic pressure for* $S_N = 0.227$.

Speed-up

Figure 4.15 shows theoretical forces, calculated considering both the incoming flow U_0 and the incoming flow $U(y,z)$ accelerated by the frames. They are compared to experimental results for which the loads acting on the empty frames were subtracted, and three solidity ratios are considered.

The experimental forces are much higher than the theoretical ones, independently of S_N, and this difference increase with U_0. The speed-up seems to be a significant component of the loads. For instance, for $S_N = 0.199$ and $U_0 = 1.5m/s$ (largest error), the loads measured in Lilletanken are around 26% higher. This difference is reduced to 16% when the speed-up is included.
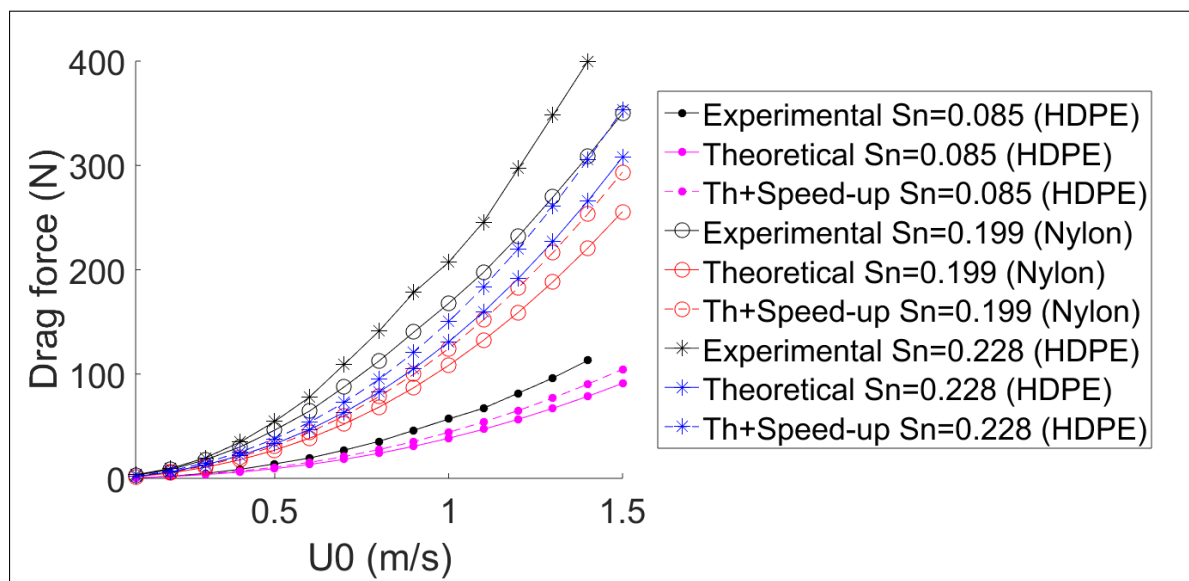
Figure 4.15: *Comparison between the theoretical and experimental loads.*

Numerical C_D

Figure 4.16 shows a comparison for to S_N between numerical (i.e. run in OpenFoam), theoretical and experimental drag forces. The CFD results were simulated with Model 2 (side view without free surface) and the second porous model (screen type load model).

Analytic and computational loads are very close, but both much lower than the experimental results (especially for the higher S_N).
This gap could probably be reduced by improving the CFD models. For example by modeling the net to the top of the domain when adding the free surface elevation (Model 3), or include the speed-up of the flow caused by the bottom wall of the tank in the analytic model.

Furthermore, some errors in the measurements of the solidity ratio, or the twine diameter which was a key parameter when calculating the Forchheimer coefficients, could have participated to increase the difference between numerical and experimental forces.
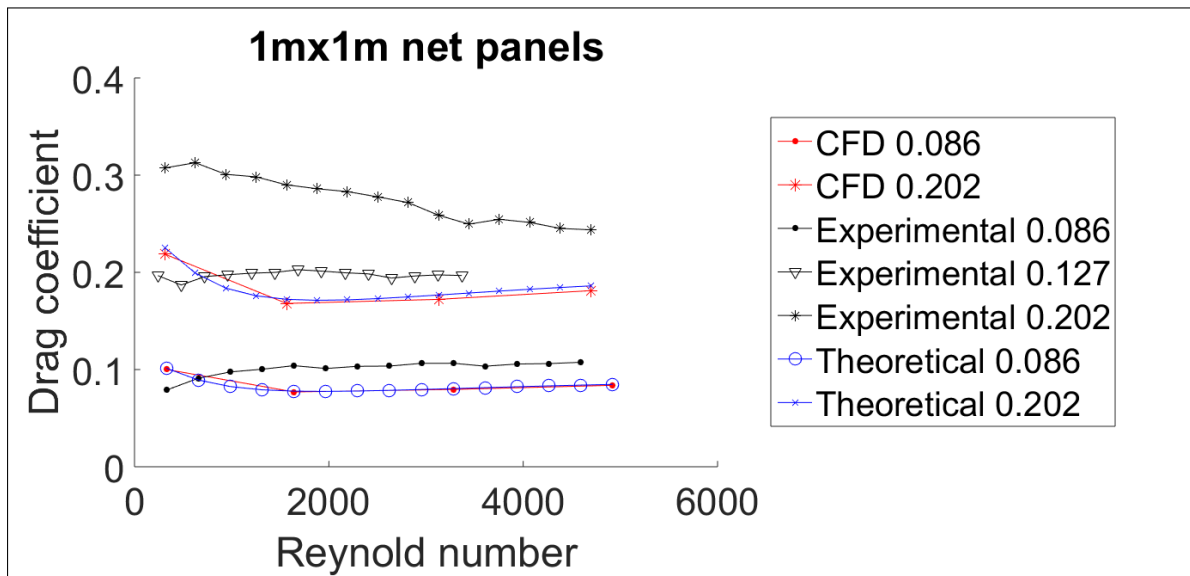
Figure 4.16: *Comparison between experimental and numerical drag coefficients.*

4.4 Experimental results - Waves

The results of the experimental data of the tests for which waves (fixed carriage) were generated are presented in this section. The main trends and observations are discussed below through examples, and the totality of the results is available in Appendix C.2 .

Only the **model scale** forces have been considered in this section in order to lighten the presentations. Furthermore, the solidity ratios estimated from Equation 2.1 have been used after the conclusion drawn when studying loads caused by currents. The curves presented for every net include the loads acting on the frame. All the amplitudes described for wave conditions are rest-to-crest amplitudes.

At first, a general description of the results obtained for wave conditions will be described through representative examples. In this part, a focus will be done on the influence of the wave periods on the drag forces. The results for different nets characterized by their solidity ratios will be compared for one wave steepness.
Then, a short presentation of the vertical forces acting on the nets will be done.
Finally the influence of the steepness on the force amplitudes will be analyzed more in details.

4.4.1 Main observations

In this part, typical graphics drawing the force amplitudes (and their harmonics) for several wave periods generated on the $1m \times 1m$ net panels are presented for $\epsilon_w = \dfrac{1}{40}$. The objective is to compare the results of the small nets for this unique steepness (a study of ϵ_w is achieved in a following section).

Similar comparisons could be done for the curves obtained with $\epsilon_w = \dfrac{1}{20}$ and $\epsilon_w = \dfrac{1}{60}$. The results for the large nets for all these steepness can also be found in Appendix C.2

It has been observed that the forces oscillated at the wave frequency. Only the amplitudes (rest to crest) of these oscillations are presented in this section. The mean drag forces (drift) are also presented in appendix. However, they are too low (most of the values are between 0 and 0.2N) to be discussed in details.

Verification of the wave periods

The wave periods measured from the wave probe in front of the nets (WP1) during the experiments were very faithful to the ones implemented in the control software of the wave makers. Figure 4.17 shows how they match with the predicted (or "theoretical") periods. Because of the technical problems met with the wave probes (often due to strong VIV), only three experiments (two nets and the empty frame) could be drawn

on this graphic over all the periods.
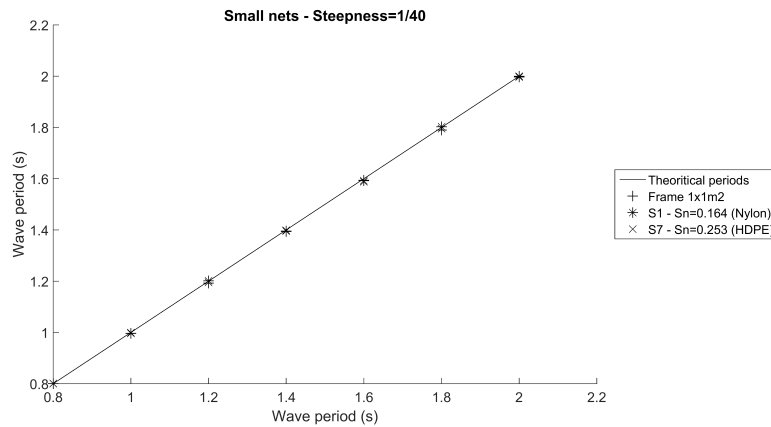
Figure 4.17: *Wave periods (WP1) of the 1m×1m net panels, compared to the theoretical periods.* $\epsilon_w = \dfrac{1}{40}$.

Force amplitude in ω
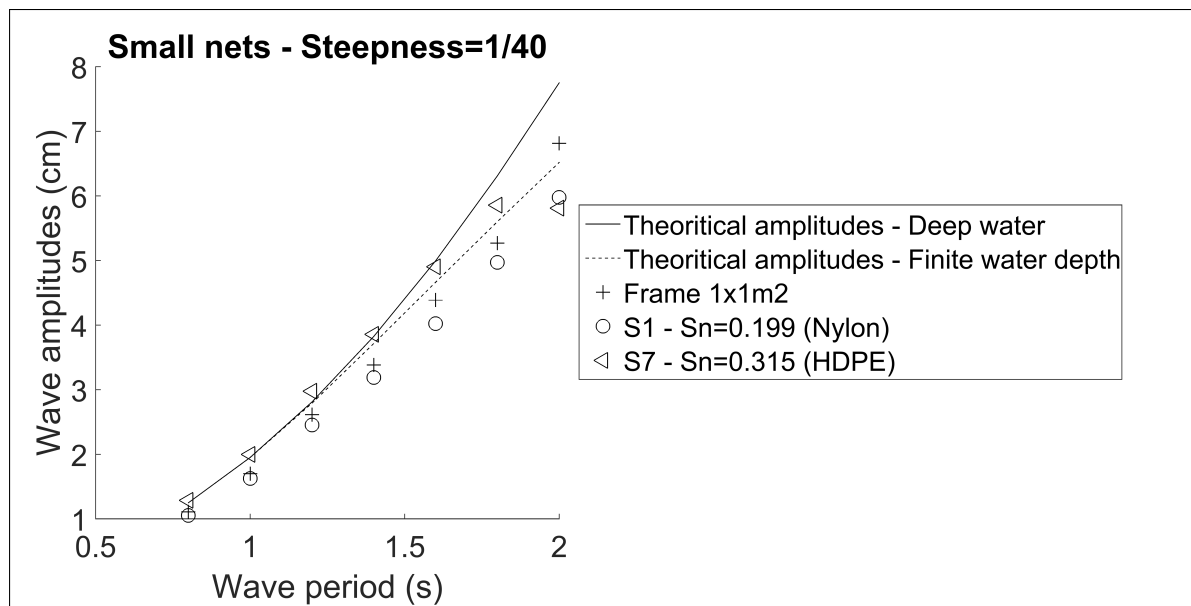
Figure 4.18: *Wave amplitude (WP1) in ω. 1m×1m net panels,* $\epsilon_w = \dfrac{1}{40}$

As for the periods, the wave amplitudes were measured from WP1 for every tests.They are compared in Figure 4.18 to the theoretical amplitudes, which were deduced from T (wave period), ϵ_w (steepness), and the dispersion relationship, with and without the deep-water assumption.

This control was sometimes useful, especially for the tests made just before that the wave maker broke, and helped to explain unexpected loads, caused by undesired waves. The points corresponding to these wrong tests have been removed. It is for example

the case for S7: the wave amplitude for $T = 2s$ is the same as for $T = 1.8s$, leading to too low loads (and so removed from the graphics).

The correspondence for the remaining points are reasonably good. The variations of ^+_-1cm of the wave amplitudes around the expected values could come from the handling of the offset. As expected, for wave periods above 1.6s, the deep-water assumption is not valid anymore.
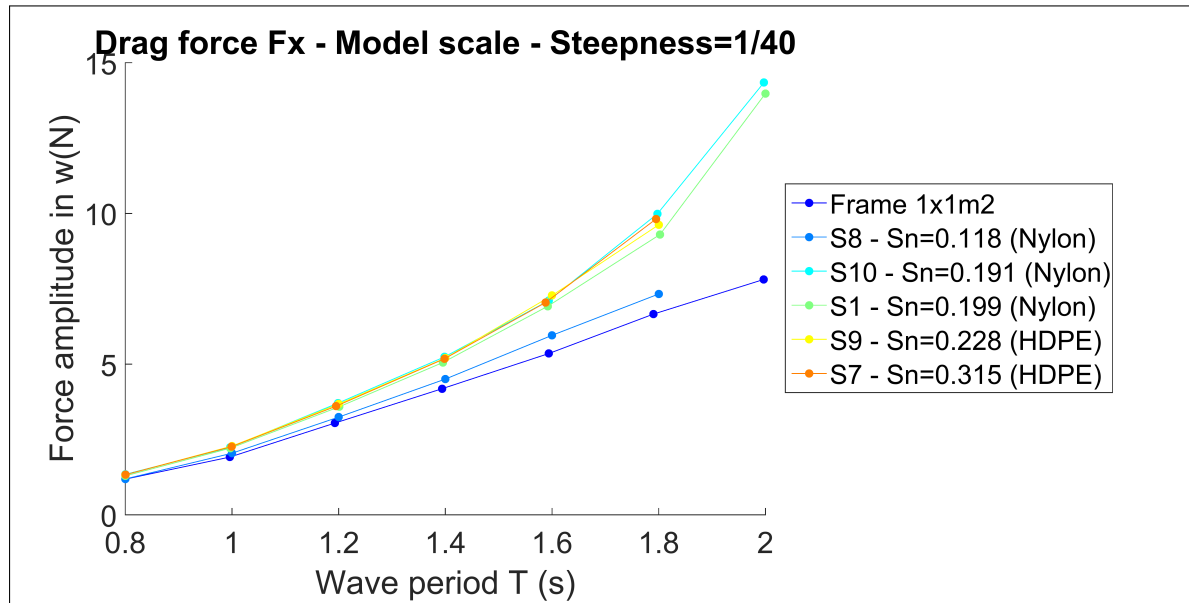
Figure 4.19: *Force amplitude in ω. 1m×1m net panels, $\epsilon_w = \dfrac{1}{40}$*

The amplitudes of the total drag forces acting on the $1m \times 1m$ net panels (including the frame) are shown in Figure 4.19. The nylon S1 and S10, with lower solidity ratios, provide higher forces than the two HDPE nets S7 and S9 (contrary to the mean loads observed in currents).
As expected, the forces increase significantly with the wave periods. The highest force observed at $T = 2s$ is about $15N/m^2$ in model scale. It corresponds to $540N/m^2$ for a period $T = 12s$ in full scale (the scale factor is $s = 36$).

Force amplitude in 2ω and 3ω

The measured wave amplitudes' harmonic in 2ω match well with the theoretical ones in Figure 4.20a, but their harmonic in 3ω are more dispersed (cf. Figure 4.21a), probably because such low amplitudes (less than 1mm) are below the level of accuracy of the wave probes.

The force responses Fx to the wave harmonics in 2 and 3ω have the same order of magnitude (cf. Figure 4.20b and 4.21b), except for the empty frame for which the3ω

(a) *Wave amplitude (WP1) in 2ω.*

(b) *Force amplitude in 2ω.*
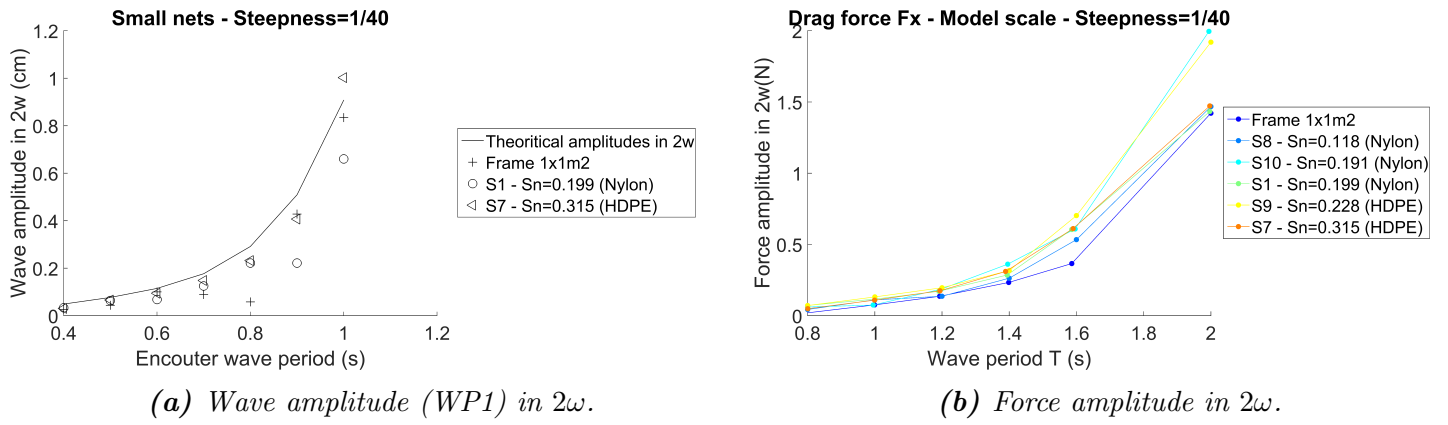
Figure 4.20: *Wave and force amplitudes in 2ω - 1m×1m net panels, $\epsilon_w = \dfrac{1}{40}$.*

(a) *Wave amplitude (WP1) in 3ω.*

(b) *Force amplitude in 3ω.*
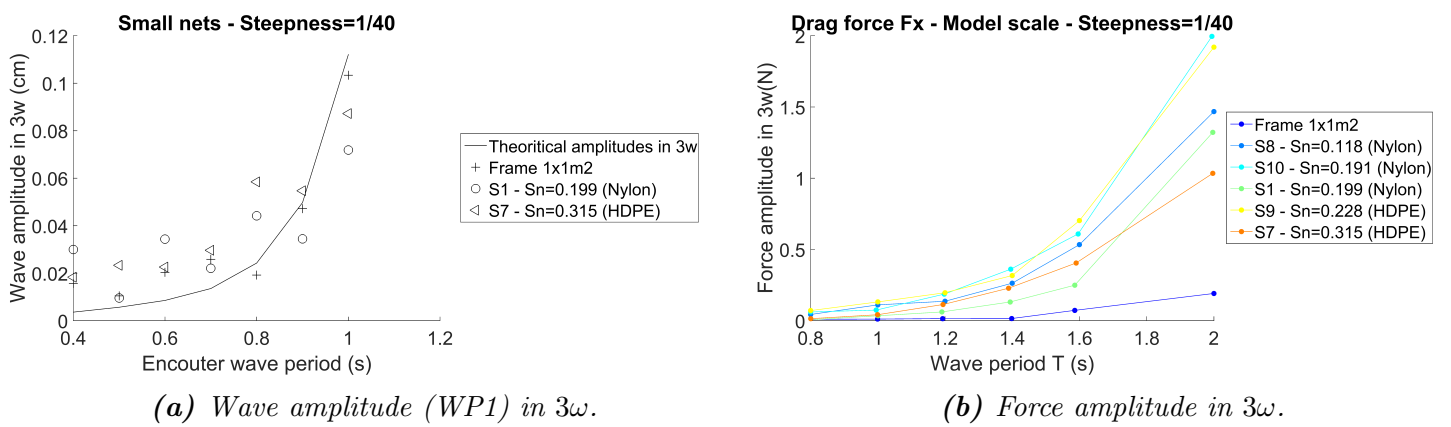
Figure 4.21: *Wave and force amplitudes in 3ω - 1m×1m net panels, $\epsilon_w = \dfrac{1}{40}$.*

component can be neglected.

The highest loads obtained for $T = 2s$ are around $2N/m^2$ ($36N/m^2$ in full scale), i.e. about 13% of the main loads' component in ω.

Vertical forces

The vertical forces acting on the 1m×1m panels for this wave steepness are shown in Figure 4.22.

They are relatively high, reaching up to $3N/m^2$ ($108N/m^2$ in full-scale), i.e. about 20% of $F_{x,\omega}$ for $T = 2s$. However, the vertical loads acting the empty frames represent a large part of these forces (more than 50%).
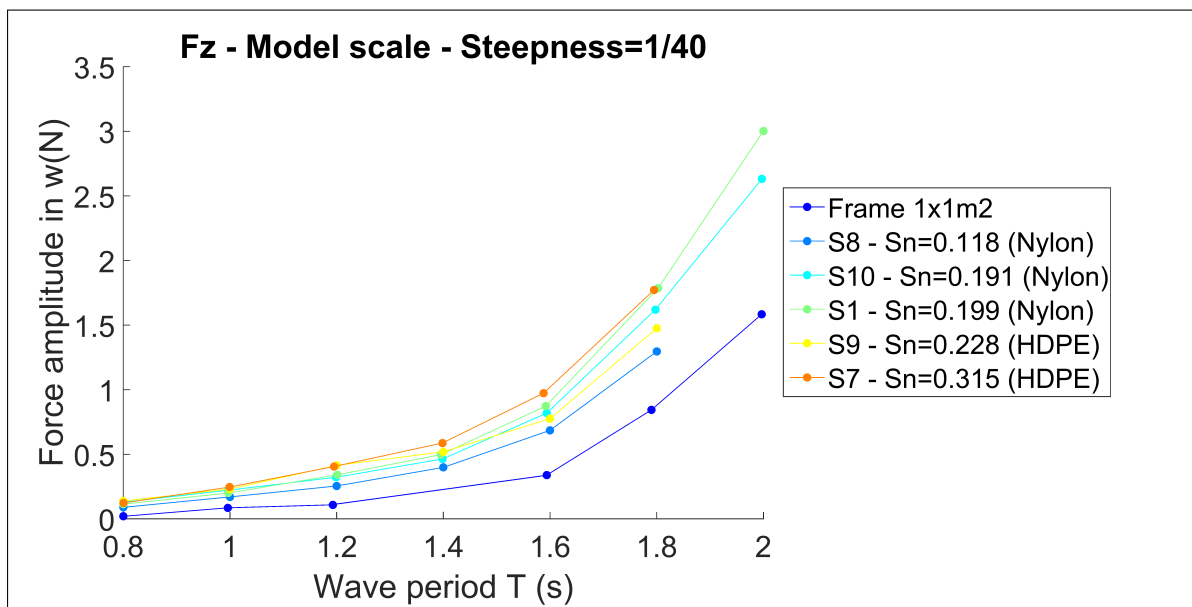
Figure 4.22: *Vertical force amplitude F_z in ω - 1m×1m net panels, $\epsilon_w = \dfrac{1}{40}$.*

4.4.2 Dependency on the steepness

The results of the loads (and their harmonics) measured for the panels S9 and L4, coming from the net (HDPE, blue), are compared below for the three steepness.
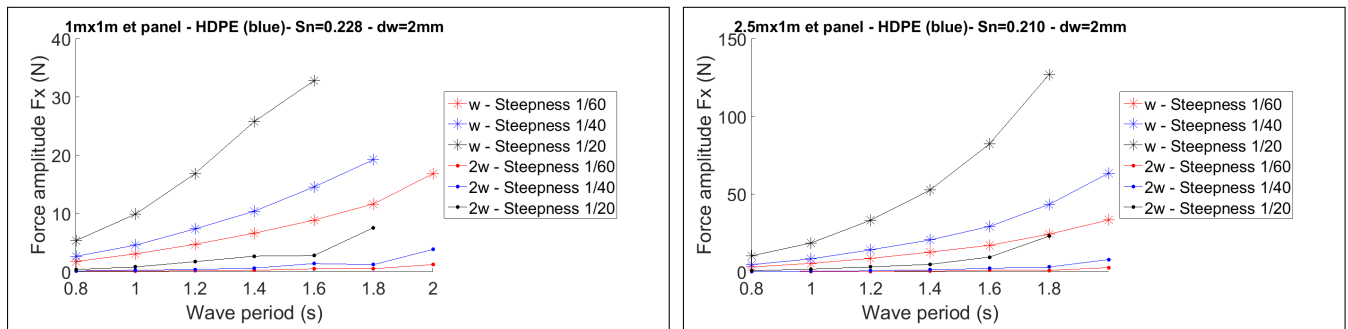
(a) *Force amplitude Fx, second and third harmonics, net S9.*

(b) *Force amplitude Fx, first and second harmonics, net L4.*

Figure 4.23: *Illustration of the influence of the wave steepness on the first and second harmonics of the force Fx for small and large net panels.*
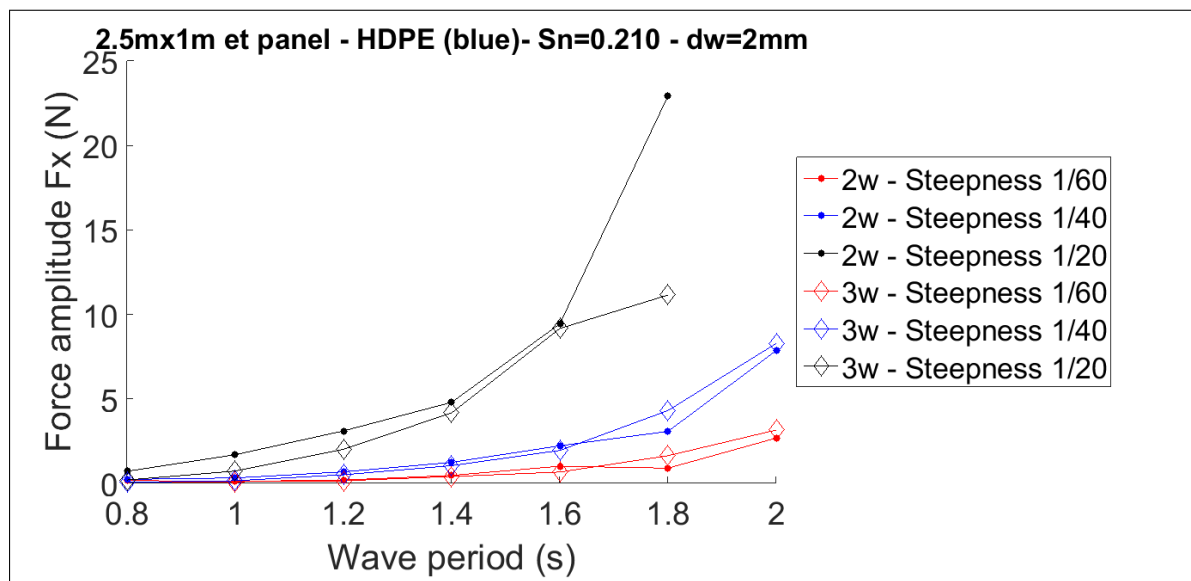
Figure 4.24: *Force amplitude Fx, second and third harmonics, net L4.*

Figure 4.23 shows the strong dependency of the force amplitude in ϵ_w. For instance, for T=1.8s, $F_{x,w}$ is multiplied by 3.5 when the steepness changes from $\dfrac{1}{40}$ to $\dfrac{1}{20}$.
The harmonics in 2 and 3ω have the same order of magnitude. As expected they increase drastically with the steepness. The second harmonic reaches up to 24N for the highest period and steepness, i.e. $360N/m^2$ in full scale (as much as the ω-component of the load for the lowest steepness at this period).

4.5   Experimental results - Waves and currents

In this section, the results of the drag tests for which the carriage was running in front of incoming waves are presented, similarly to those for which the nets were fixed and subjected to waves only (previous section). The few but important differences between these two types of experiment are reminded below:

- The drag forces are now studied and plotted against the encounter wave periods T_e (shorter than the wave periods because of the carriage's speed).

- Two steepness have been tested: $\epsilon_w = \dfrac{1}{20}$ and $\dfrac{1}{40}$.

- Two velocities of currents have been considered: $U_0 = 0.1 m/s$ and $U_0 = 0.2 m/s$. Contrary to the experiments carried out in currents, these speeds are in model-scale (leading to $U_0 = 0.6 m/s$, respectively $U_0 = 1.2 m/s$ in full-scale).

- Because of the noise made by the vibration of the installation during the run, the third harmonics of the loads were not investigated.

- The results are still discussed in model-scale to lighten the presentation. The total forces are considered (i.e. all the loads include the forces acting on the frames).

The totality of the results is presented in Appendix C.3 .

Firstly, the main trends emerging from the results will be described through representative examples. Secondly, the influence of both the wave steepness ϵ_w and the velocity U_0 will be described.
As previously the solidity ratios considered in this section, but also in appendix, were calculated (i.e. obtained from Equation 2.1), and the amplitudes are from rest-to-crest.

4.5.1   Main observations

General trends have been observed in most of the post-treated data. Particular cases, i.e. the $2.5m \times 1m$ net panels for $U_0 = 0.2m/s$ and $\epsilon_w = \dfrac{1}{20}$, are discussed below to reflect these observations.

Hence, the mean loads and the force amplitudes in ω and 2ω are described below for different wave periods. Several solidity ratios are compared, with the same conclusion: it turns out that for these three types of loads, higher S_N tends to lead to higher forces.
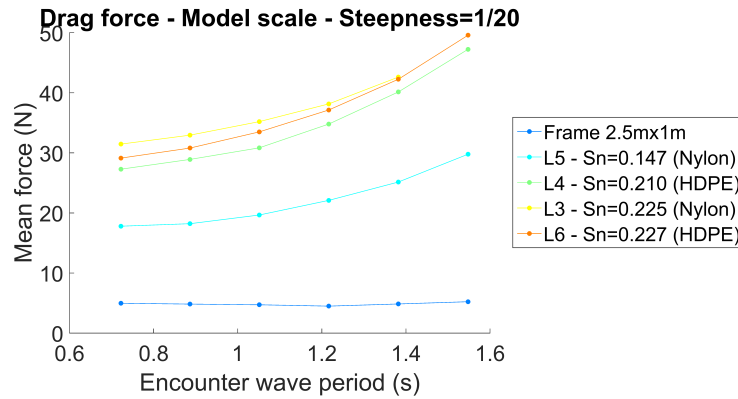
Figure 4.25: *Mean drag force - 2.5m×1m net panels, $U_0 = 0.2m/s$ and $\epsilon_w = \dfrac{1}{20}$.*

The mean forces are presented in Figure 4.25. Now that currents are added, these loads are significant, reaching 50N for the highest values (i.e. $720N/m^2$ in full-scale). The forces acting on the empty frames do not seem to be influenced by the wave periods, contrary to the net panels for which F_x increase by 40% between $T_e = 0.72s$ and $T_e = 1.64s$ for the highest S_N (L6).
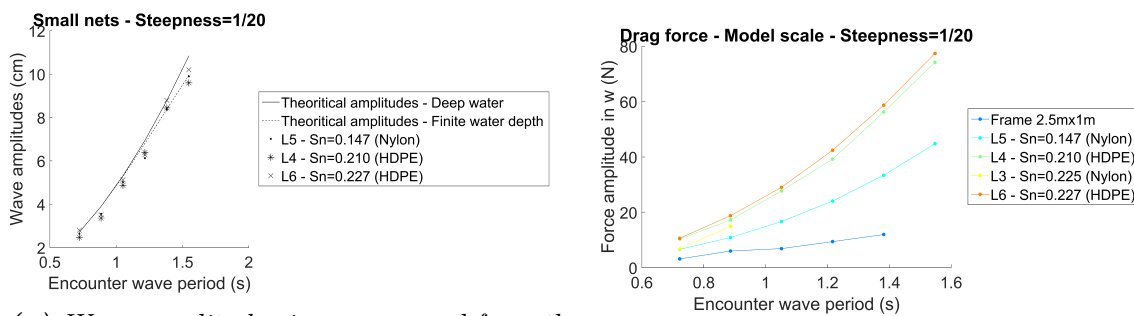
(a) *Wave amplitudes in ω measured from the carriage, in front of the net (WP1).*

(b) *Drag force amplitudes in ω.*

Figure 4.26: *Wave and force amplitudes in ω. 2.5m×1m net panels, $U_0 = 0.2m/s$ and $\epsilon_w = \dfrac{1}{20}$.*

The wave amplitudes measured from WP1, observed in Figure 4.26a match well with the expected and theoretical curves, with an error of approximately 0.3cm. The resulting loads corresponding to these waves, presented in Figure 4.26b, show a strong dependency on the wave period, leading for the highest period to approximately 45N

(i.e. $648N/m^2$ in full-scale) for $S_N = 0.147$, and 78N (i.e. $1123N/m^2$ in full-scale) for $S_N = 0.227$.
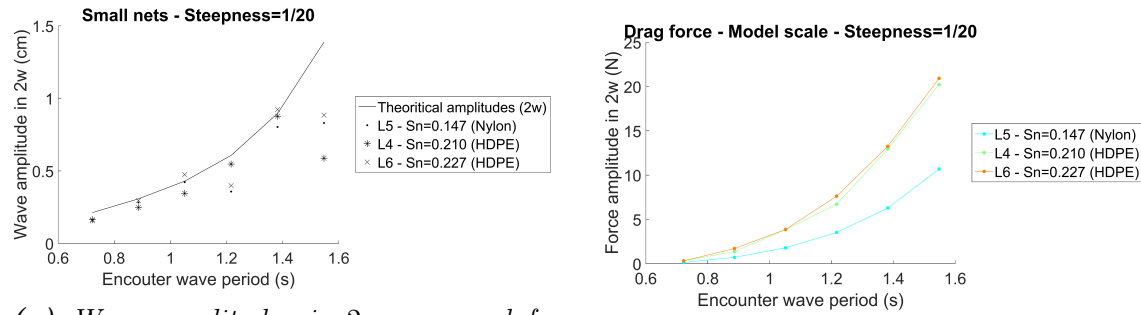
(a) *Wave amplitudes in 2ω measured from the carriage in front of the net (WP1).*

(b) *Drag force amplitudes in 2ω.*

Figure 4.27: *Wave and force amplitudes in 2ω. 2.5m×1m net panels, $U_0 = 0.2m/s$ and $\epsilon_w = \dfrac{1}{20}$.*

The second harmonic of the wave amplitudes measured in Lilletanken (Figure 4.27a) match also well with the theoretical values, expect for the highest periods. Such strange values were very common, and could come from the fact that too few periods were considered in the WP1's time series, when it came to calculate the spectrum of the wave amplitudes during the data analysis. Thus, the spectra could have been too "coarse" to study the wave amplitude's harmonics in detail.

However, the resulting load amplitudes in 2ω have been caught properly, as shown in Figure 4.27b. As for the curves in ω, a parabolic trend is observed, but the forces seem to increase faster with T_e, e.g. from around 1N (i.e. $14.4N/m^2$ in full-scale) at $T_e = 0.72s$, to 21N (i.e. $302N/m^2$ in full-scale) at $T_e = 1.54s$ for $S_N = 0.227$.

4.5.2 Influence of ϵ_w and U_0 on the loads

In this section, the loads on the panels S9 ($1m \times 1m$) and L4 ($2.5m \times 1m$) are presented for the two wave steepness, and the two velocities tested in Lilletanken. These panels come from the same net, and have almost the same properties: HDPE (blue), $d_w = 2mm$, $S_N = 0.228$ for S9, and $S_N = 0.210$ for L4. S_N depends on the stretching of the nets on the frames so they are not exactly identical.

Mean forces

(a) *1m×1m net panel S9 (HDPE).*

(b) *2.5m×1m net panel L4 (HDPE).*
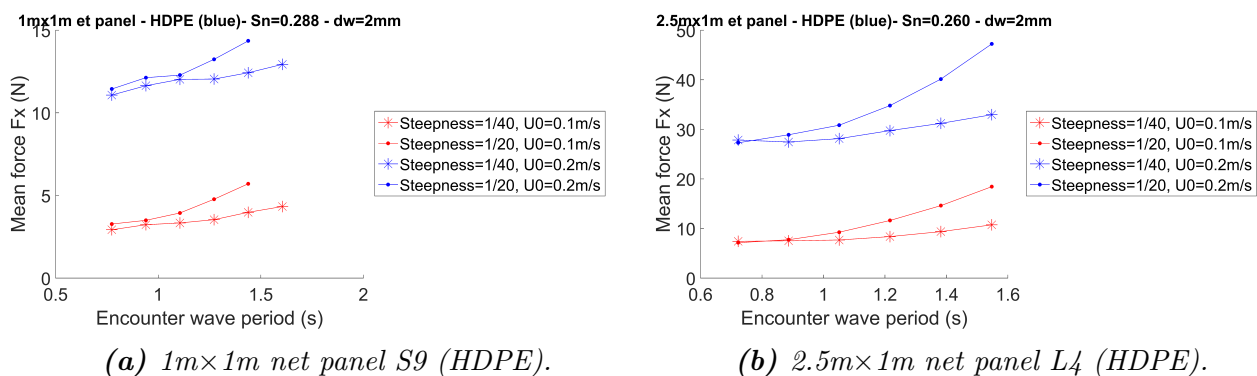
Figure 4.28: *Mean drag force. Influence of the current's velocity and wave's steepness for two different sizes of the same net (Sn determined from the photos).*

Figure 4.28 presents the mean drag forces in model-scale for the two nets S9 and L4. The values read for the lowest wave periods correspond to the values found for current conditions at the same velocities without wave. Thus, U_0 is clearly the main cause of this mean load.

However a stokes drift is also acting since for $\epsilon_w = \dfrac{1}{20}$, the loads measured for high wave periods are about 35% higher than the initial values. The maximum drift is obtained for L4 and reaches $648N/m^2$ in full-scale.

Force amplitude in ω

As expected, the wave steepness is preponderant when looking at the force amplitudes in Figure 4.29, even if U_0 still plays an important role. For example for L4 and $T = 1.6s$, $F_x(\epsilon_w = \dfrac{1}{40}, U_0 = 0.1m/s)$ increases by approximately 71% when the steepness doubled (i.e. from $619N/m^2$ to $1555N/m^2$ in full scale), and by %35 when the velocity doubled (i.e. from $619N/m^2$ to $956N/m^2$ in full scale). The maximum reached is $2160N/m^2$ in full scale.

(a) *1m×1m net panel S9 (HDPE).*

(b) *2.5m×1m net panel L4 (HDPE).*
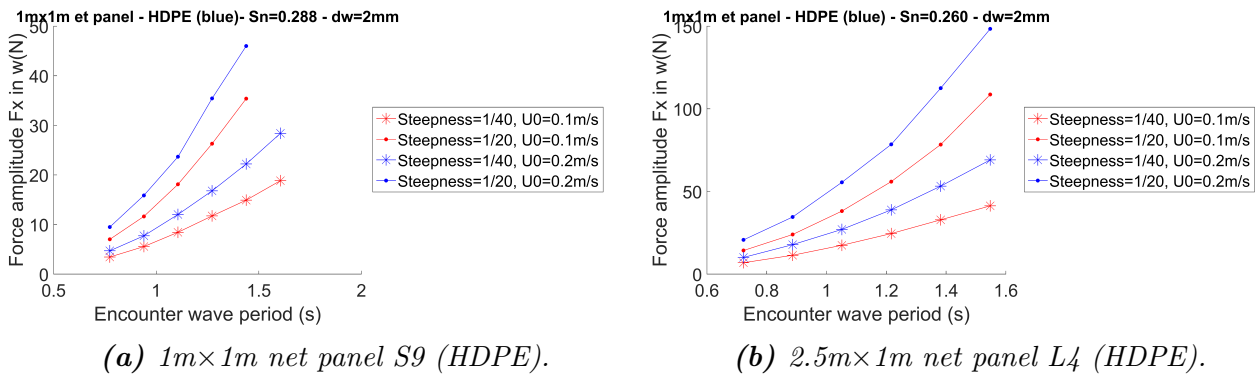
Figure 4.29: *Force amplitude in ω. Influence of the current's velocity and wave's steepness for two different sizes of the same net (Sn determined from the photos).*

Force amplitude in 2ω

(a) *1m×1m net panel S9 (HDPE).*

(b) *2.5m×1m net panel L4 (HDPE).*
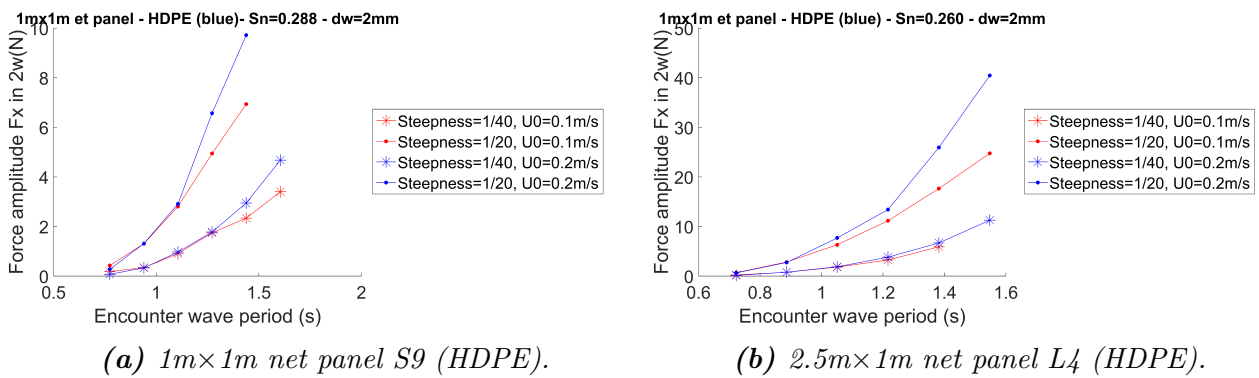
Figure 4.30: *Force amplitude in 2ω. Influence of the current's velocity and wave's steepness for two different sizes of the same net (Sn determined from the photos).*

Figure 4.30 shows the second harmonics of the loads. The curves for both U_0 are overlapped for low wave periods, but still influence the results for high periods.

The components of the loads in 2ω are significant for $\epsilon_w = \dfrac{1}{20}$, reaching $576 N/m^2$ for $T = 9.6s$ (both in full-scale).

Globally, the forces acting on the $2.5m \times 1m$ panels were a little more than 2.5 times higher than the $1m \times 1m$. It could come from the fact that the real wet area of the nets was maybe higher for the large panels because of the wave elevation in front of the nets.

4.6   Uncertainties and errors

Many sources of errors were mentioned all along this project, and many uncertainties remain on the final results provided in the previous section. The main causes and effects met in both the numerical and experimental works are presented below.

Uncertainties on the net properties and stretching

S_N is a key parameter, and two methods were used to estimate it: from photos and from calculations based on the twine diameters. However, the values obtained were significantly different, with $S_{N,photos}$ around 20% higher than $S_{N,calculations}$ (in average). One cause could be the stretching of the nets, which was not uniform (some meshes were more stretched than other over the all surface of the net), and S_N was suspected to be higher near the bars of the frames. But the main error probably came from the poor quality of the photos.
Besides, the measurement of the twine diameter (very low) was not very accurate neither.

Furthermore, the nets were loosening, more or less quickly, during the experiments. It was observed from the videos taken under the carriage that the nylon nets were loosening particularly quickly after few tests.
The stretching seemed also to be a key factor to understand the variations of the loads measured in the same conditions during the repetitive tests achieved on the $1m \times 1m$ net S2.

Finally, the nets were designed in full-scale, but tested in model-scale for wave conditions. Thus, some model-scale effects are expected.

Environmental conditions

The wave reflections at the end of the towing tank, and to a lesser extent to the side walls, interfered with the incoming waves. It was especially the case for wave and current conditions (in the same time) because the carriage had to start at the end of the towing tank and the reflected waves were interfering much quicker at the begining of the tests.

A seiching wave was also observed for these tests, the "mean" forces were then oscillating at low frequency with very large variations for few extreme cases (up to $^{+}10\%$ around the mean signals).

The water free surface was assumed to be the same for each tests, and a break of 180s was automatically imposed between two experiments. However, for high U_0 or high wave steepness, it was maybe not sufficient for the water to be at rest again.

Besides, a "drift" was observed in the offset of the loads during the same time series (several tests were recorded in the same time series). It could come from the transducers themselves (fatigue, change of temperature, etc.).

Post-treatment of the raw data

The post-treatment of the data was also source of errors and uncertainties. An important error was brought by subtracting the loads acting on the empty frame to "only" kept the contribution of the nets. However, loads acting on the only frames were suspected to be much increased with the presence of the nets: because the water elevation (due to the nets) was higher, and because the flows around the bars composing the frame were probably affected by the nets. For instance, the mere presence of the strips on the frames led to about 14% lower forces.

Other errors have been brought when filtering (the amplitudes of the loads could be very slightly lowered), interpolating, etc.

Numerical and analytic errors and uncertainties

The analytic speed-up of the flow calculated analytically did not integrated any acceleration of the flow between the frame and the bottom wall of the tank (less than 10cm).

The solving of the NSE in OpenFoam brought few errors from the numerical schemes that were used (rounding, truncation errors, etc.), but one of the most important error probably came from the mesh, which was chosen a little coarse in order to keep reasonable computational times.

Bias errors linked to the set-up and measuring equipment

The noises caused y the vibrations of the installation while the carriage was running, or maybe by the electronic equipment, polluted the recorded time series. It was an important concern, especially when studying the harmonics of the loads which were sometimes "drowned" in the noise.
Besides, the VIV of the wave probes were very strong and frequent, and most of the recorded wave elevations could not be used.

The accuracy of the transducers, and measurement of the carriage's velocity played a role in the accuracy of the results. Few errors coming from the calibration could have remained.
In addition, the installation was probably not perfectly symmetric, i.e. not exactly centered in the middle of the tank (as discussed from the F_y curves). The screwing of the frame, made manually, could have also been asymmetric, e.g. the two front screws more tightened than the tow back ones. Thus, the frames could have been very slightly inclined during the tests.

However, one of the main error concern the wave elevation saw just in front of the nets. The wet surface was increased (up to 12.7% higher in the two example treated), as well as the loads acting on the nets, making the comparison with CFD results very difficult.

Conclusion

Several net panels, characterized by their solidity ratios, their widths, their twine diameters and their materials were provided by Aqualine. Drag tests on these aquaculture net panels were achieved in the towing tank Lilletanken at NTNU. The loads caused by different conditions of waves and currents were recorded and analysed.

Numerical investigations were carried out in parallel to the experimental study. The nets were modeled as porous media, and the two main theories found in the literature - the Morison type loads and screen type loads - have been simulated and compared.

The results obtained for the different nets have then been compared and discussed.

Overall conclusions

This estimation of the solidity ratio thanks to pictures did not bring accurate results because of the poor quality of the photos, and the calculation of this number, as proposed in Fredheim (2005) and based on the twine diameters and mesh's length, has been preferred.

Loads from 400N to 1000N have been measured for the largest nets (S_N from 0.085 to 0.227) when subtracting the loads on the empty frames. However the uncertainties on the loads acting the frames could be significant, especially because of the water elevation observed on the net panels during the tests.

The numerical were lower than the experimental ones, and large differences were obtained for high S_N. An important speed-up of the flow between the panels and the bottom wall was observed in the numerical models. Between the two porous models tested, the screen type load model provided the best results.

Further works

From the conclusions made in the previous part, several improvements or further works could be imagined:

- Improve the turbulent model. Very strong velocity gradients were observed in the CFD results, they are questionable. Furthermore, large eddies were observed during the experiments. LES methods could be more adapted.

- Include the design of the knots (HDPE nets) in the determination of the porous coefficients, since the porous models used in this thesis are based on knot-less nets. Fredheim (2005) proposes for example to decompose the drag coefficients into two terms: $C_D = C_{D,twines} + C_{D,knots}$.

- Increase the height of the porous volume to the top of the domain when adding the free-surface elevation. The water elevation on the panels would then be incuded, and the loads more realistic.

- Change the set-up of the installation to avoid side effects are water elevation. For instance, by testing the nets in Flume tanks.

- Achieve sensitive analysis to estimate more precisely the accuracy of the results, and the dependence of the drag force on several parameters, as S_N or Re.

- Improve and control the stretching of the net panels.

References

[1] F. an Agriculture Organization of the United Nations, *The state of world fisheries and aquaculture, contributing to food security and nutrition for all* (2016).

[2] F. R. Menter, "Zonal two equation k- turbulence models for aerodynamic flows", (1993).

[3] J. D. Anderson, *Fundamentals of aerodynamics*, Third Edition (McGraw Hill Higher Education, 2001), pp. 206–243, ISBN: 0072373350.

[4] S. Steen, *Experimental methods in marine hydrodynamics, lecture notes*, Marine Technology Center, Department of Marine Technology (Faculty of Engineering Science and Technology, Norwegian University of Science and Technology, Trondheim, Aug 2014).

[5] A. Fredheim, *Current forces on net structures*, Ph.D. Dissertation (Norwegian University of Science and Technology, Trondheim, April 2005).

[6] G. Ducrozet, *Environnement marin et chargements, presentation*, LHEEA (Ecole Centrale de Nantes, France, 2014).

[7] H. Chanson, "Current knowledge in hydraulic jumps and related phenomena. a survey of experimental results", **28**, 191–210 (2009) `https://doi.org/10.1016/j.euromechflu.2008.06.004`.

[8] T. Kristiansen and O. M. Faltinsen, "Modelling of current loads on aquaculture net cages", **34**, 218–235 (2012) `http://dx.doi.org/10.1016/j.jfluidstructs.2012.04.001`.

[9] O. M. Faltinsen, *Sea loads on ships and offshore structures (Cambridge Ocean Technology Series)*, Reprint Edition (Cambridge University Press, 1993), ISBN: 0521458706.

[10] H. Chen and E. D. Christensen, "Investigations on the porous resistance coefficients for fishing net structures", **65**, 76–107 (2016) `http://dx.doi.org/10.1016/j.jfluidstructs.2016.05.005`.

[11] Ø. Patursson, *Flow through and around fish farming nets*, Ph.D. Dissertation, Ocean Engineering (University of New Hampshire, Durham, NH, USA, 2008).

[12] Y.-P. Zhao, C.-W. Bi, G.-H. Dong, F.-K. Gui, C.-T. Guan, T.-J. Xu, and Y. Cui, "Numerical simulation of the ow around shing plane nets using the porous media model", **62**, 25–37 (2013) `http://dx.doi.org/10.1016/j.oceaneng.2013.01.009`.

[13] B. Jensen, N. G. Jacobsen, and E. D. Christensen, "Investigations on the porous media equations and resistance coefcients for coastal structures", **84**, 56–72 (2014) `http://dx.doi.org/10.1016/j.coastaleng.2013.11.004`.

[14] Ø. Patursson, M. R. Swift, I. Tsukrov, K. Simonsen, K. Baldwin, D. W. Fredriksson, and B. Celikkol, "Development of a porous media model with application to ow through and around a net panel", **37**, 314–324 (2010) `http://dx.doi.org/10.1016/j.oceaneng.2009.10.001`.

[15] H. Darcy, *Les fontaines publiques de la ville de dijon* (Victor Dalmont, Paris, 1856).

[16] P. Forchheimer, "Wasserbewegung durch boden. z. ver. deutsch. ing.", **45**, 1782–1788 (1901).

[17]C. J. Greenshields, *The openfoam foundation - user guide* (OpenFOAM Foundation Ltd., 2016).

[18]R. D. Blevins, *Applied fluid dynamics handbook*, New York (Van Nostrand Reinhold Co., 1984), ISBN: 0442212968.

[19]H. Werlé, *Le tunnel hydrodynamique au service de la recherche aérospatiale* (Publ. no. 156, ONERA, France, 1974).

[20]S. F. Hoerner, *Fluid dynamic drag, practical information on aerodynamic drag and hydrodynamic resistance*, Second Edition (Hoerner Fluid Dynamics, 1965).

[21]P. F. Lader, B. Enerhaug, A. Fredheim, and J. Krokstad, *Modelling of 3d net structures exposed to waves and current*, 3rd International conference on Hydroelasticity in Marine Technology (Oxford, UK, 2003).

[22]P. Lader and B. Enerhaug, "Experimental investigation of forces and geometry of a net cage in uniform flow", **30**, 79–84 (2005) `http://dx.doi.org/10.1109/JOE.2004.841390`.

[23]T. Kristiansen, "A numerical parameter study on current forces on circular aquaculture net cages", (June 2013) `http://dx.doi.org/10.1115/OMAE2013-10915`.

[24]G. Løland, "Current forces on, and water flow through and around, floating fish farms", **1**, 72–89 (1993) `http://dx.doi.org/10.1007/BF00692665`.

[25]S. Ergun, "Fluid flow through packed columns", **48**, 89–94 (1952).

[26]G. Løland, *Current forces on and flow through fish farms*, Ph.D. Dissertation (Norwegian University of Science and Technology, Trondheim, 1991).

[27]S. Goldstein, *Modern developments in fluid dynamics* (Dover Publications, 1965).

[28]J. N. Newman, *Marine hydrodynamics*, Cambridge, Massachusetts (MIT Press, 1977), ISBN: 062140268.

A | Tests in Lilletanken
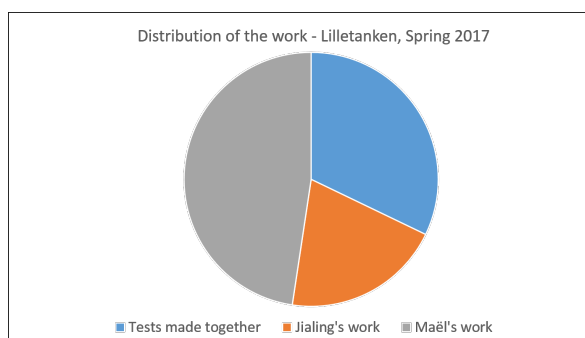
Figure A.1: *Division of the work in Lilletanken (test by test).*

A.1   Wave probe calibrations
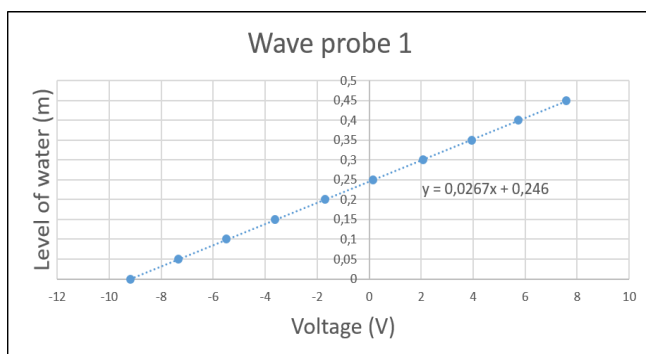
(a) *WP1.*
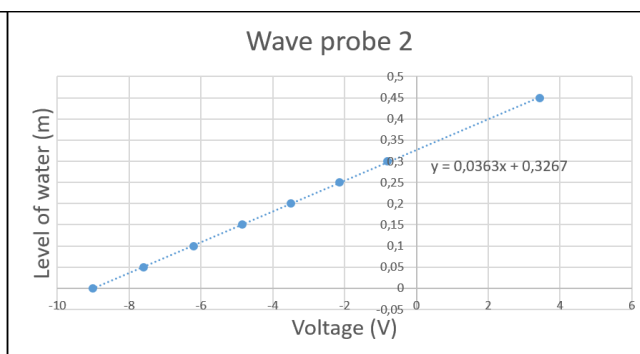
(b) *WP2.*
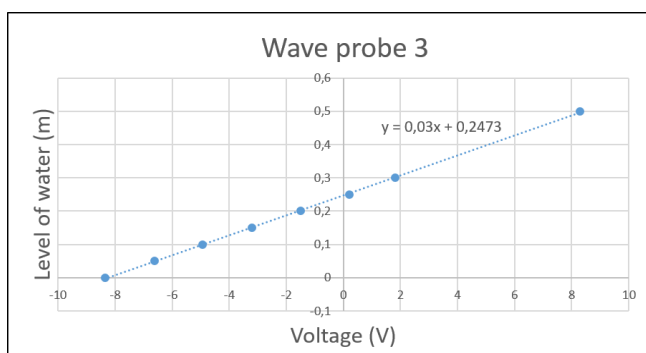
(c) *WP3.*
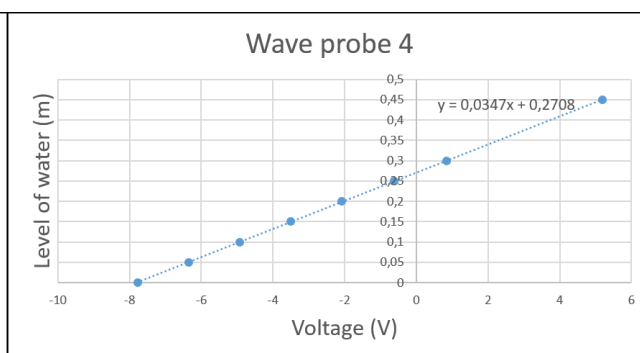
(d) *WP4.*
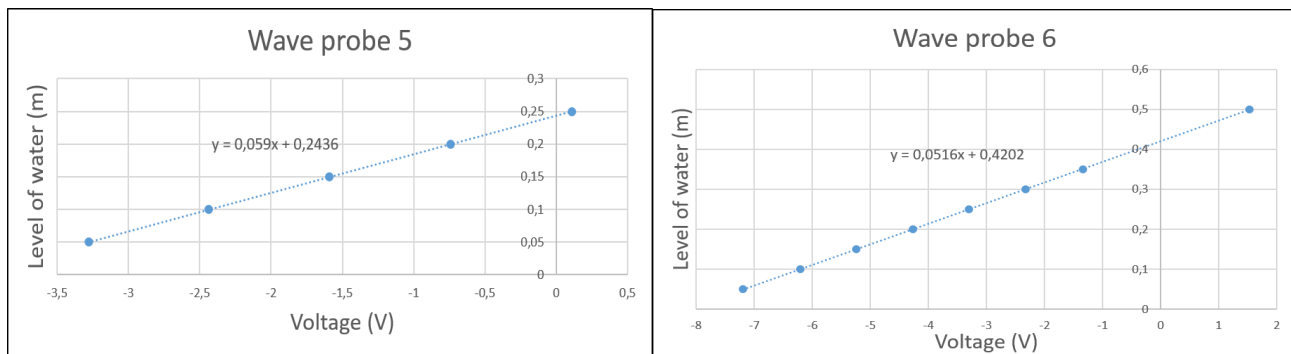
(e) *WP5.*   **(f)** *WP6.*

Figure A.2: *Calibration of the wave probes.*

A.2   Main dimensions of the frames
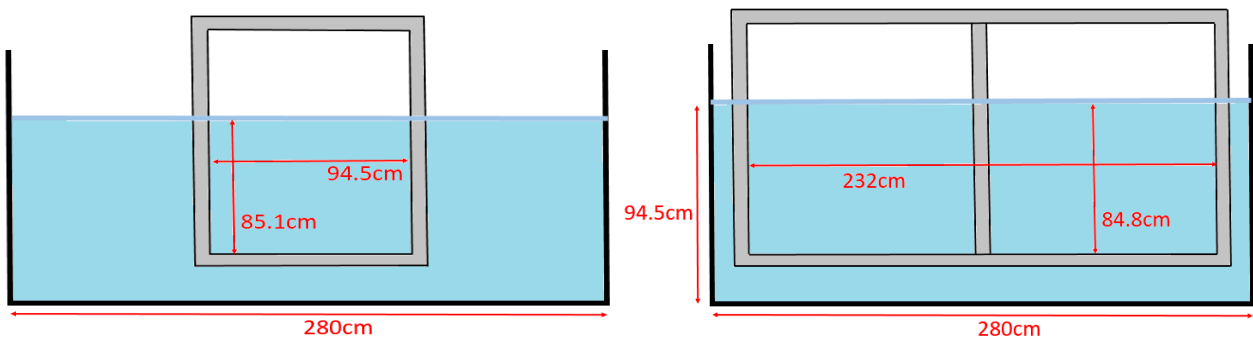
(a) *1m×1m empty frame.*

(b) *2.5m×1m empty frame.*

Figure A.3: *Measures taken in the towing tank when the frames were placed in the water and fixed to the carriage.*
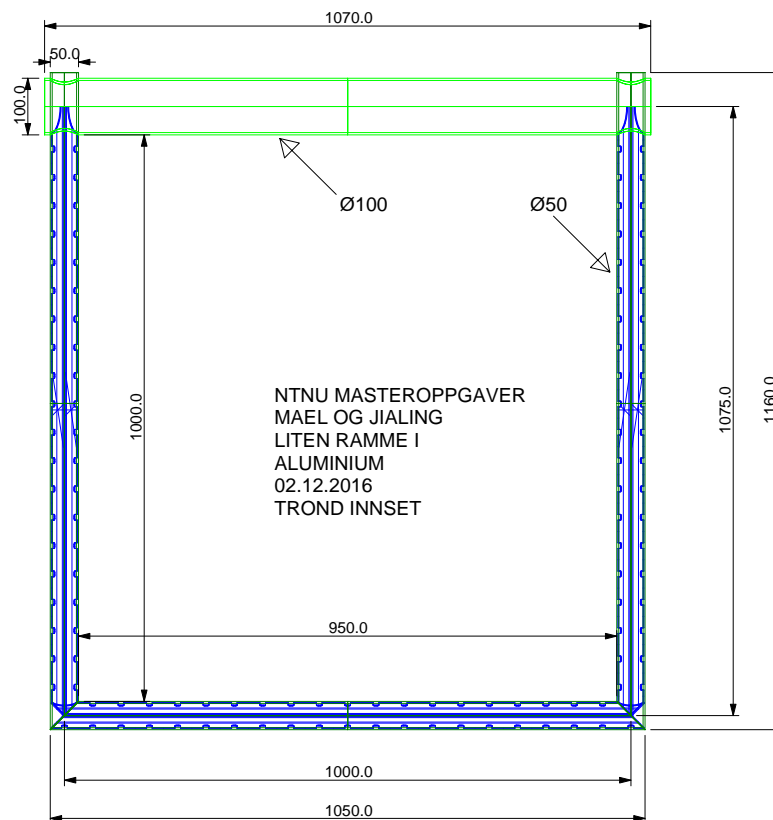
Figure A.4: *1m×1m frame dimensions - Conceived by Trond Innset.*

A.3   Modal test
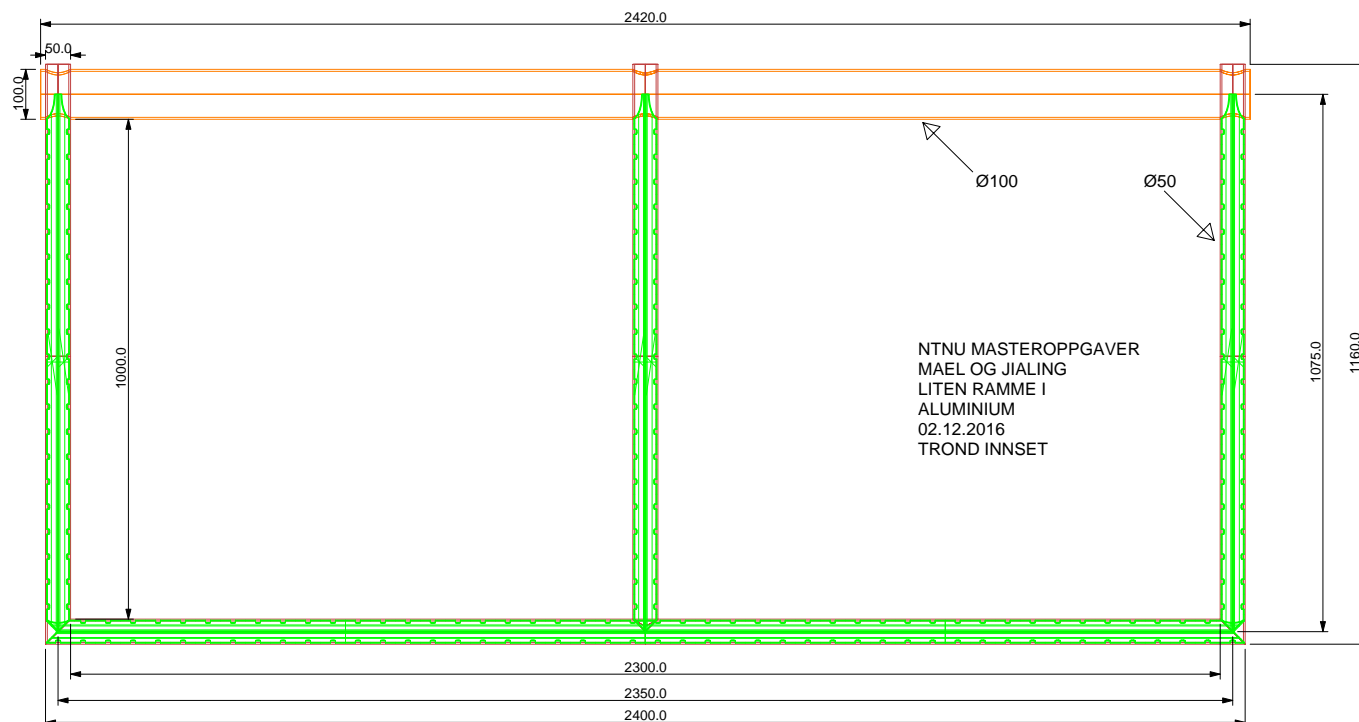
Figure A.5: *2.5m×1m frame dimensions - Conceived by Trond Innset.*
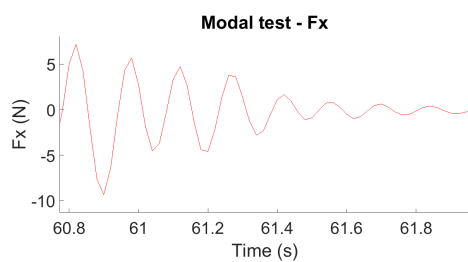
(a) *1m*2.5m frames - Fx.*
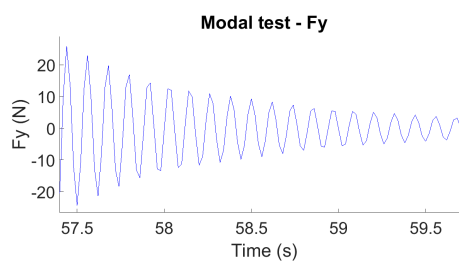
(b) *1m*2.5m frames - Fy.*
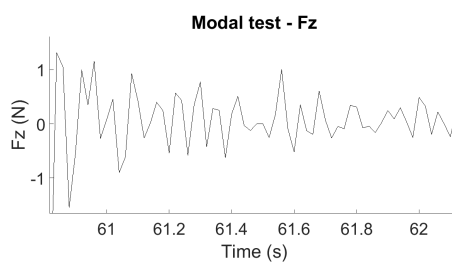
(c) *1m*2.5m frames - Fz.*

Figure A.6: *Modal tests of the 1m*2.5m frames - Time series of the forces just after the hit.*
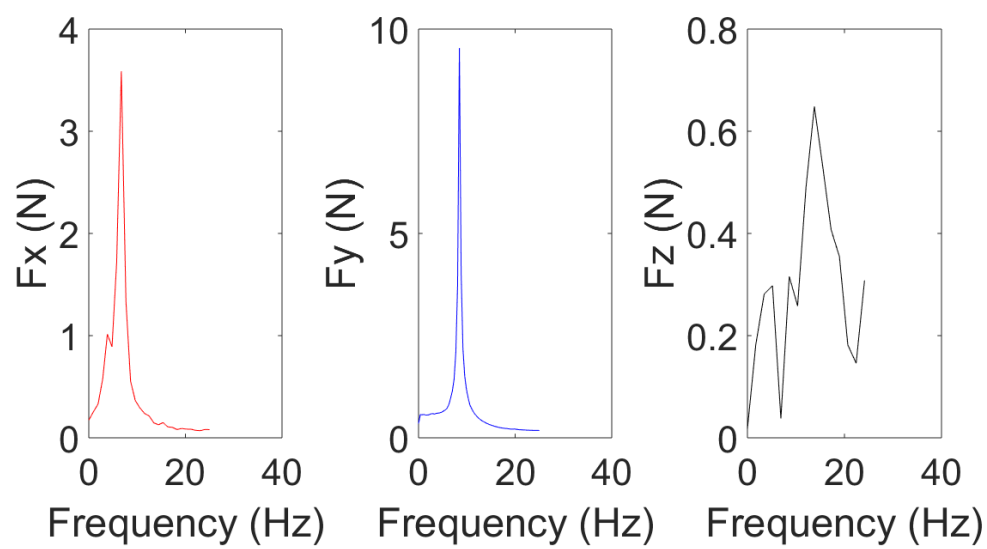
Figure A.7: *Fourier transform (spectral analysis) of the forces' time series. Modal test achieved on the 2.5m × 1m empty frame without strips.*

A.4   Nets' solidity ratio
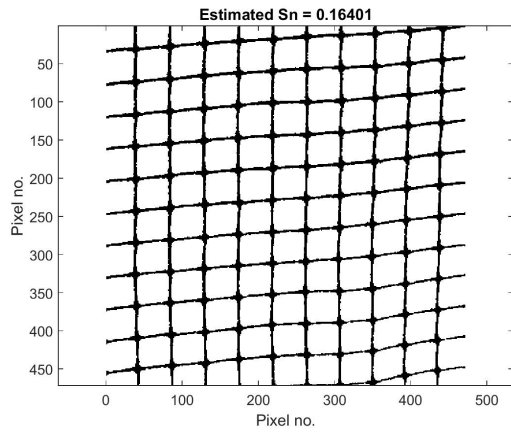
(a) *Net S1.*
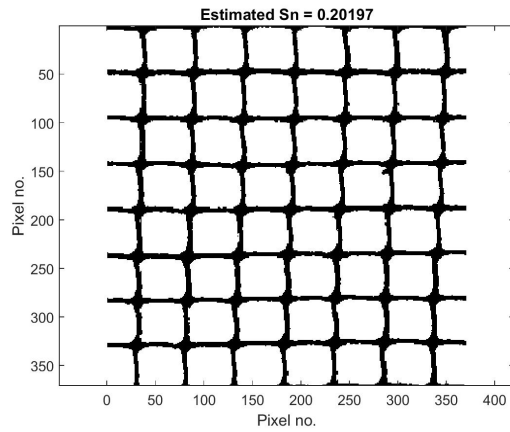
(b) *Net S2.*
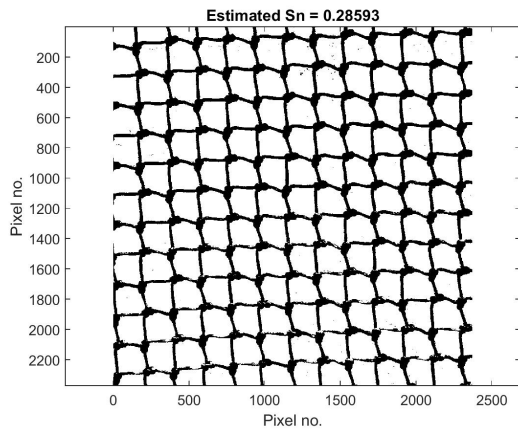
(c) *Net S3.*
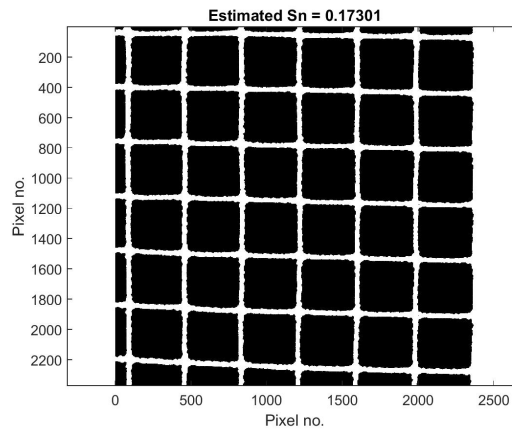
(d) *Net S4.*
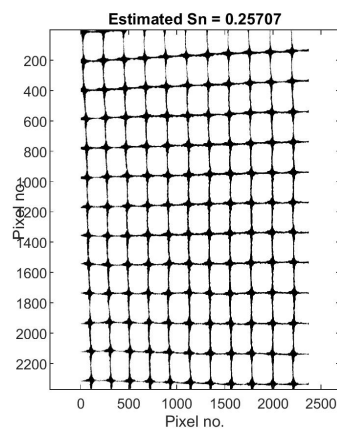
(e) *Net S5.*
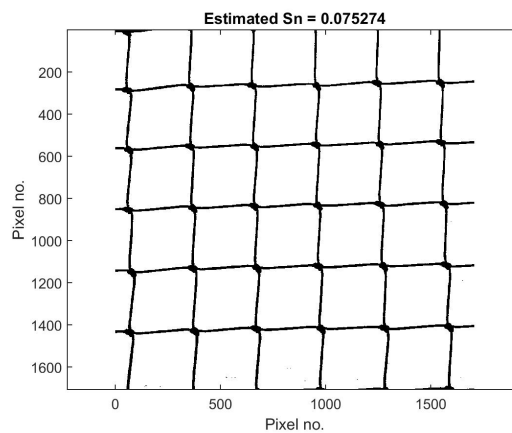
(f) *Net S6.*
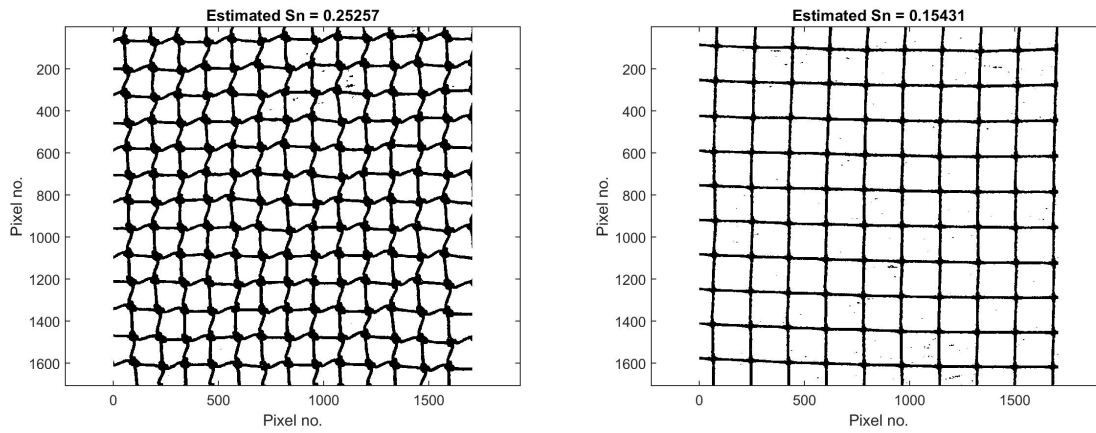
(g) *Net S7. This S_N is expected to be too high because of the impurities on the walls.*

(h) *Net S8. This S_N is also expected to be too high because of the impurities on the walls.*
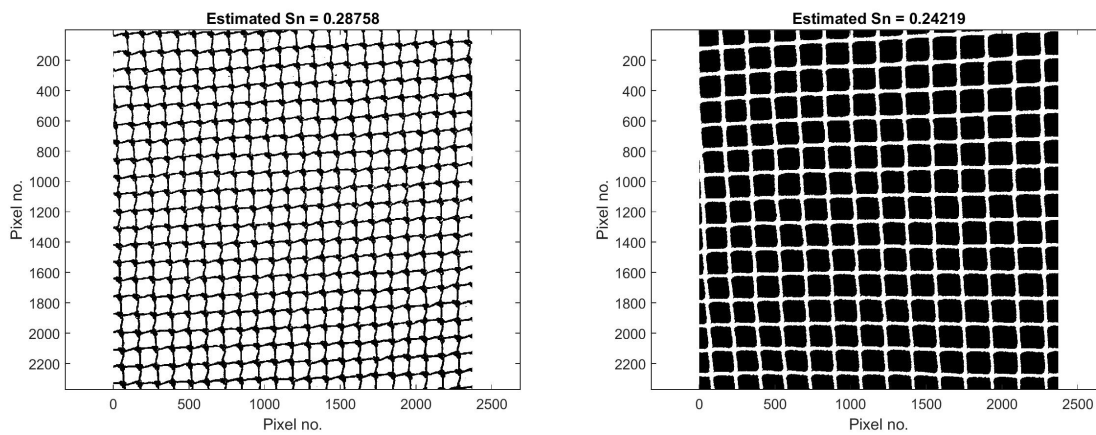
(i) *Net S9.*

(j) *Net S10.*

Figure A.8: *Solidity ratios of the 1m*1m net panels calculated with Matlab from the photos.*
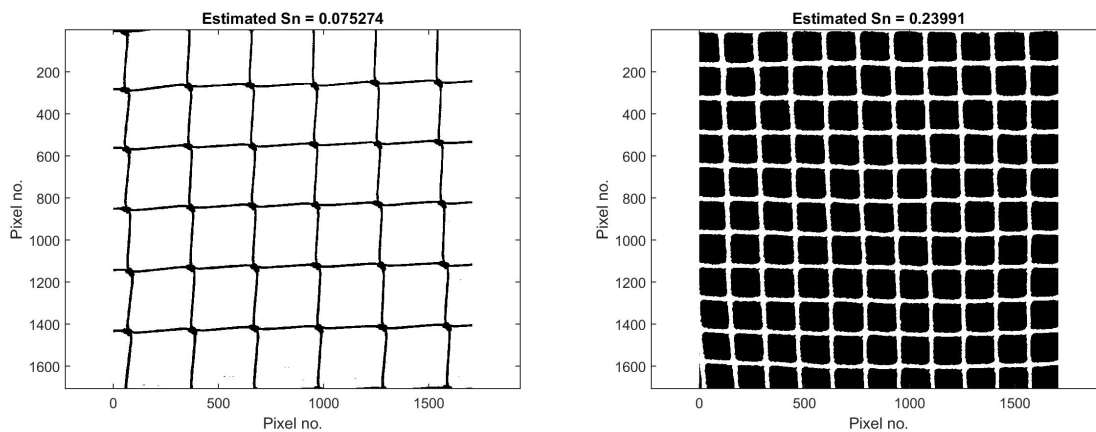
(a) *Net L1.*

(b) *Net L2.*
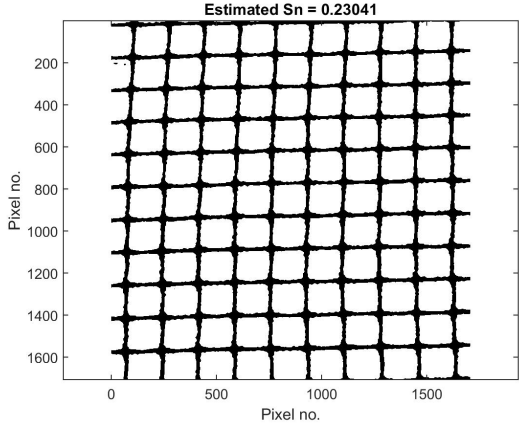
(c) Net L3.
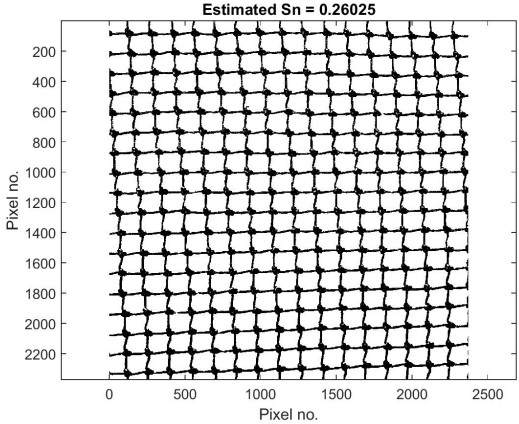
(d) Net L4.
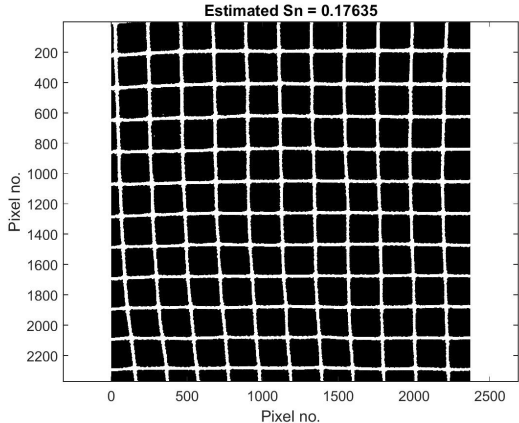
(e) Net L5.
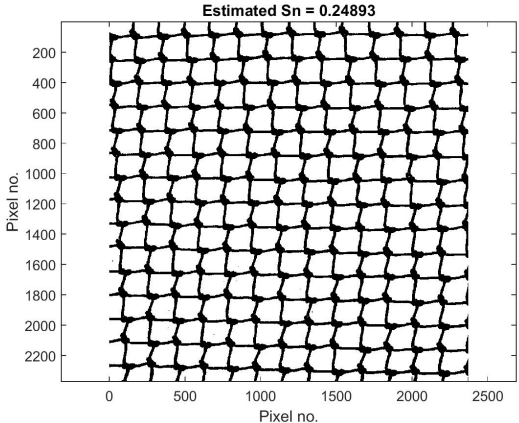
(f) Net L6.

Figure A.9: *Solidity ratios of the 2.5m*1m net panels calculated with Matlab from the photos.*

A.5   Nets' properties

A.5.1   Nets' tags

Some of the net panels have been provided with tags on them giving information about theirs twine length l and diameters d_w, and theirs sizes (as defined during their fabrication). However the measured values of these parameters, more reliable, have been used. The Tables A.1 and A.2 report the information written on the tags found attached to the tested nets.

Table A.1: *Tags - Small net panels.*

Net	Inscription on the tag	Material - Color
$S1$	"N0.36x22.5mmsqx1.2mx1.2m"	Nylon - Black
$S2$	"N0.28x18mmsqx1.2mx1.2m"	Nylon - Black
$S3$	"2.2mm*25mmsqx1.2mx1.2m"	HDPE - Red
$S4$	"N0.36x29mmsqx1.2mx1.2m"	Nylon - White
$S5$	"N0.20x15.5mmsqx1.2mx1.2m"	Nylon - Black
$S6$	"3.1mmx75mmsqx1.2mx1.2m"	HDPE - Red
$S7$	"1.7mmx18mmsqx1.2mx1.2m"	HDPE - Red
$S8$	"N0.24x30.5mmsqx1.2mx1.2m"	Nylon - Black
$S9$	No tag	HDPE - Blue
$S10$	"N0.40x22.5mmsqx1.2x1.2m"	Nylon - White

Table A.2: *Tags - Large net panels.*

Net	Inscription on the tag	Material - Color
$L1$	"2.7mx2.1m""	HDPE - Red
$L2$	"N0.40x22.5mmsqx2.7x1.2m"	Nylon - White
$L3$	"N0.20x15.5mmsqx2.7mx1.2m"	Nylon - Black
$L4$	"1.9mmx18mm"	HDPE - Blue
$L5$	"N0.36x29mmsqx2.7mx1.2m"	Nylon - White
$L6$	"2.2mmx25mmsqx2.7mx1.2m"	HDPE - Red

A.5.2   Large and small nets correspondance

Table A.3: *Correspondence between the large and small net panels.*

2.5m×1m	1m×1m	Material	Color
$L1$	$S6$	HDPE	Red
$L2$	$S10$	Nylon	White
$L3$	$S5$	Nylon	Black
$L4$	$S9$	HDPE	Blue
$L5$	$S4$	Nylon	White
$L6$	$S3$	HDPE	Red

A.6   Data analysis

(a) $U_0 = 0.2 m/s$.   **(b)** $U_0 = 1.5 m/s$.
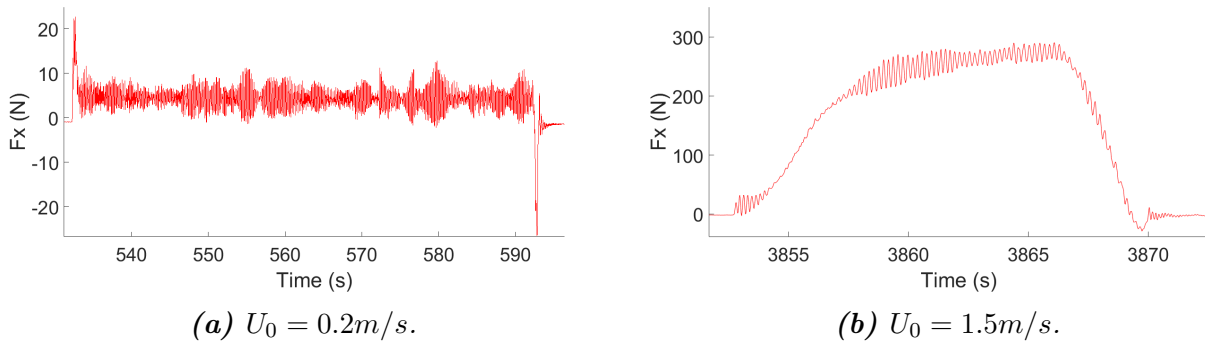
Figure A.10: *Example of time series for the drag force - Net S6.*
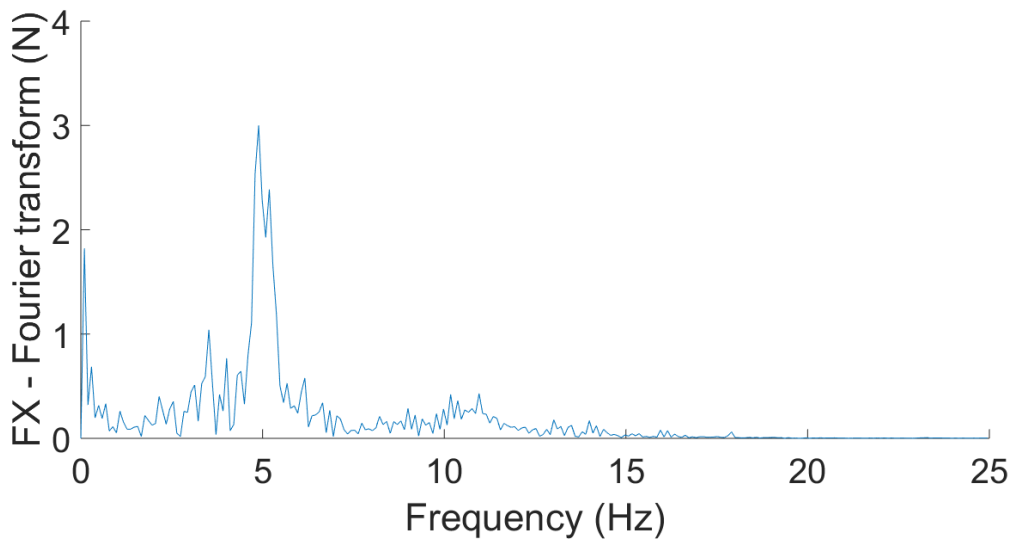
Figure A.11: *Fourier transform for $U_0 = 1 m/s$ - Example, net S6.*

(a) *All the signal.*

(b) *Zoom on the mean value over the tests for which $\epsilon = \dfrac{1}{40}$.*
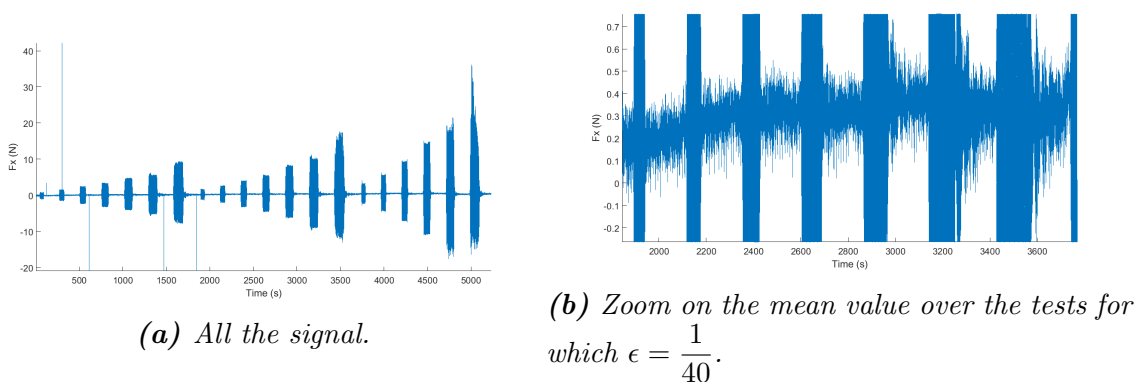
Figure A.12: *Time series of the drag force for wave conditions applied to the 1m×1m empty frame.*

Table A.4 presents the scaling factors of the variables needed to convert the results in waves in full scale, knowing that the scale used for these tests was $s = 36$.
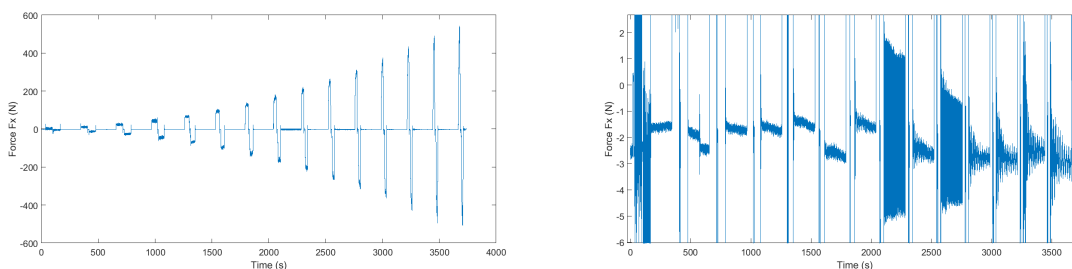
(a) *All the signal.*

(b) *Zoom on the mean value over the tests.*

Figure A.13: *Time series of the drag force for current conditions applied to the 1m×1m net S2.*
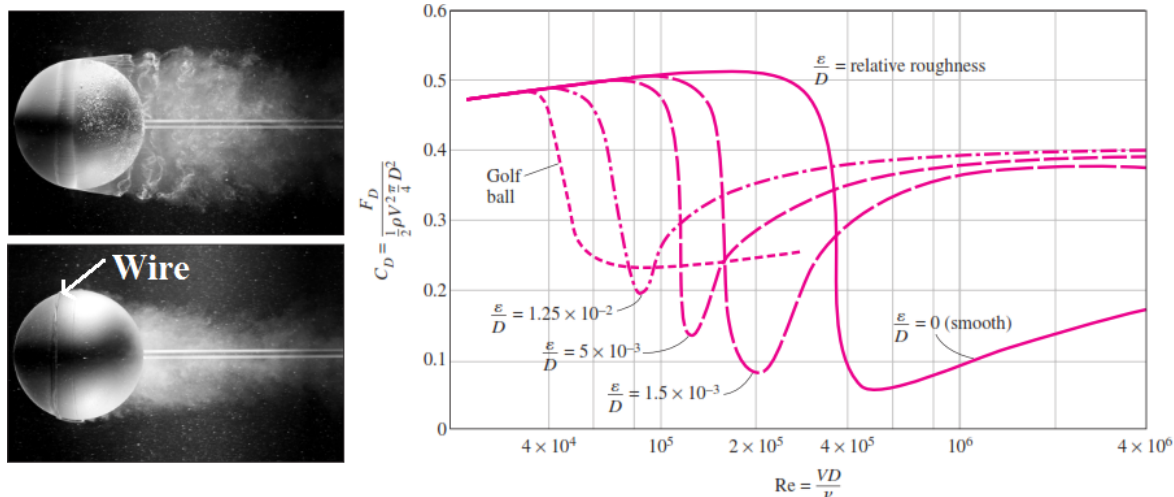
Figure A.14: *To the left: pictures of the flows around a sphere without (top) and with (bottom) a wire, from Werlé (1974). To the right: influence of the roughness on the drag coefficient of a sphere from Blevins (1984).*

Table A.4: *Full scale conversions.*

Variable	Conversion factors
Length (m)	s
Time (s)	$\sqrt{s}$
Force (N)	s^3

A.7   Wave elevations - Example of time series.
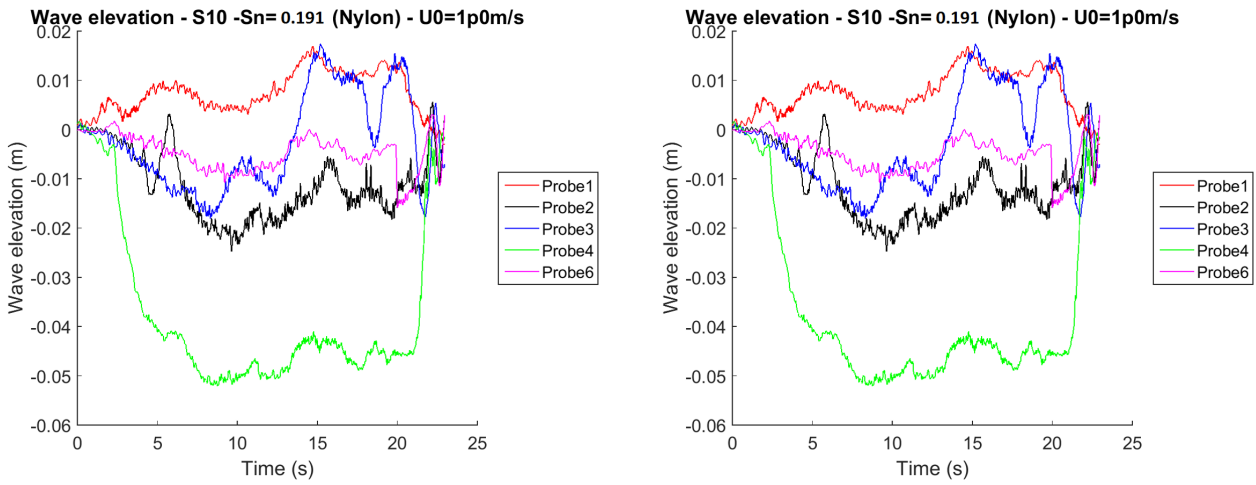
(a) *Net S10 (Nylon, $S_N = 0.191$).*   **(b)** *Net L2 (Nylon, $S_N = 0.171$).*

Figure A.15: *Experimental measured from the wave probe in front of the panels (WP1). $U_0 = 1m/s$.*
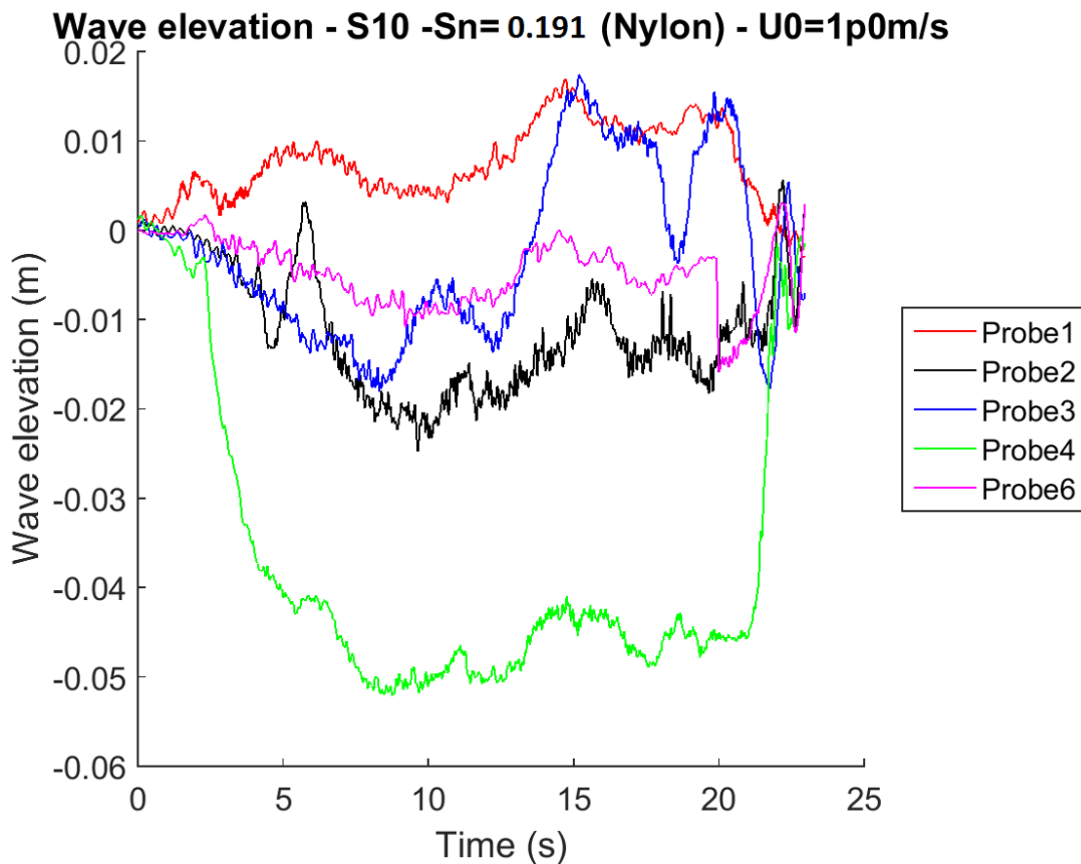
Figure A.16: *Experimental measured from the wave probe in front of the panels (WP1). Net L2 (Nylon, $S_N = 0.171$), $U_0 = 1.5m/s$.*

B | CFD model

B.1   Meshes - Convergence study

Time series
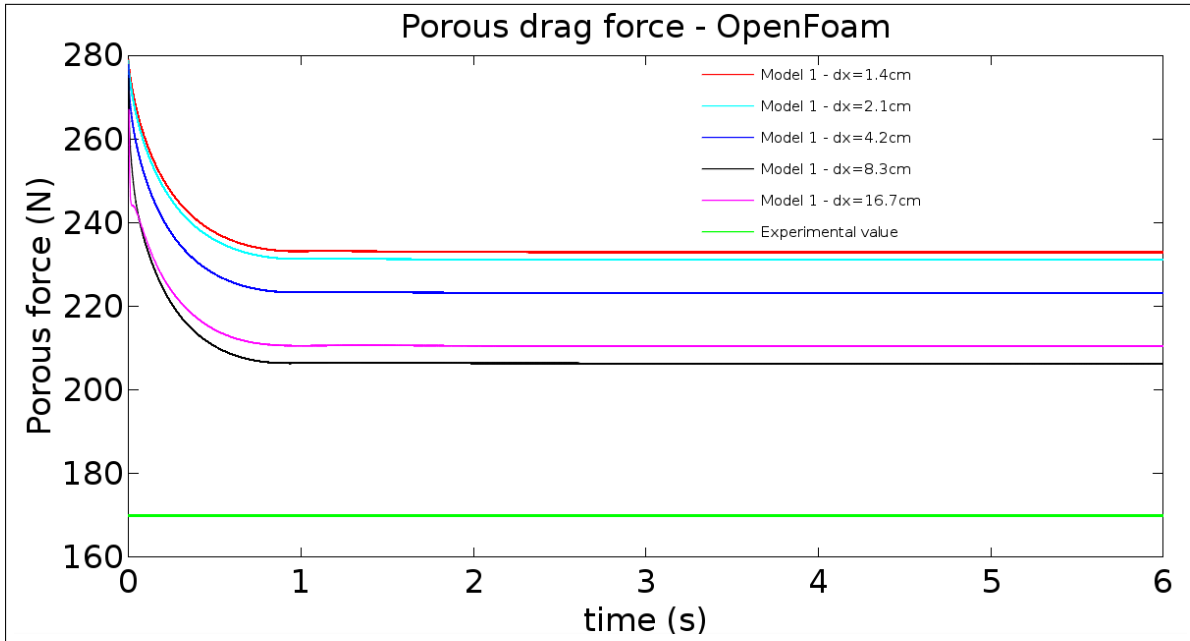
Figure B.1: *Model 1, time series. Mesh convergence study (Ergun porous model).*
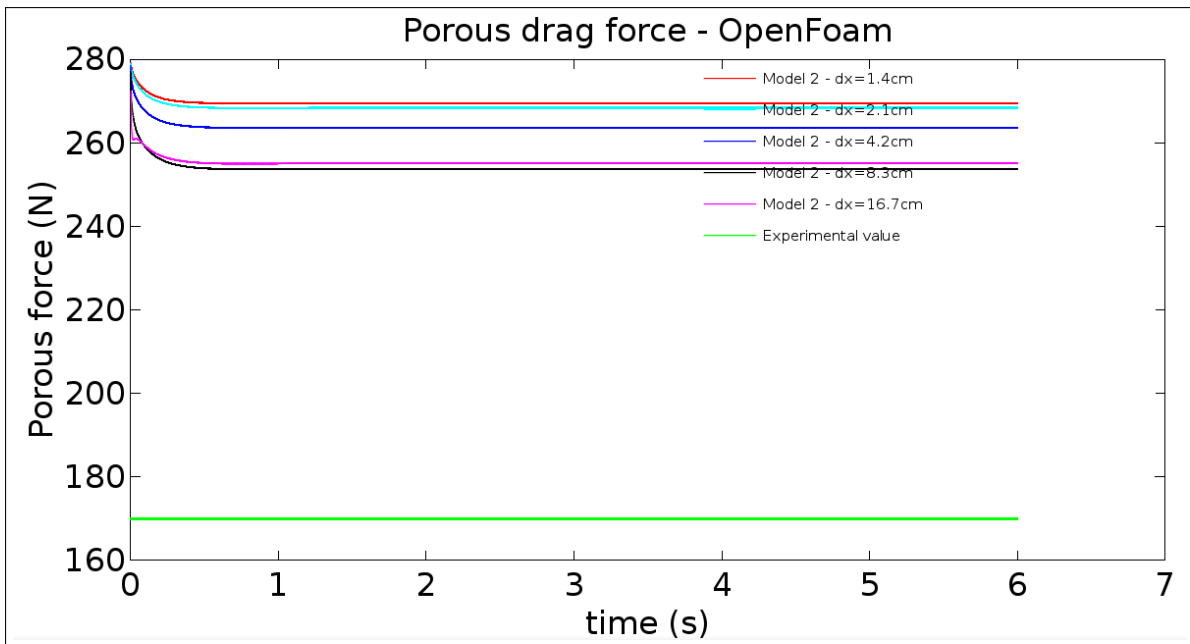
Figure B.2: *Model 2 - Time series. Mesh convergence study (Ergun porous model).*

Mesh sizes
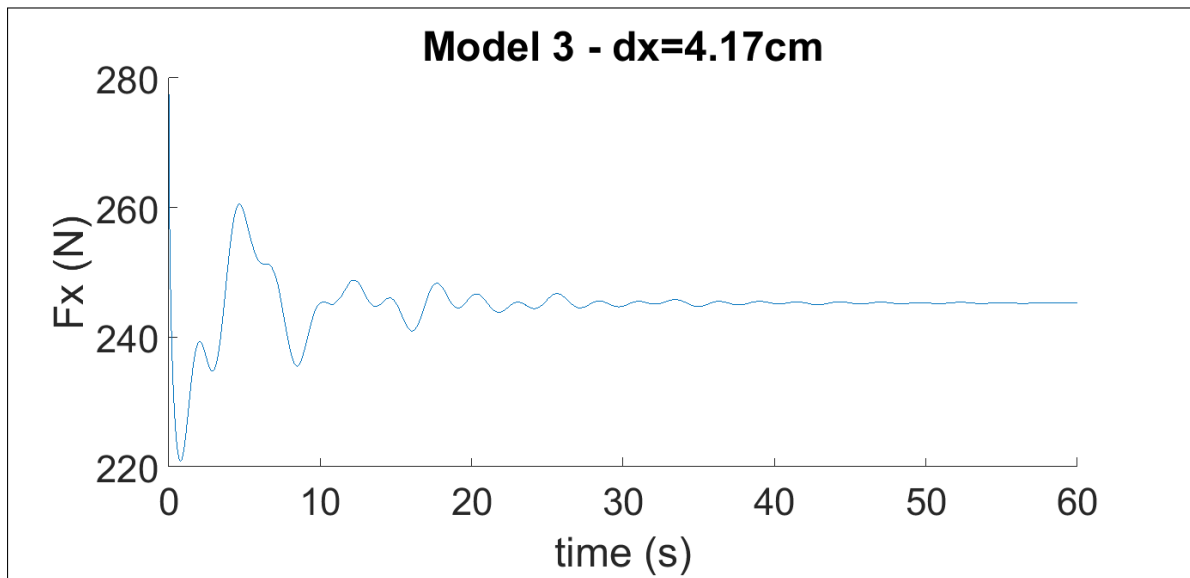
Figure B.3: *Model 3 - Time series. Mesh convergence study (Ergun porous model).*
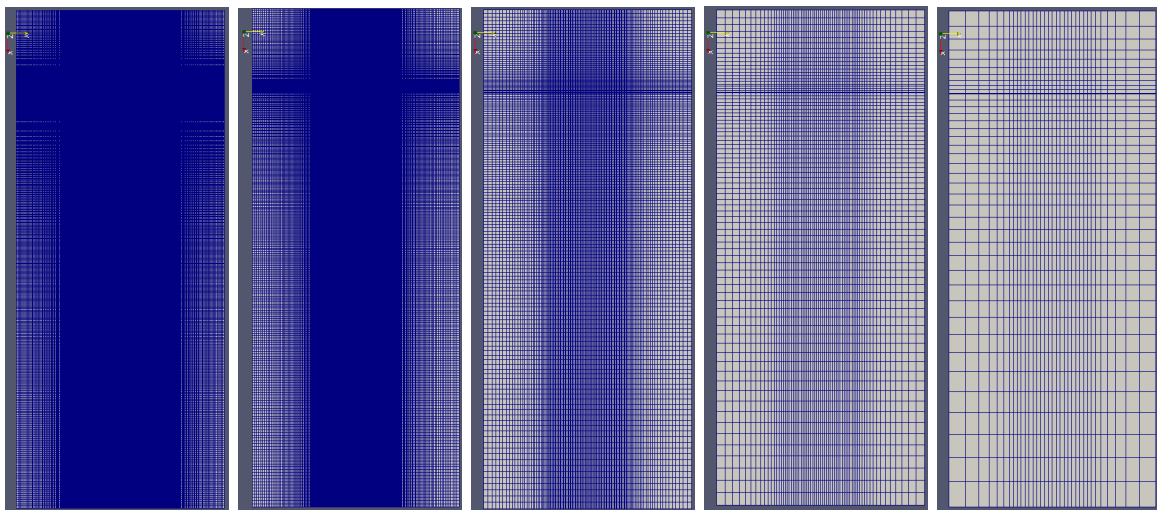
(a) $dx = 1.4cm$ **(b)** $dx = 2.1cm$ **(c)** $dx = 4.2cm$ **(d)** $dx = 8.3cm$ **(e)** $dx = 16.7cm$

Figure B.4: *Model 1 on ParaView - All meshes.*

B.2   Ergun porous drag forces
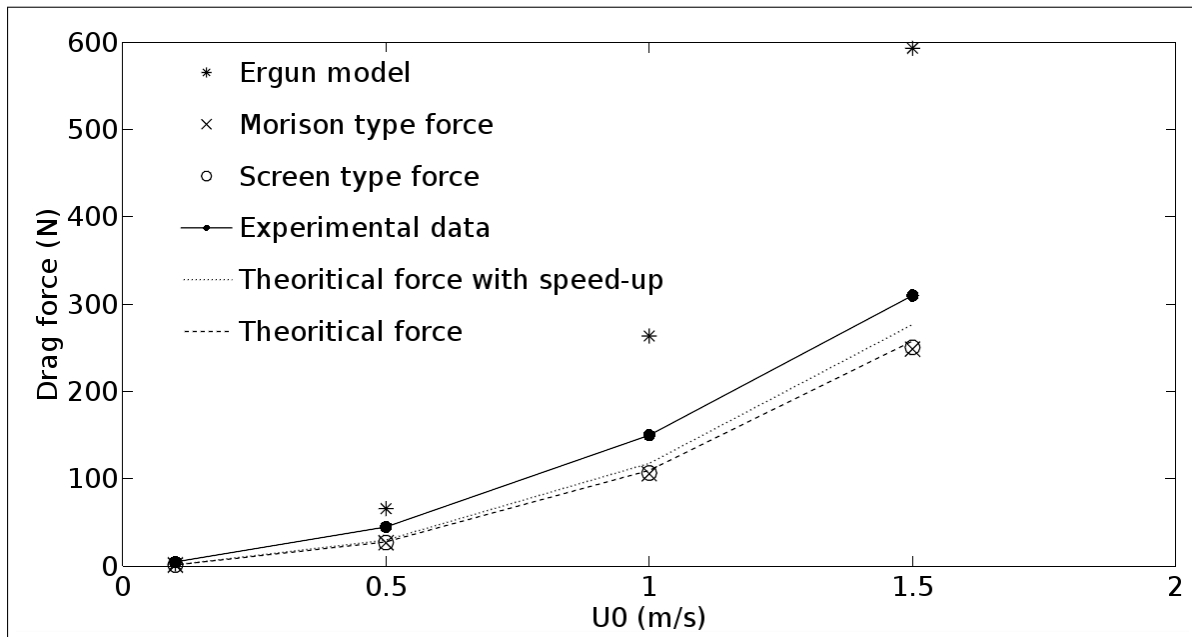
Figure B.5: *Model 2 - Comparison of numerical porous models with analytic and experimental forces. The Ergun porous forces are excessively high ($S_N = 0.20$).*
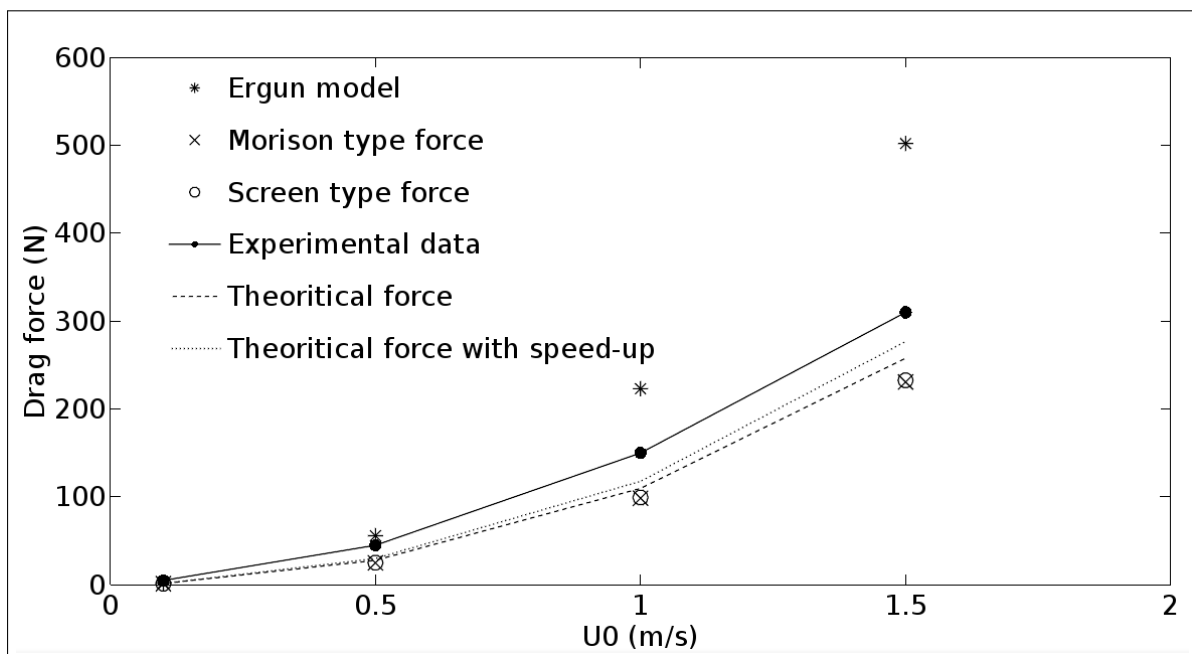
Figure B.6: *Model 1 - Comparison of numerical porous models with analytic and experimental forces. The Ergun porous forces are still excessively high ($S_N = 0.20$).*
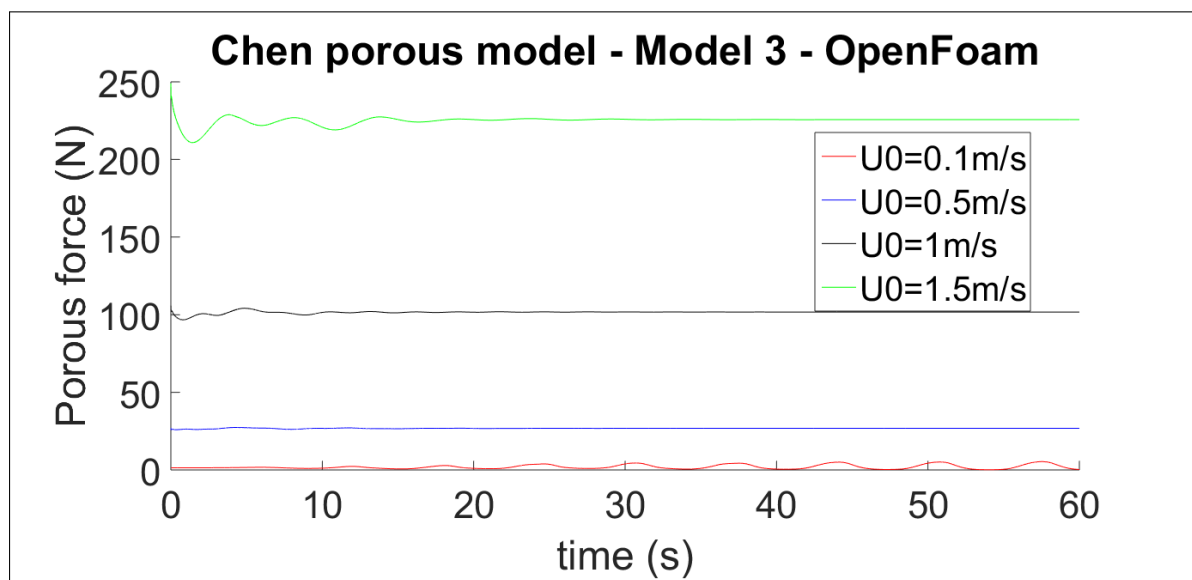
Figure B.7: *Time series of the Model 3, simulations run with the Chen porous model ($S_N = 0.202$).*

B.3   Wave lengths in the wake - Model 3
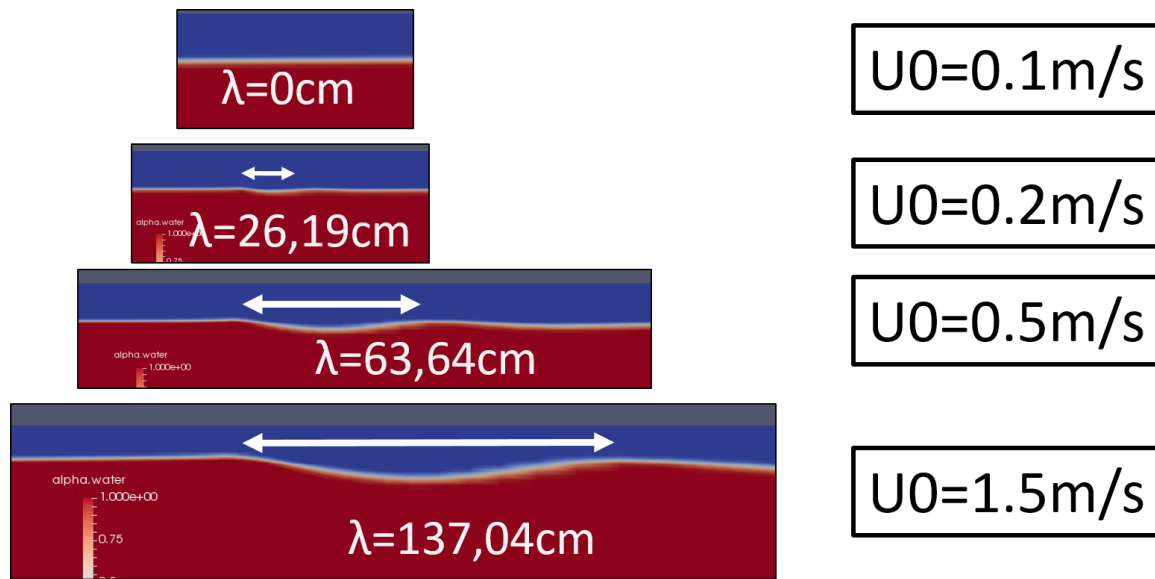
Figure B.8: *Wave lengths in the wake of the panels, measured in ParaView from the numerical model (Model 3).*

Table B.1: *Theoretical wave lengths of the wave generated behind the net (steady currents). The standing wave created by an obstacle placed in a steady flow (like a rock in a river) is discussed in "Marine Hydrodynamics" of J.N. Newman. Based on this theory, the theoretical was found as: $\lambda = \dfrac{2\pi U_0^2}{g}$*

U_0 [m/s]	0.1	0.2	0.3	0.4	0.5	0.6	0.7	0.8	0.9	1.0
λ [cm]	0.64	2.56	5.76	10.25	16.01	23.06	31.38	40.99	51.88	64.05

U_0 [m/s]	1.1	1.2	1.3	1.4	1.5
λ [cm]	77.50	92.23	108.24	125.54	144.11

C | Experimental results

Only S_N determined from the photos has been used for the results with waves conditions.

C.1   Results - Nets in currents

C.1.1   Small net panels

(a) C_D - S_N from photos.

(b) C_D - S_N from Equation 2.1.
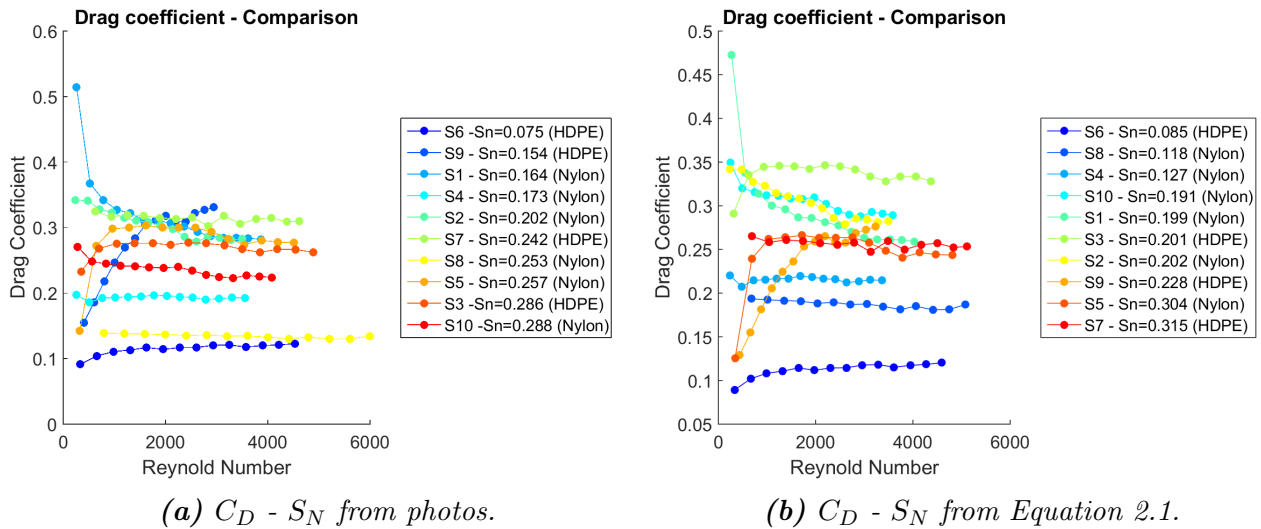
Figure C.1: *Drag coefficients - 1m×1m net panels.*

(a) C_L - S_N from photos.

(b) C_L - S_N from Equation 2.1.
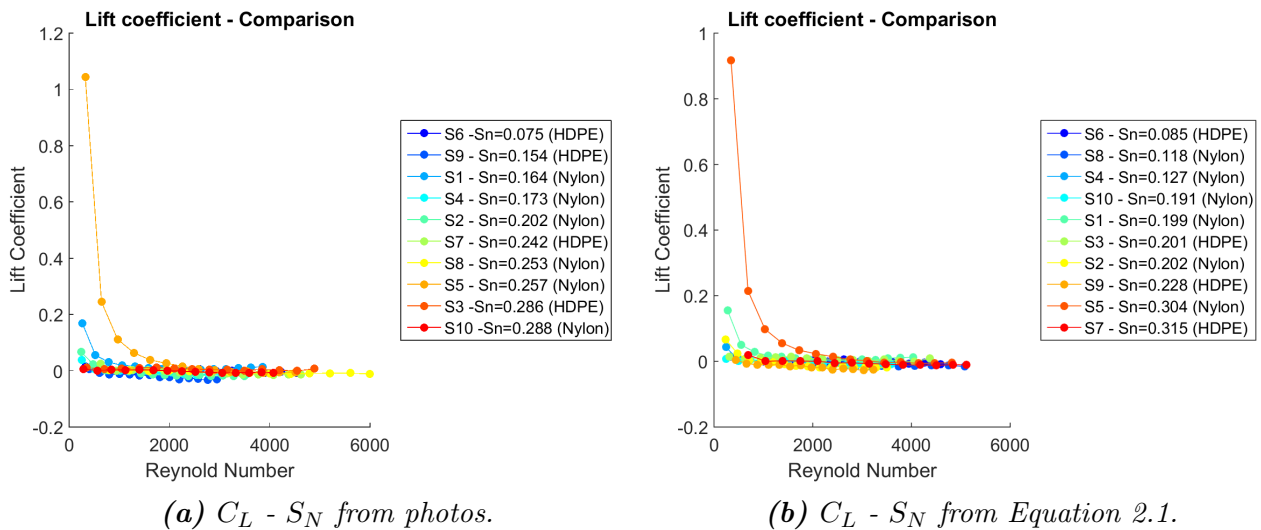
Figure C.2: *Lift coefficients - 1m×1m net panels.*

C.1.2   Repetitive tests

C.1.3   Large net panels

(a) F_X - S_N from photos.   **(b)** F_X - S_N from Equation 2.1.
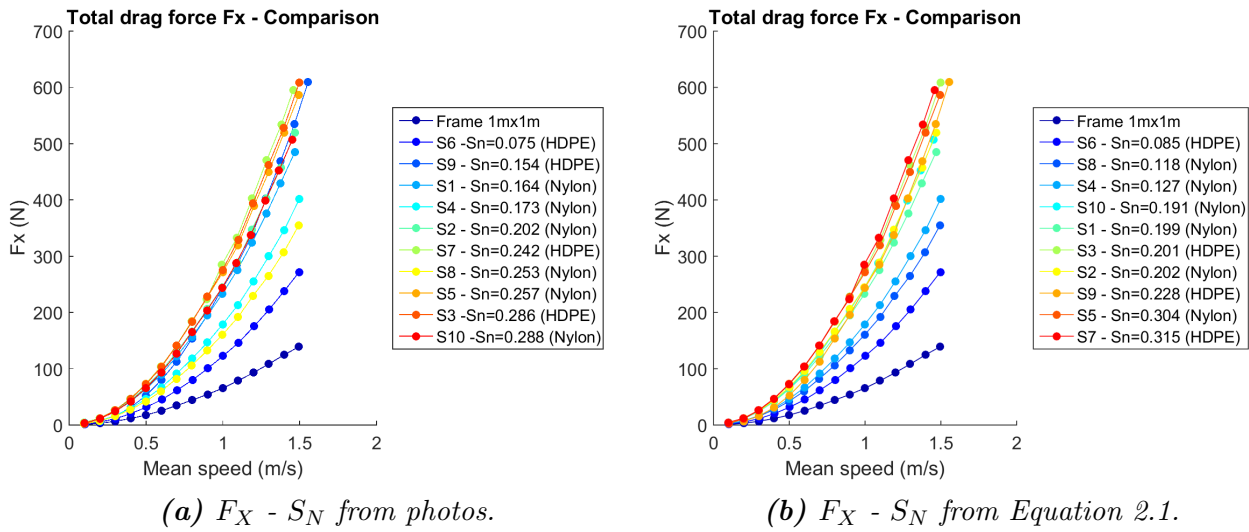
Figure C.3: *Total drag force - 1m×1m net panels.*

Figure C.4: *Force F_y, parallel to the transverse axis. It points out the asymmetry of the installation. $1m \times 1m$ net panels, S_N from Equation 2.1.*
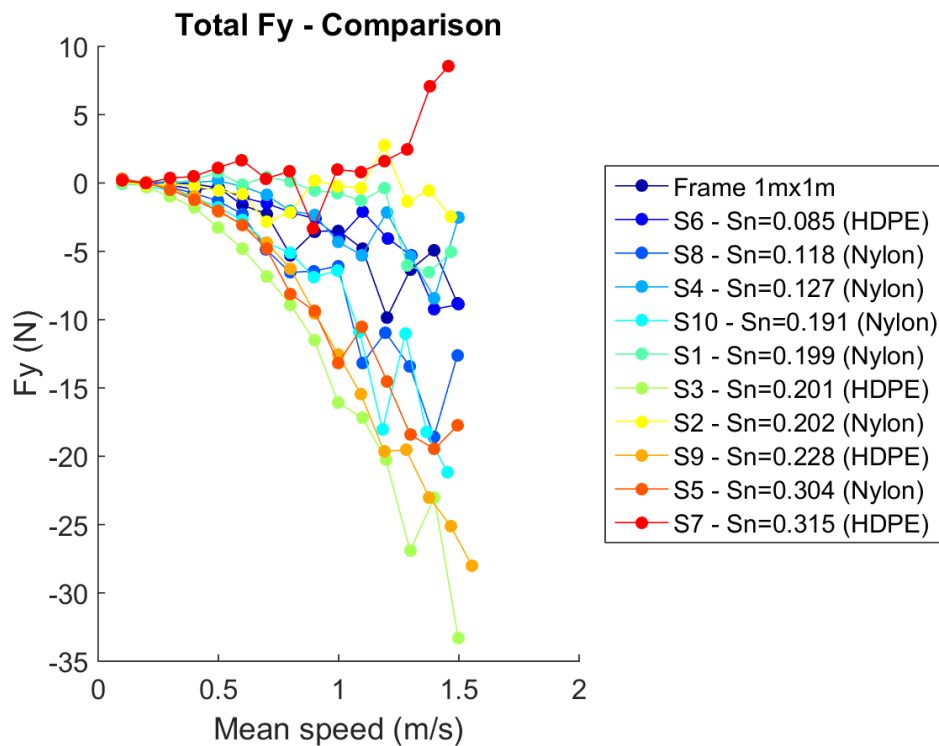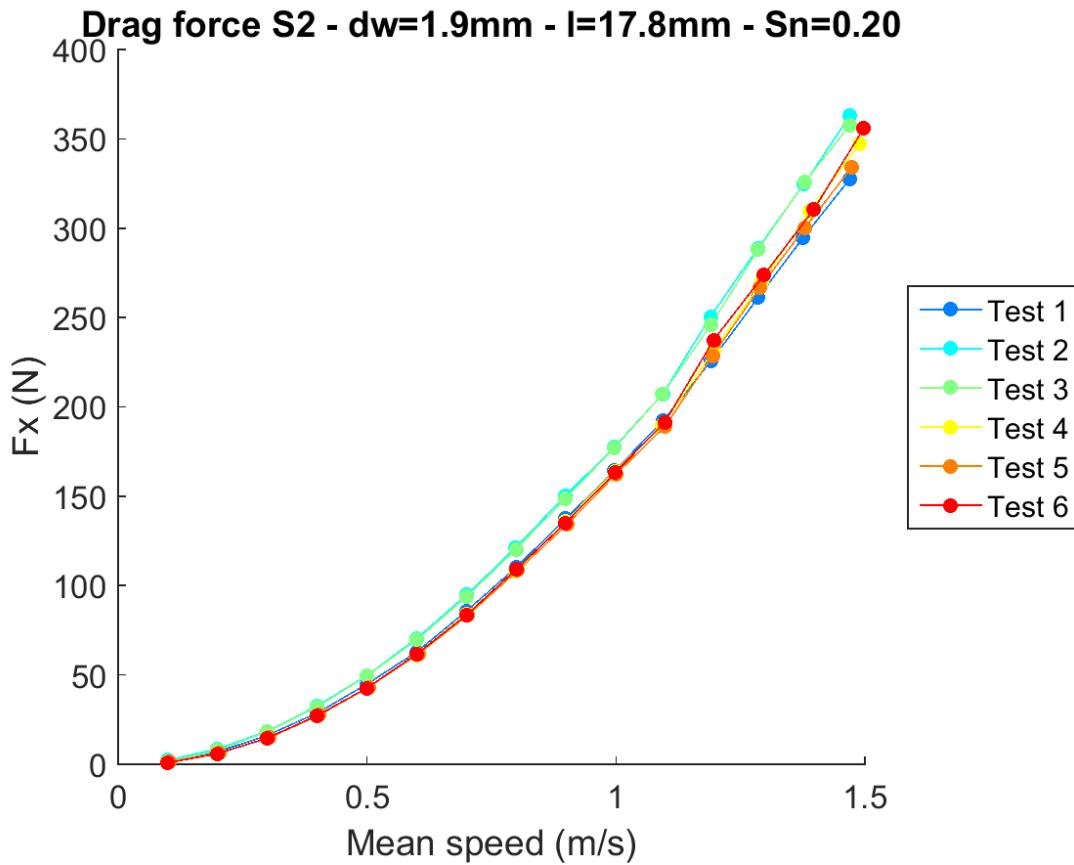
Figure C.5: *Drag force, repetitive tests (net S2). The force acting on the 1m×1m empty frames has been subtracted.*
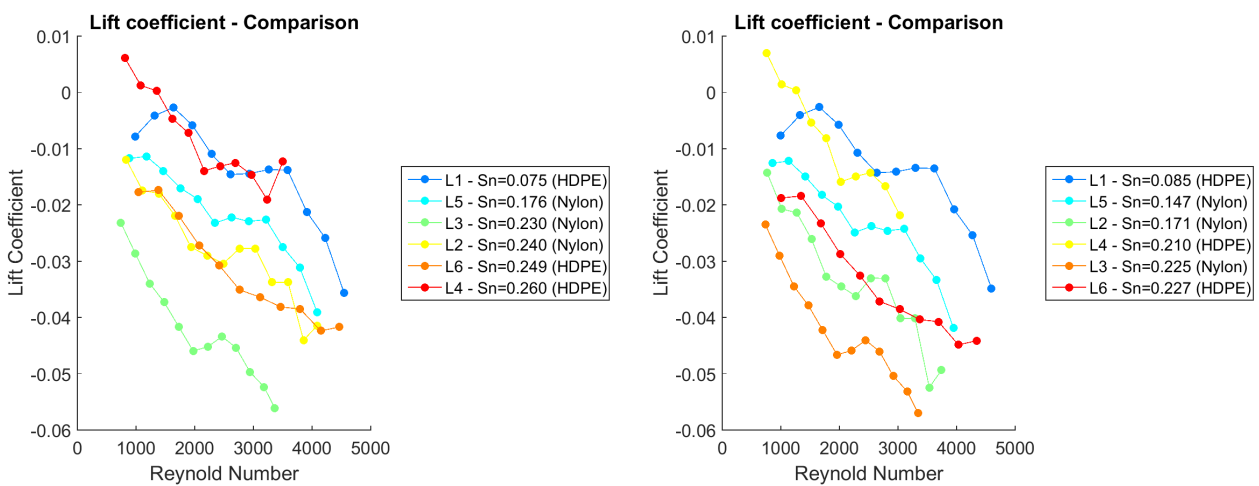
(a) C_L - S_N from photos.   **(b)** C_L - S_N from Equation 2.1.

Figure C.6: *Lift coefficients - 2.5m×1m net panels.*

C.2   Results - Nets in waves

C.2.1   Small net panels

(a) $\epsilon_w = \dfrac{1}{60}$.

(b) $\epsilon_w = \dfrac{1}{20}$.
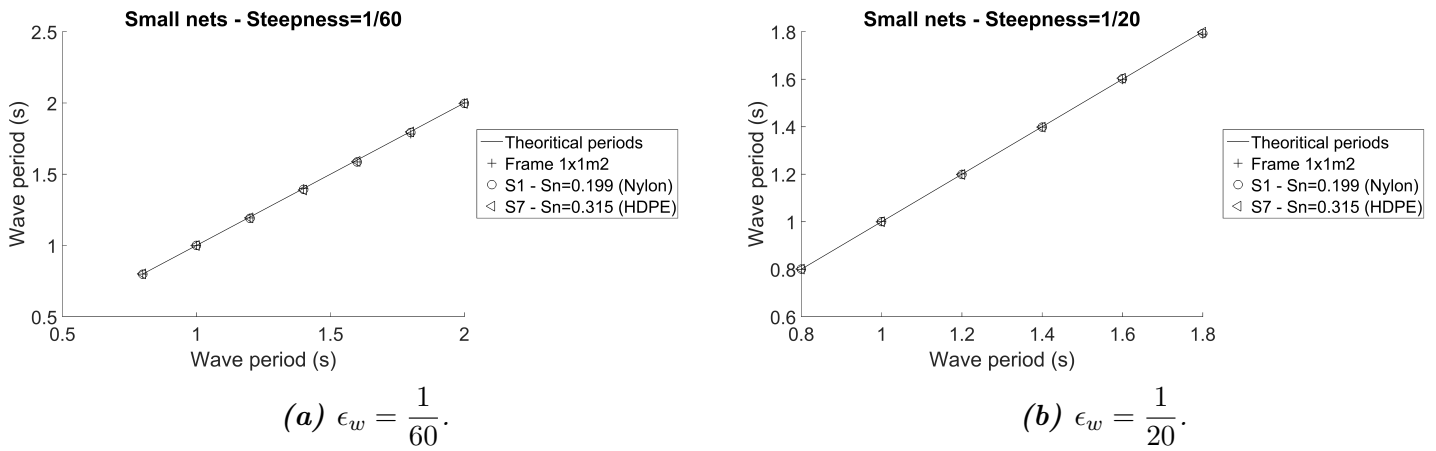
Figure C.7: *Wave periods measured from the carriage in front of the net (WP1) - 1m×1m net panels.*

(a) *Wave amplitude (WP1) in ω.*

(b) *Force amplitude in ω.*
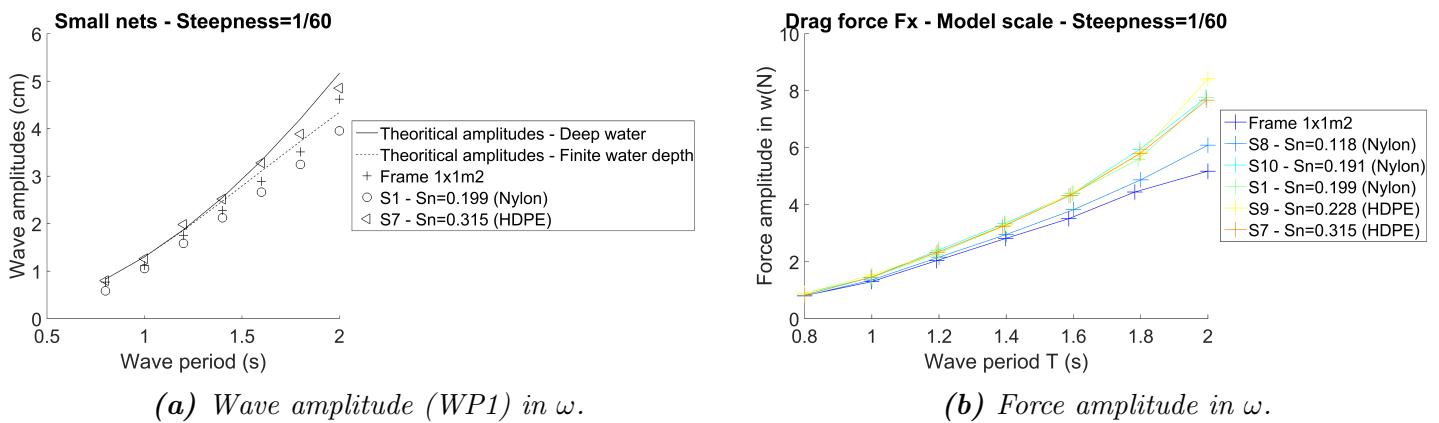
Figure C.8: *Wave and force amplitudes in ω - 1m×1m net panels, $\epsilon_w = \dfrac{1}{60}$.*

**(a)** *Wave amplitude (WP1) in* 2ω.

(b) *Force amplitude in* 2ω.
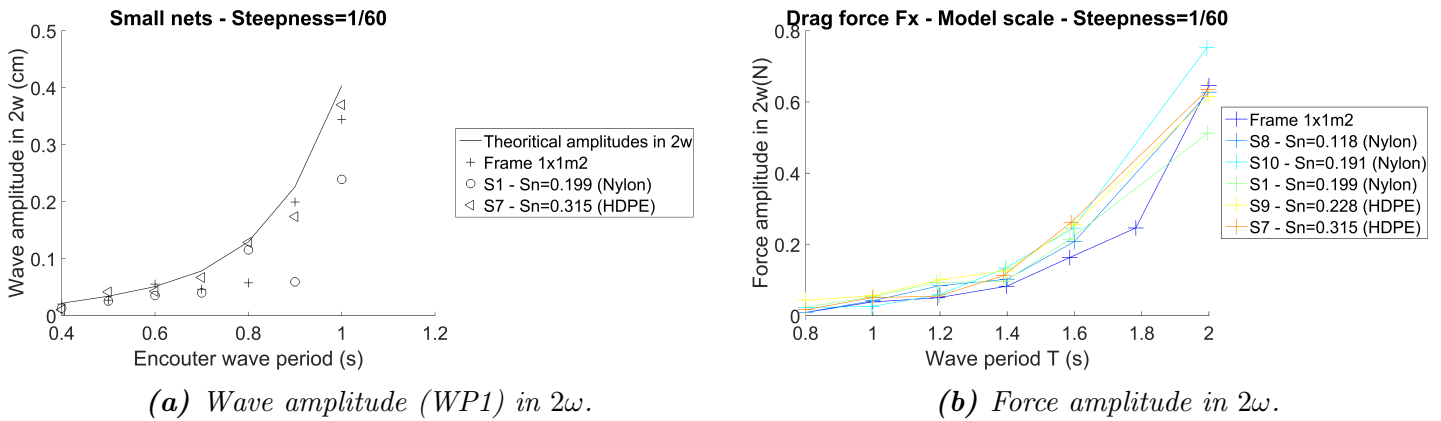
Figure C.9: *Wave and force amplitudes in* 2ω *-* $1m \times 1m$ *net panels,* $\epsilon_w = \dfrac{1}{60}$.

(a) *Wave amplitude (WP1) in* 3ω.

(b) *Force amplitude in* 3ω.
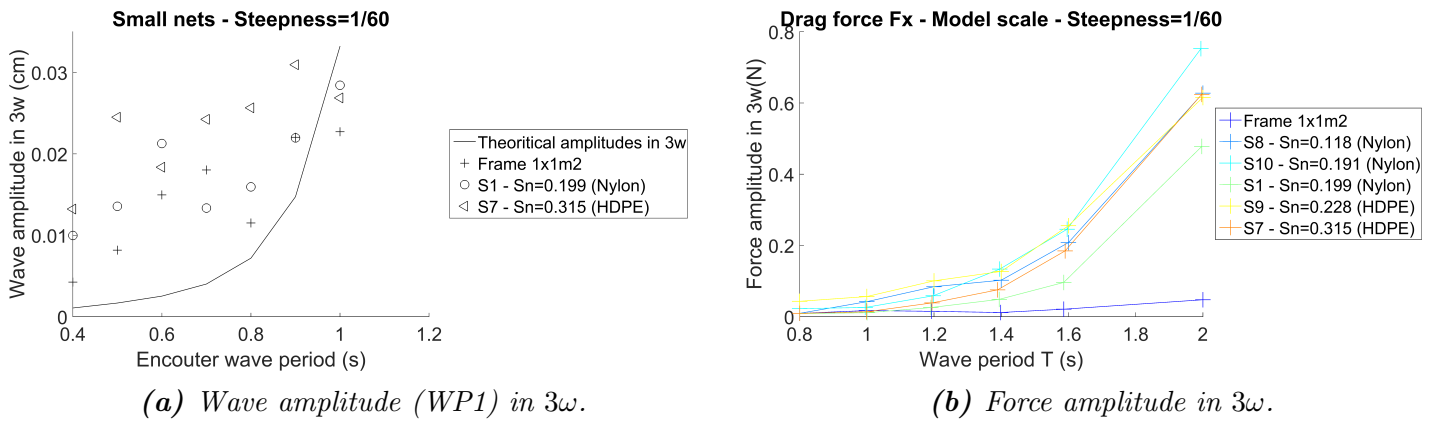
Figure C.10: *Wave and force amplitudes in* 3ω *-* $1m \times 1m$ *net panels,* $\epsilon_w = \dfrac{1}{60}$.
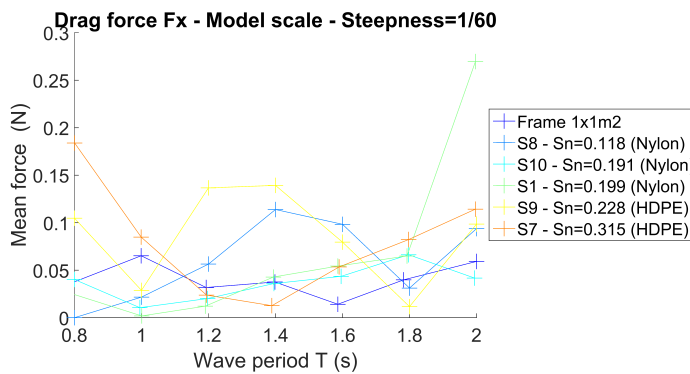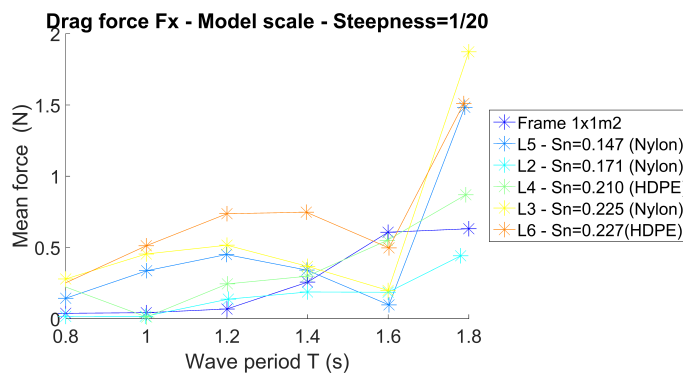

Figure C.11: *Mean drag force -* $1m \times 1m$ *net panels,* $\epsilon_w = \dfrac{1}{60}$.
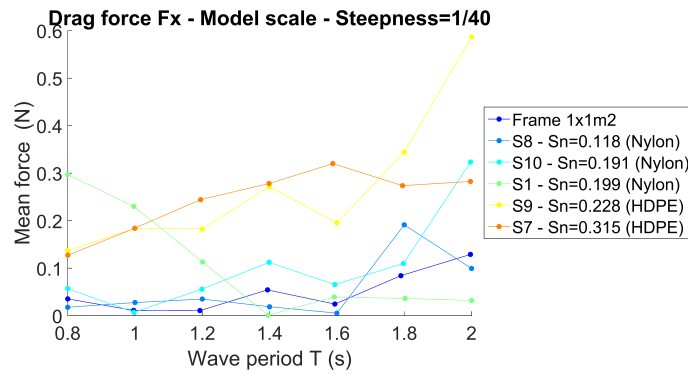
Figure C.12: *Mean drag force - 1m×1m net panels, $\epsilon_w = \dfrac{1}{40}$.*
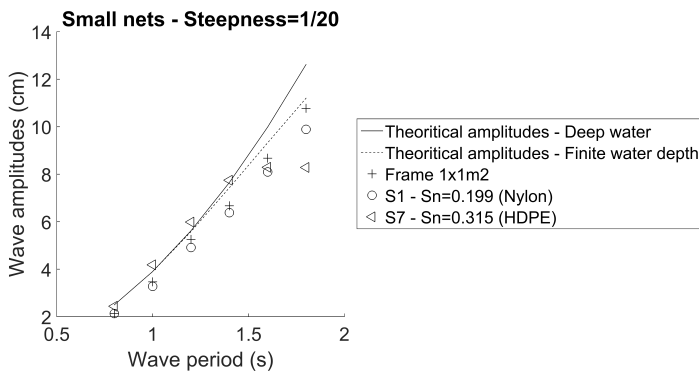
(a) *Wave amplitude (WP1) in ω.*
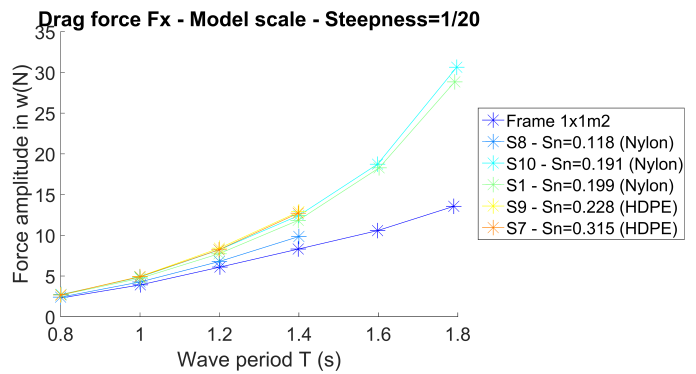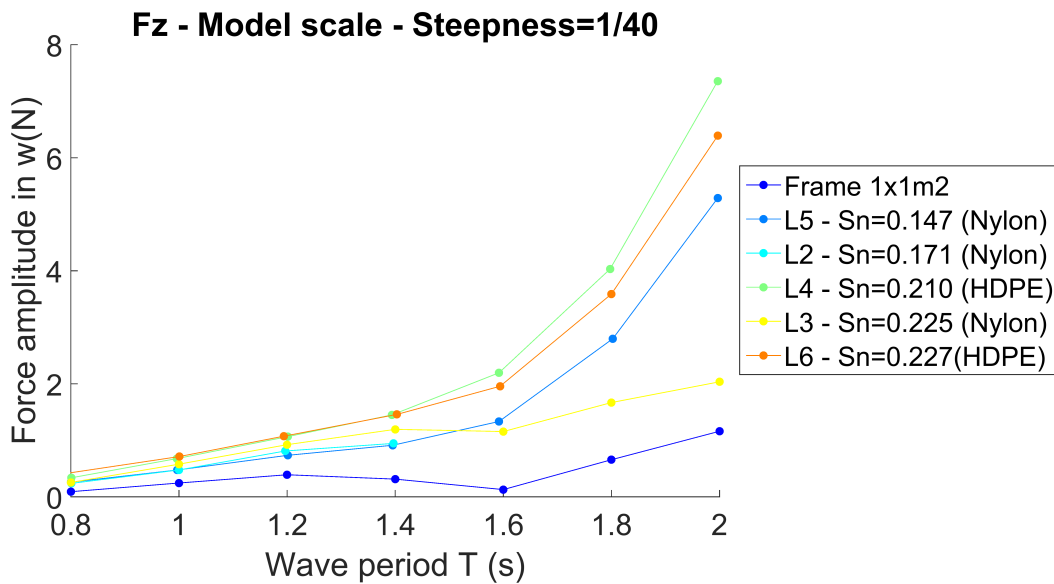

(b) *Force amplitude in ω.*

Figure C.13: *Wave and force amplitudes in ω - 1m×1m net panels, $\epsilon_w = \dfrac{1}{20}$.*
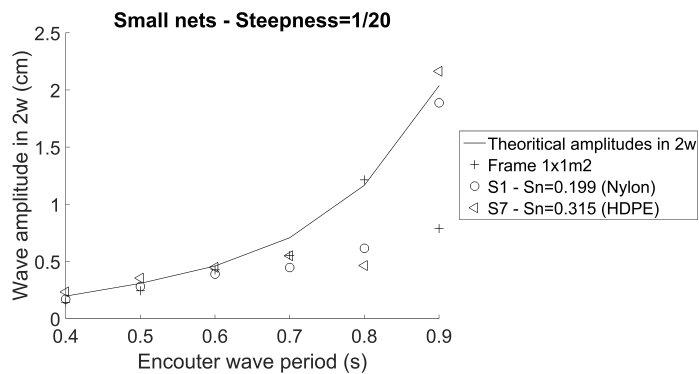
(a) *Wave amplitude (WP1) in 2ω.*
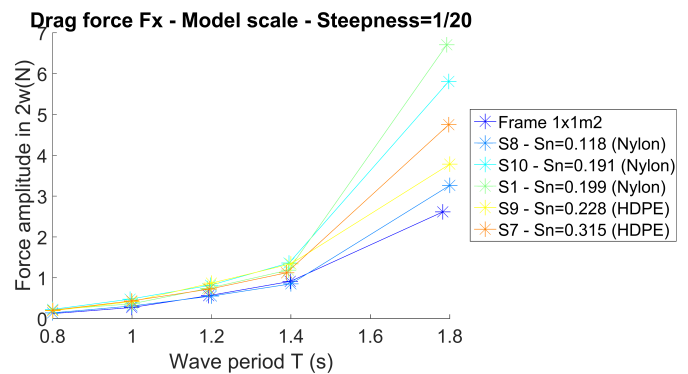
(b) *Force amplitude in 2ω.*

Figure C.14: *Wave and force amplitudes in 2ω - 1m×1m net panels, $\epsilon_w = \dfrac{1}{20}$.*

(a) *Wave amplitude (WP1) in* 3ω.

(b) *Force amplitude in* 3ω.
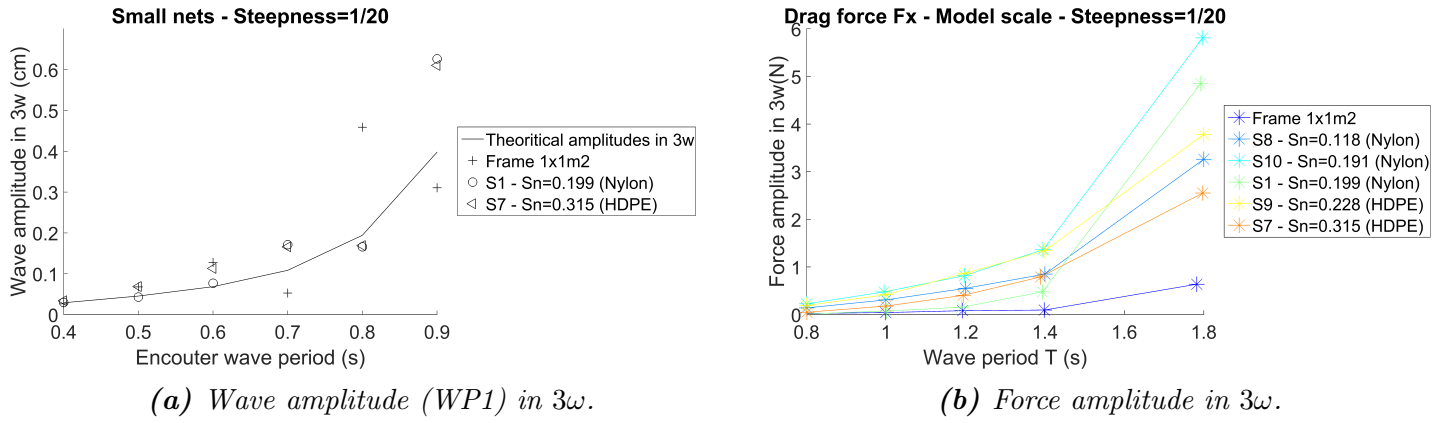
Figure C.15: *Wave and force amplitudes in* 3ω *- 1m×1m net panels,* $\epsilon_w = \dfrac{1}{20}$.
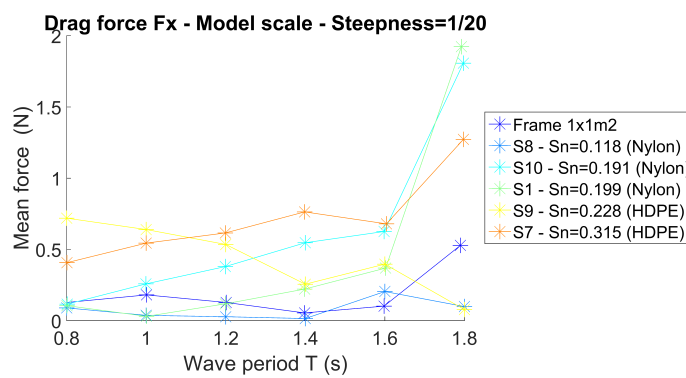
Figure C.16: *Mean drag force - 1m×1m net panels,* $\epsilon_w = \dfrac{1}{20}$.

C.2.2   Large net panels

(a) $\epsilon_w = \dfrac{1}{60}$.

(b) $\epsilon_w = \dfrac{1}{40}$.

(c) $\epsilon_w = \dfrac{1}{20}$.
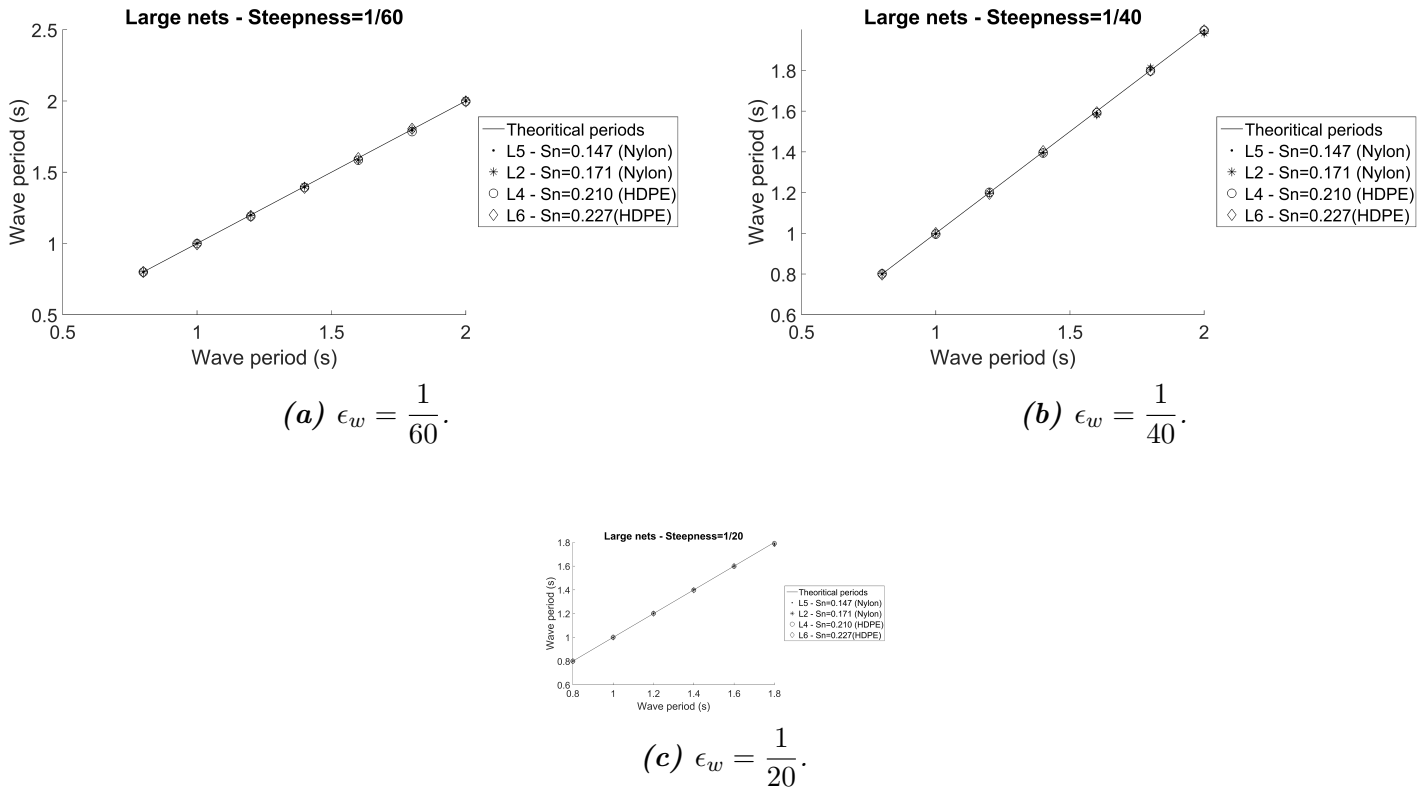
Figure C.17: *Wave periods measured from the carriage in front of the net (WP1), $\epsilon_w = \dfrac{1}{20}$ - 2.5m×1m net panels.*

(a) *Wave amplitude (WP1) in ω.*

(b) *Force amplitude in ω.*
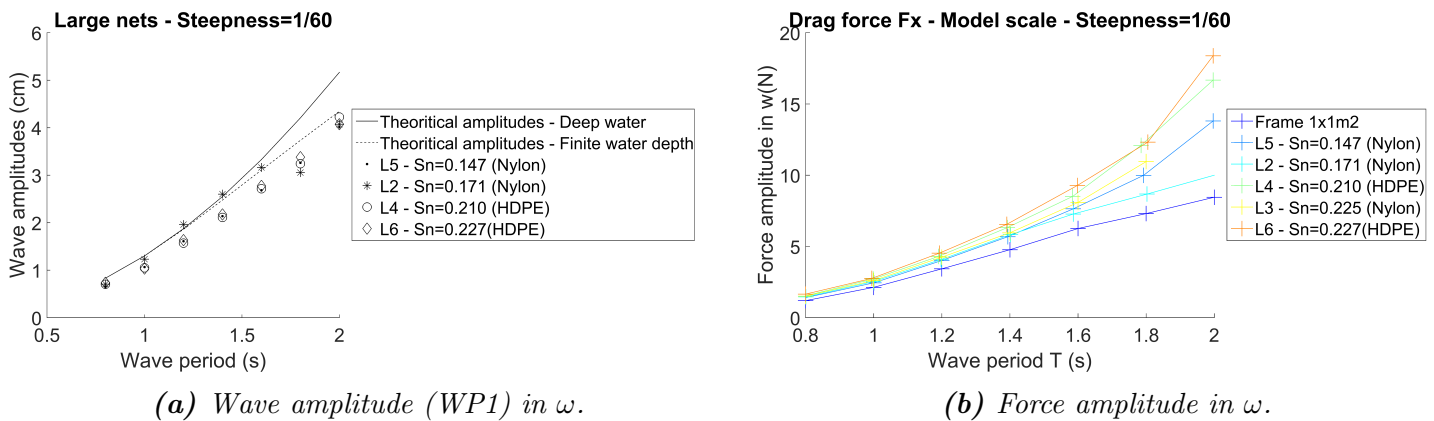
Figure C.18: *Wave and force amplitudes in ω - 2.5m×1m net panels, $\epsilon_w = \dfrac{1}{60}$.*

(a) *Wave amplitude (WP1) in* 2ω.

(b) *Force amplitude in* 2ω.
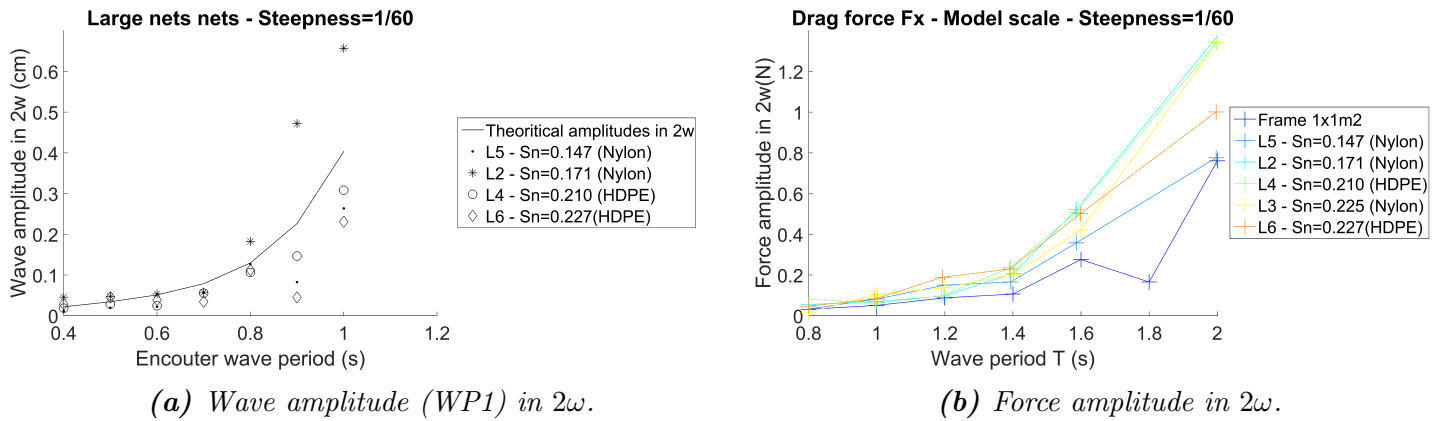
Figure C.19: *Wave and force amplitudes in* 2ω *- 2.5m×1m net panels,* $\epsilon_w = \dfrac{1}{60}$.

(a) *Wave amplitude (WP1) in* 3ω.

(b) *Force amplitude in* 3ω.
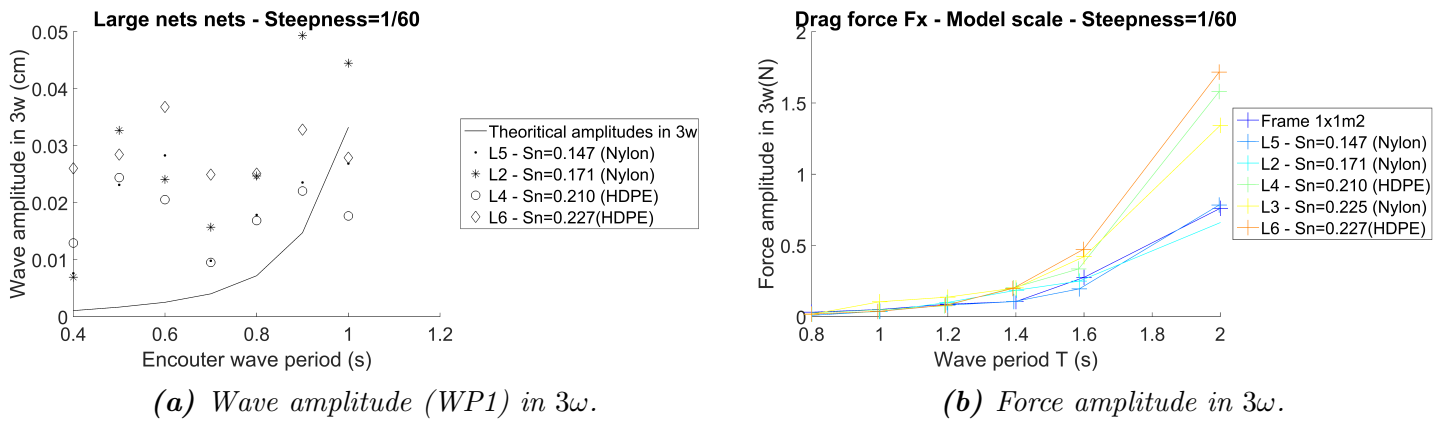
Figure C.20: *Wave and force amplitudes in* 3ω *- 2.5m×1m net panels,* $\epsilon_w = \dfrac{1}{60}$.
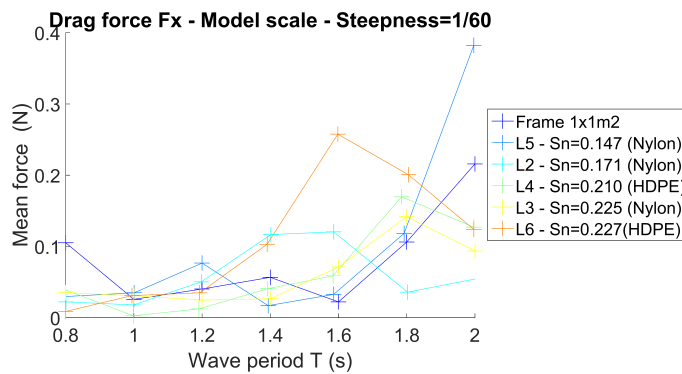
Figure C.21: *Mean drag force - 2.5m×1m net panels,* $\epsilon_w = \dfrac{1}{60}$.
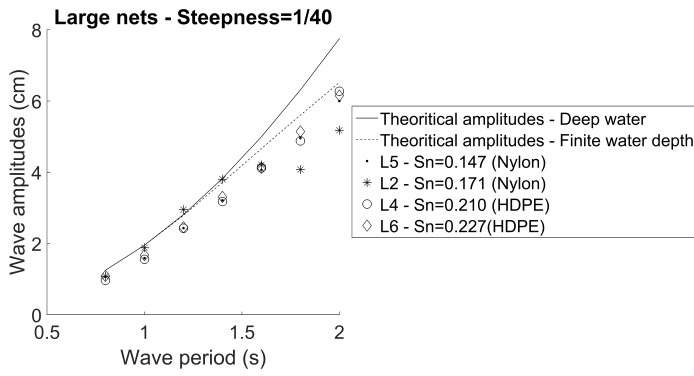
(a) *Wave amplitude (WP1) in ω.*
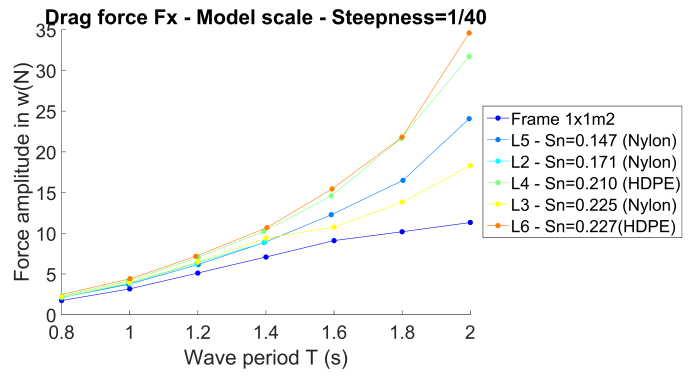
(b) *Force amplitude in ω.*

Figure C.22: *Wave and force amplitudes in ω - 2.5m×1m net panels, $\epsilon_w = \dfrac{1}{40}$.*
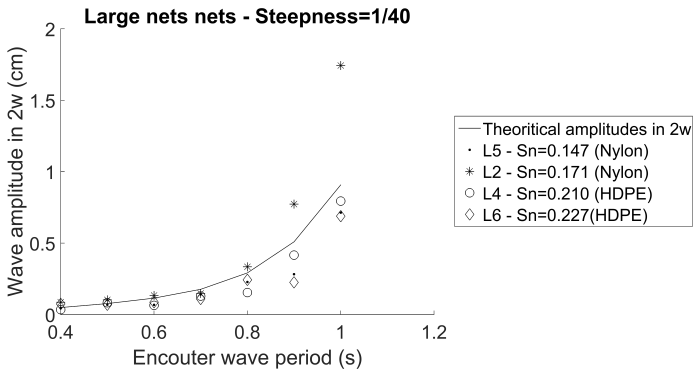
(a) *Wave amplitude (WP1) in 2ω.*
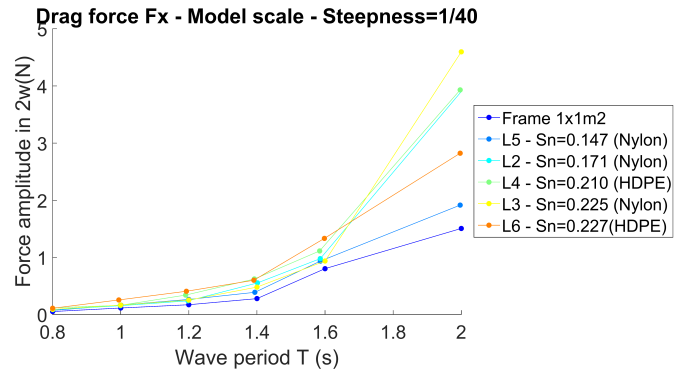
(b) *Force amplitude in 2ω.*

Figure C.23: *Wave and force amplitudes in 2ω - 2.5m×1m net panels, $\epsilon_w = \dfrac{1}{40}$.*
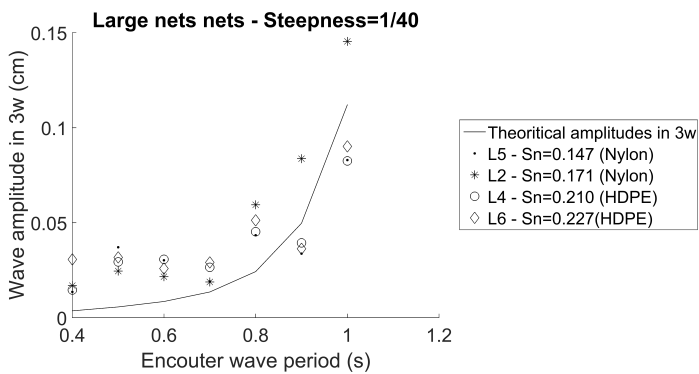
(a) *Wave amplitude (WP1) in 3ω.*
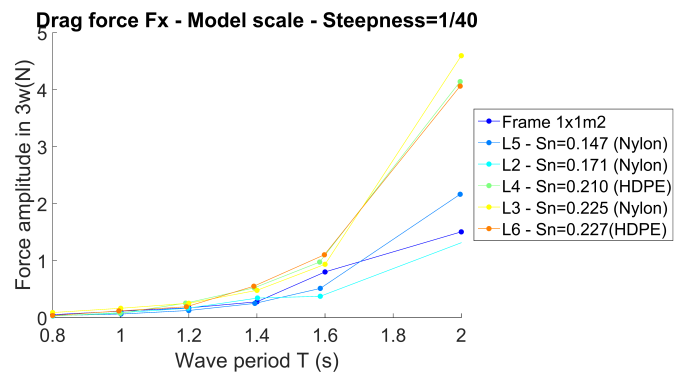
(b) *Force amplitude in 3ω.*

Figure C.24: *Wave and force amplitudes in 3ω - 2.5m×1m net panels, $\epsilon_w = \dfrac{1}{40}$.*
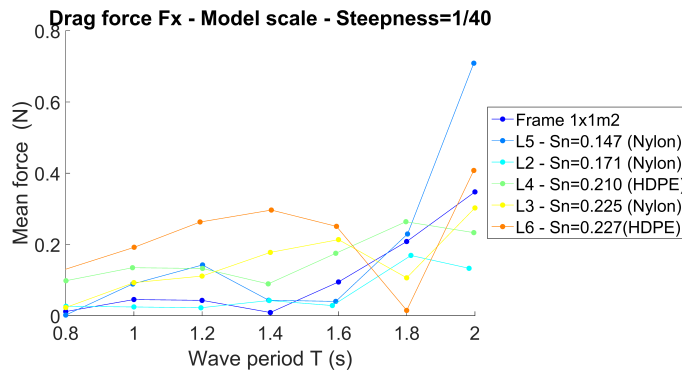
Figure C.25: *Mean drag force - 2.5m×1m net panels, $\epsilon_w = \dfrac{1}{40}$.*
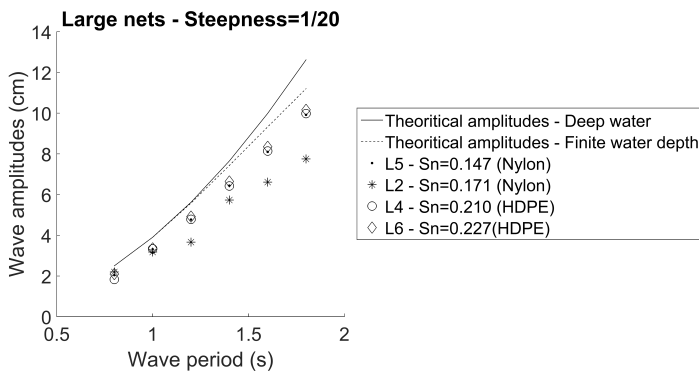
(a) *Wave amplitude (WP1) in ω.*
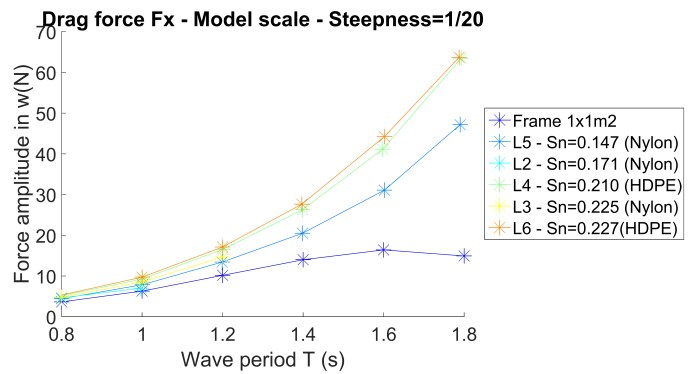
(b) *Force amplitude in ω.*

Figure C.26: *Wave and force amplitudes in ω - 2.5m×1m net panels, $\epsilon_w = \dfrac{1}{20}$.*
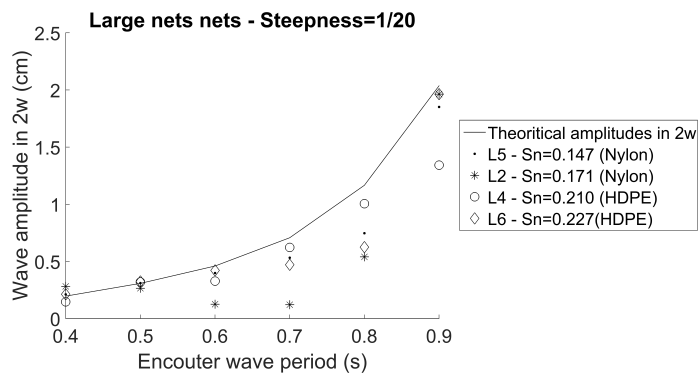
(a) *Wave amplitude (WP1) in 2ω.*
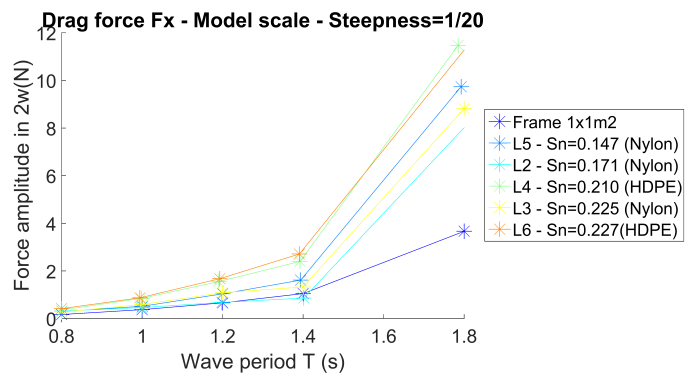
(b) *Force amplitude in 2ω.*

Figure C.27: *Wave and force amplitudes in 2ω - 2.5m×1m net panels, $\epsilon_w = \dfrac{1}{20}$.*
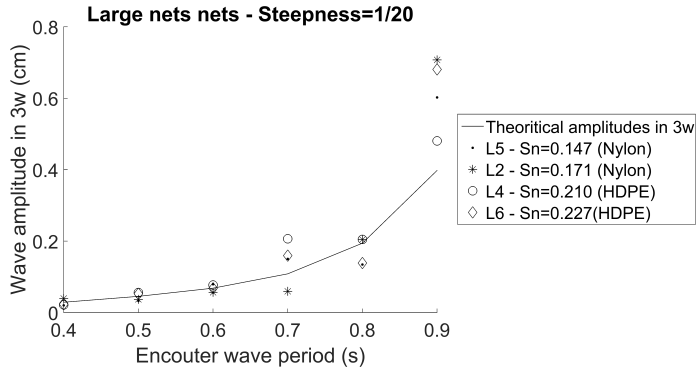
(a) *Wave amplitude (WP1) in* 3ω.
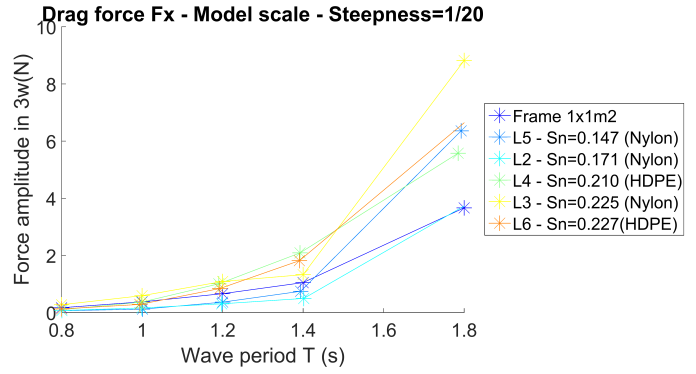
(b) *Force amplitude in* 3ω.

Figure C.28: *Wave and force amplitudes in* 3ω *- 2.5m×1m net panels,* $\epsilon_w = \dfrac{1}{20}$.

Figure C.29: *Mean drag force - 2.5m×1m net panels,* $\epsilon_w = \dfrac{1}{20}$.

C.2.3   Vertical loads F_z
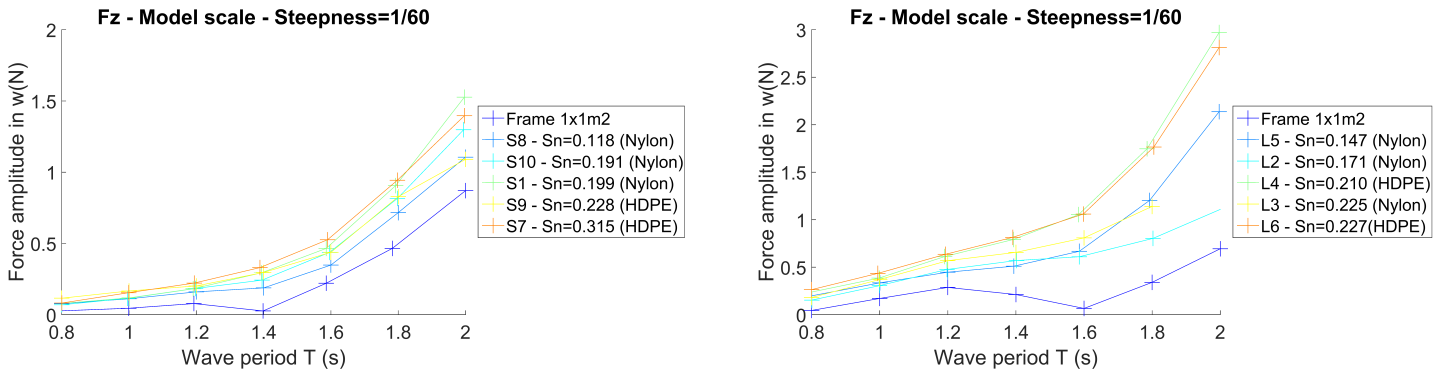
(a) *1m×1m net panels.*

(b) *2.5m×1m net panels.*

Figure C.30: *Vertical force amplitude F_z in ω, $\epsilon_w = \dfrac{1}{60}$.*

Figure C.31: *Vertical force amplitude F_z in ω - 2.5m×1m net panels, $\epsilon_w = \dfrac{1}{40}$.*
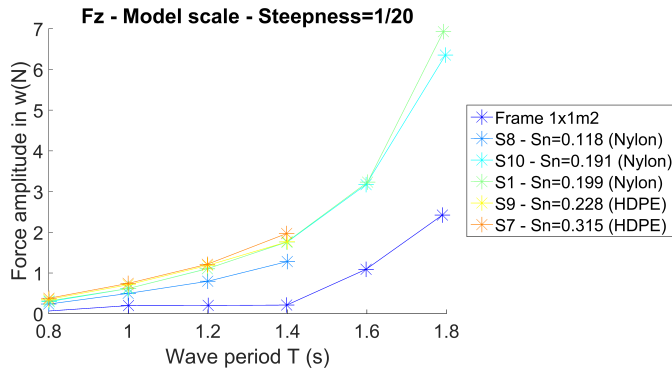
(a) *1m×1m net panels.*
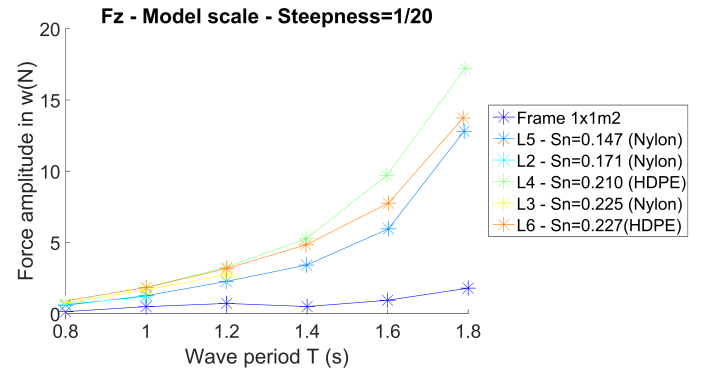
(b) *2.5m×1m net panels.*

Figure C.32: *Vertical force amplitude F_z in ω, $\epsilon_w = \dfrac{1}{20}$.*
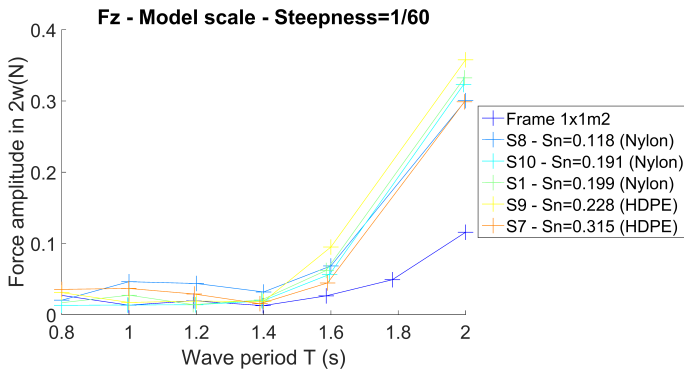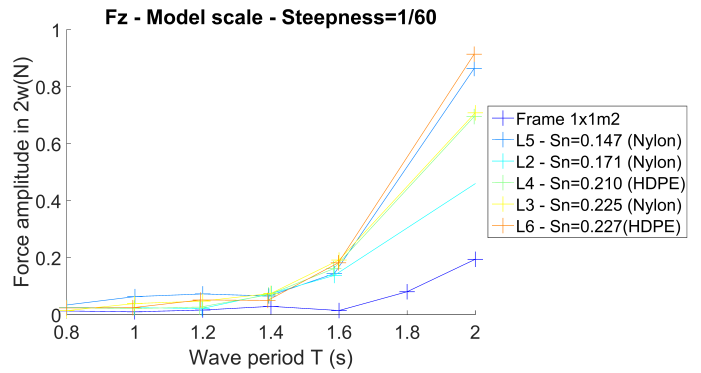
(a) *1m×1m net panels.*

(b) *2.5m×1m net panels.*

Figure C.33: *Vertical force amplitude F_z in 2ω, $\epsilon_w = \dfrac{1}{60}$.*
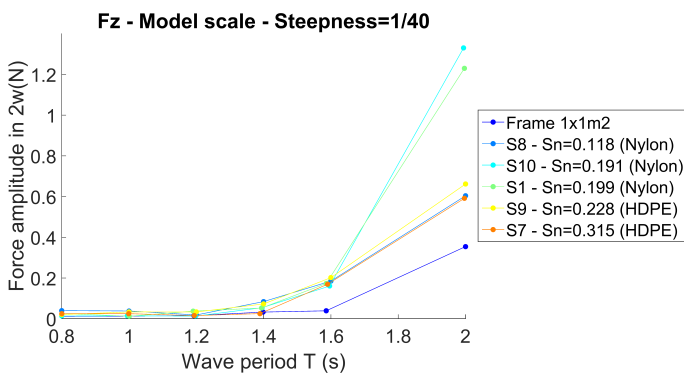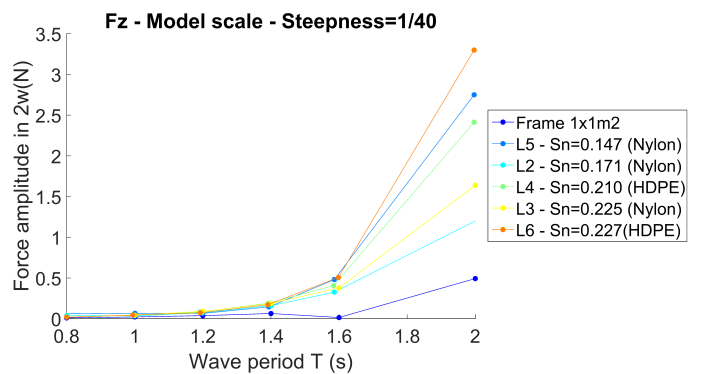
(a) *1m×1m net panels.*

(b) *2.5m×1m net panels.*

Figure C.34: *Vertical force amplitude F_z in 2ω, $\epsilon_w = \dfrac{1}{40}$.*
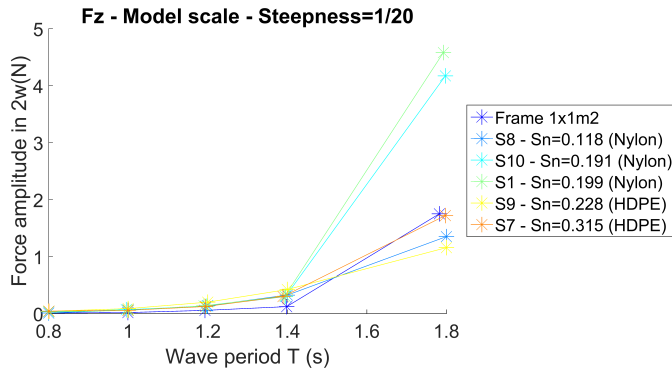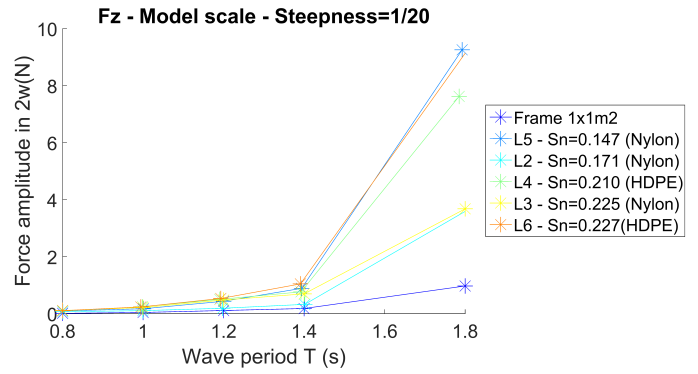
(a) *1m×1m net panels.*

(b) *2.5m×1m net panels.*

Figure C.35: *Vertical force amplitude F_z in 2ω, $\epsilon_w = \dfrac{1}{20}$.*
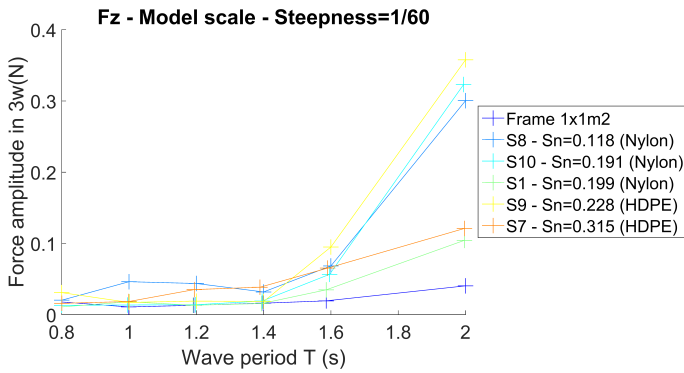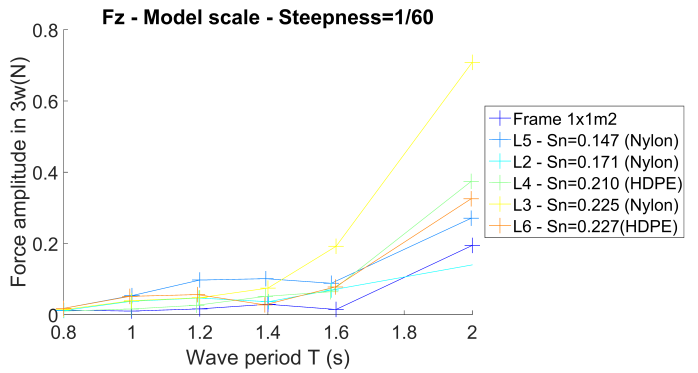
(a) *1m×1m net panels.*

(b) *2.5m×1m net panels.*

Figure C.36: *Vertical force amplitude F_z in 3ω, $\epsilon_w = \dfrac{1}{60}$.*
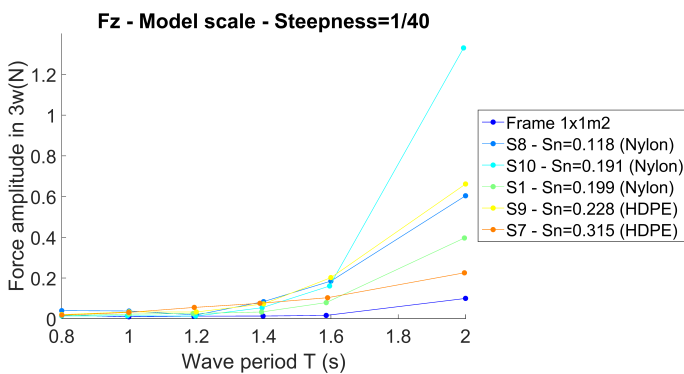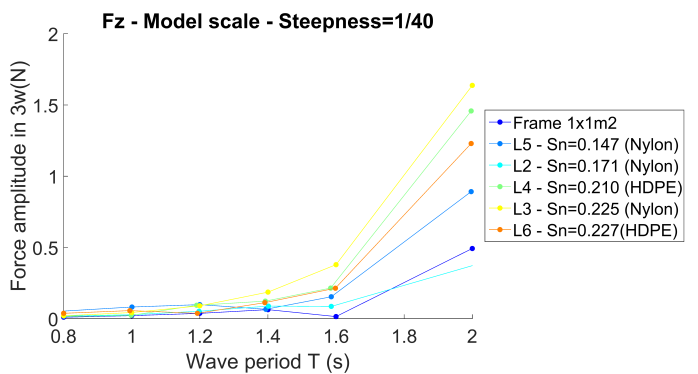
(a) *1m×1m net panels.*

(b) *2.5m×1m net panels.*

Figure C.37: *Vertical force amplitude F_z in 3ω, $\epsilon_w = \dfrac{1}{40}$.*

(a) *1m×1m net panels.*
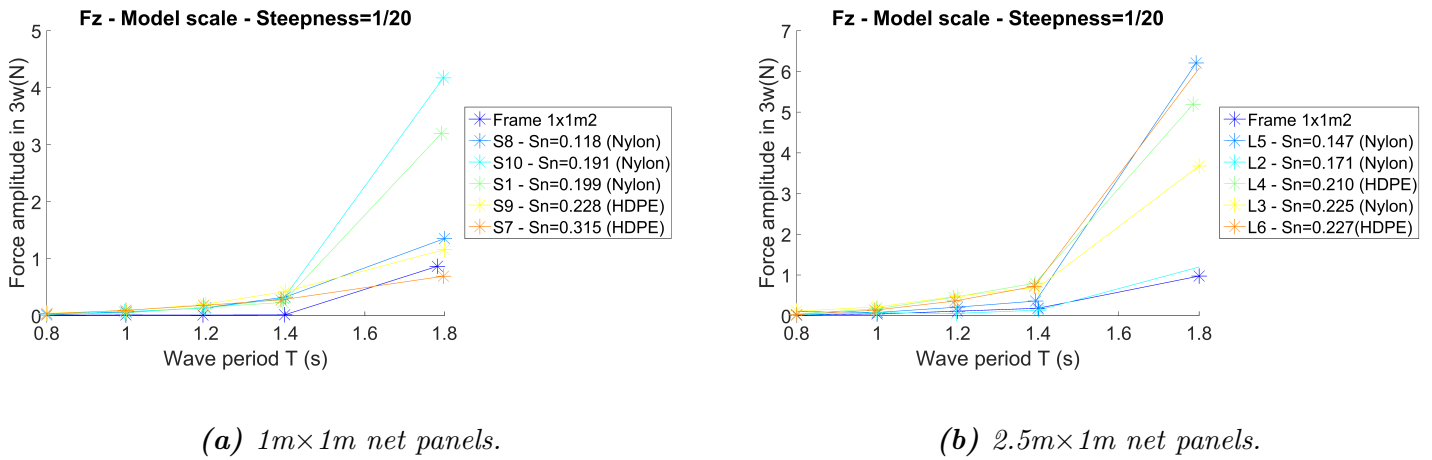
(b) *2.5m×1m net panels.*

Figure C.38: *Vertical force amplitude F_z in 3ω, $\epsilon_w = \dfrac{1}{20}$.*
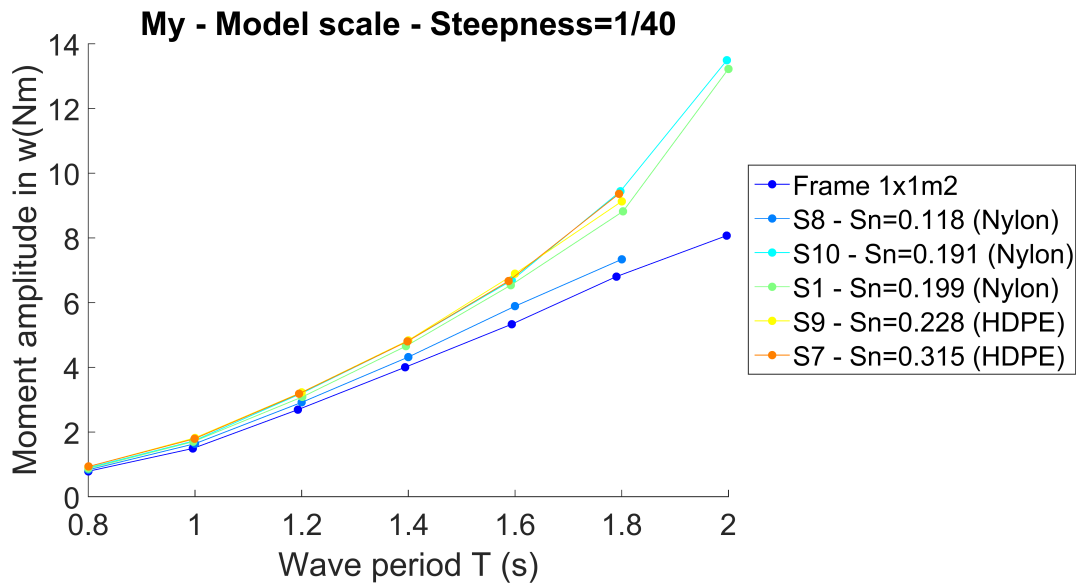
Figure C.39: *Example of results in moment. Amplitude of M_y in ω - 1m×1m net panels, $\epsilon_w = \dfrac{1}{40}$.*

C.3   Results - Nets in waves and currents

C.3.1   1m×1m net panels

(a) $\epsilon_w = \dfrac{1}{40}$.

(b) $\epsilon_w = \dfrac{1}{20}$.
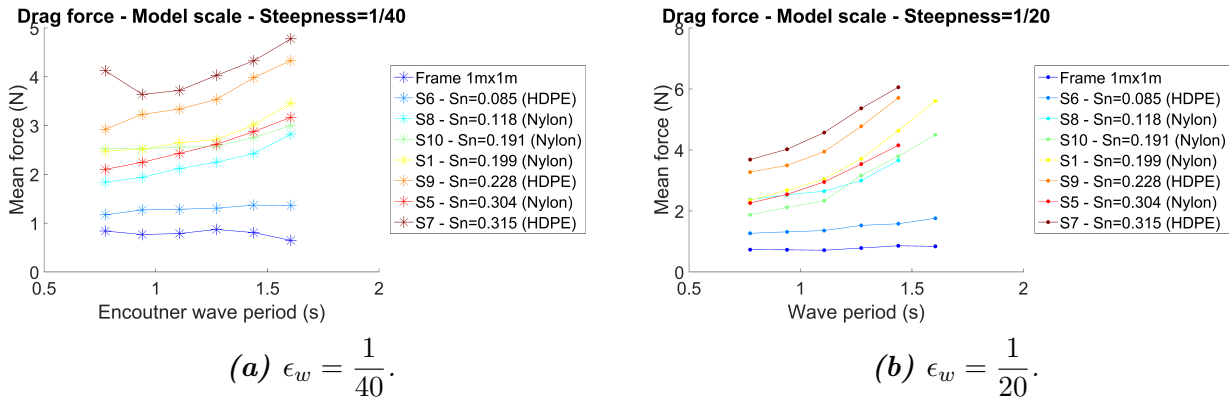
Figure C.40: *Mean drag force - 1m×1m net panels, $U_0 = 0.1m/s$.*

(a) $\epsilon_w = \dfrac{1}{40}$.

(b) $\epsilon_w = \dfrac{1}{20}$.
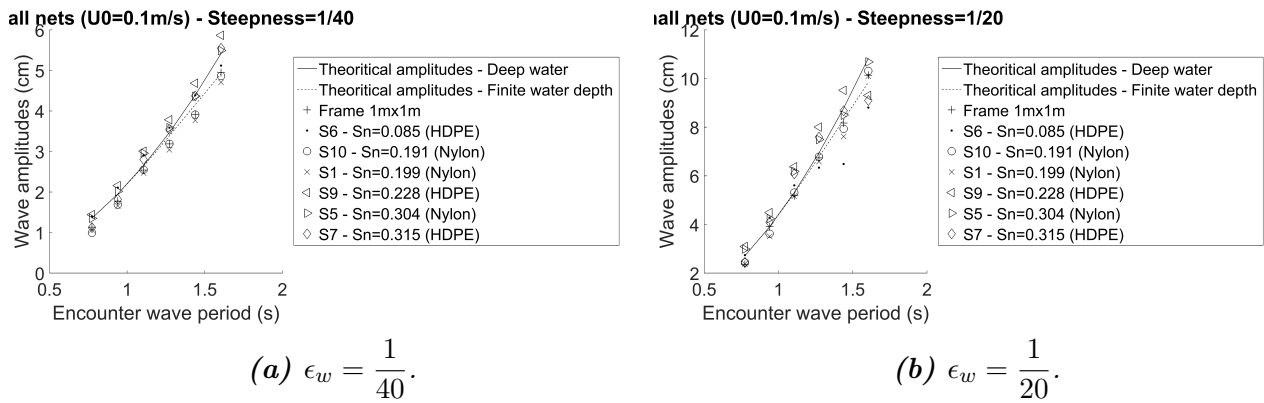
Figure C.41: *Wave amplitudes measured from the carriage in front of the net (WP1) - 1m×1m net panels, $U_0 = 0.1m/s$.*

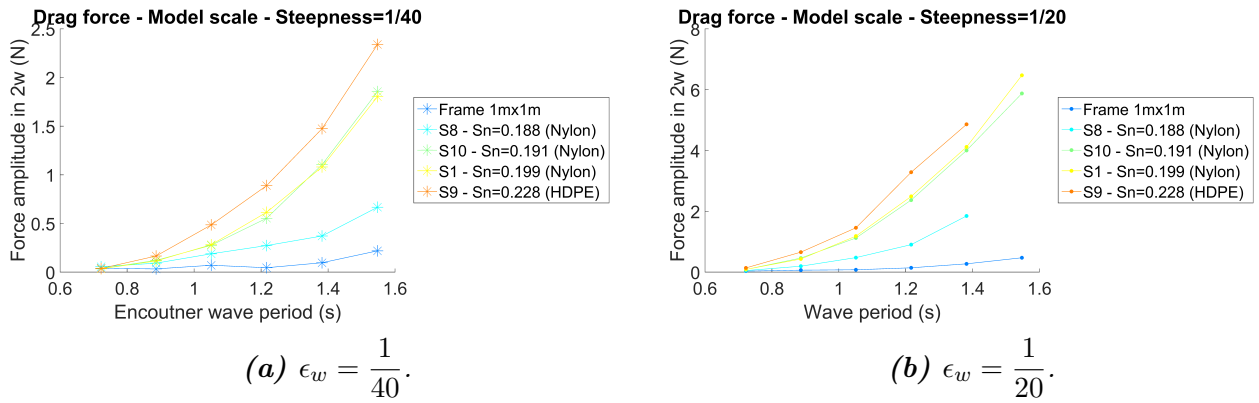**(a)** $\epsilon_w = \dfrac{1}{40}$.

(b) $\epsilon_w = \dfrac{1}{20}$.
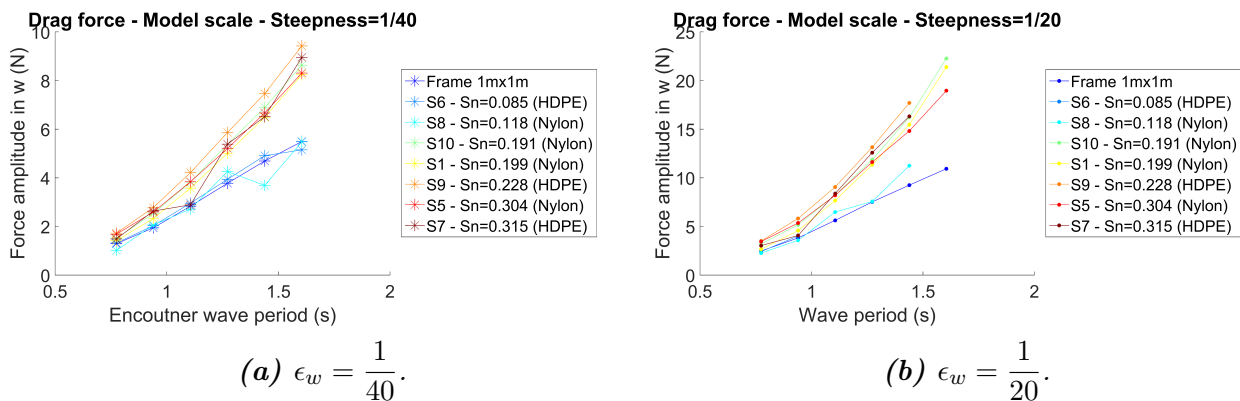
Figure C.42: *Force amplitudes (in ω) - 1m×1m net panels, $U_0 = 0.1m/s$.*

(a) $\epsilon_w = \dfrac{1}{40}$.

(b) $\epsilon_w = \dfrac{1}{20}$.
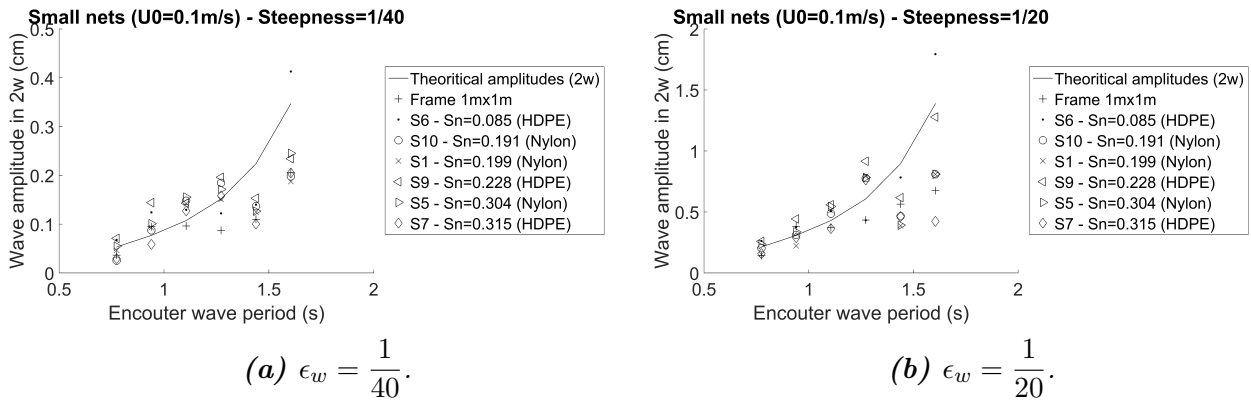
Figure C.43: *Wave amplitudes in 2ω measured from the carriage in front of the net (WP1) - $1m \times 1m$ net panels, $U_0 = 0.1m/s$.*

(a) $\epsilon_w = \dfrac{1}{40}$.

(b) $\epsilon_w = \dfrac{1}{20}$.
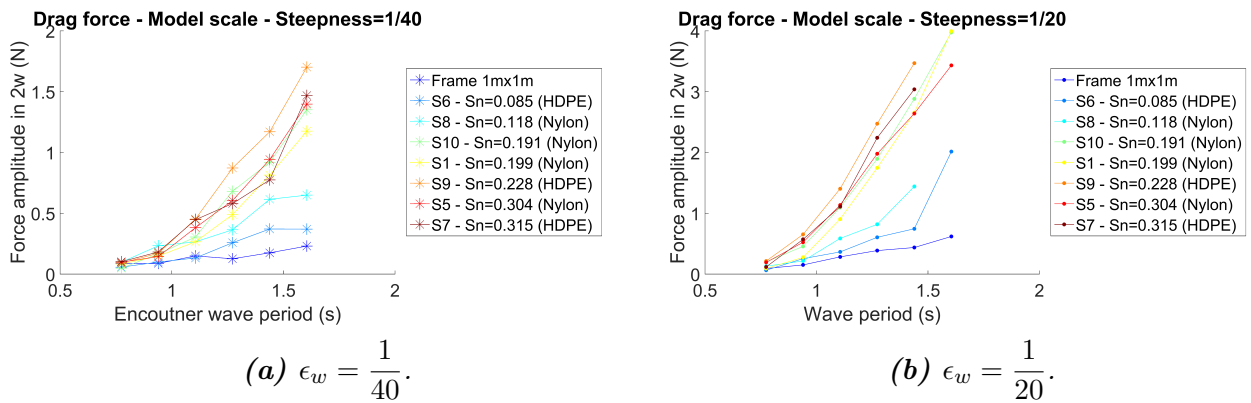
Figure C.44: *Force amplitudes in 2ω - $1m \times 1m$ net panels, $U_0 = 0.1m/s$.*

(a) $\epsilon_w = \dfrac{1}{40}$.

(b) $\epsilon_w = \dfrac{1}{20}$.
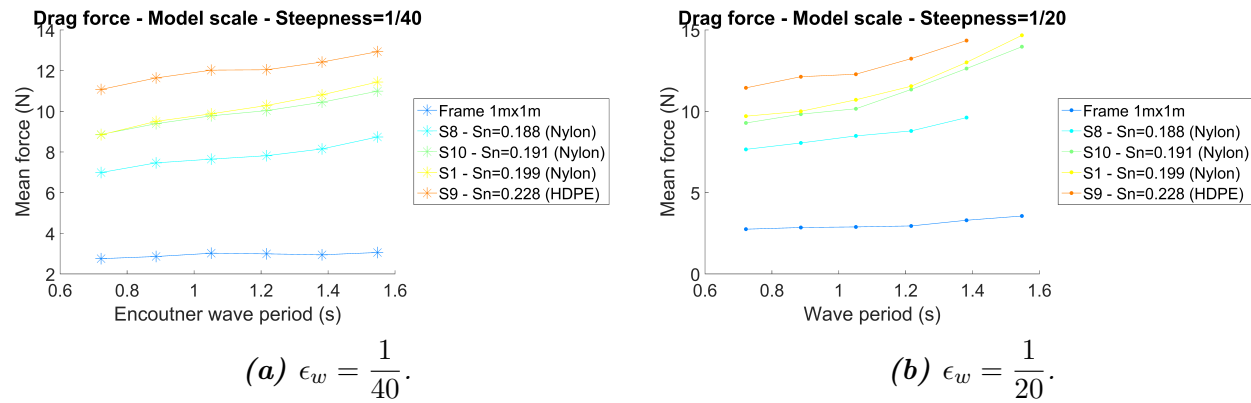
Figure C.45: *Mean drag force - $1m \times 1m$ net panels, $U_0 = 0.2m/s$.*

(a) $\epsilon_w = \dfrac{1}{40}$.
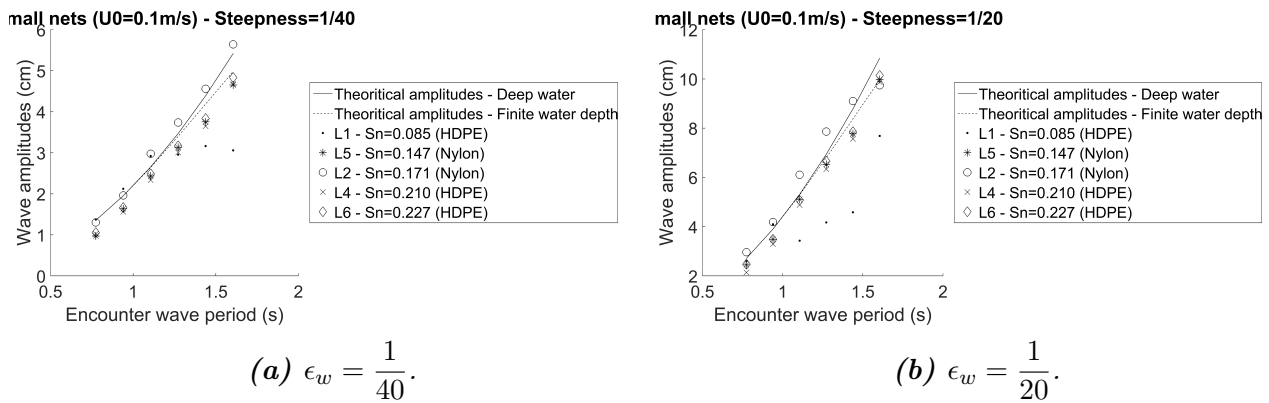
(b) $\epsilon_w = \dfrac{1}{20}$.
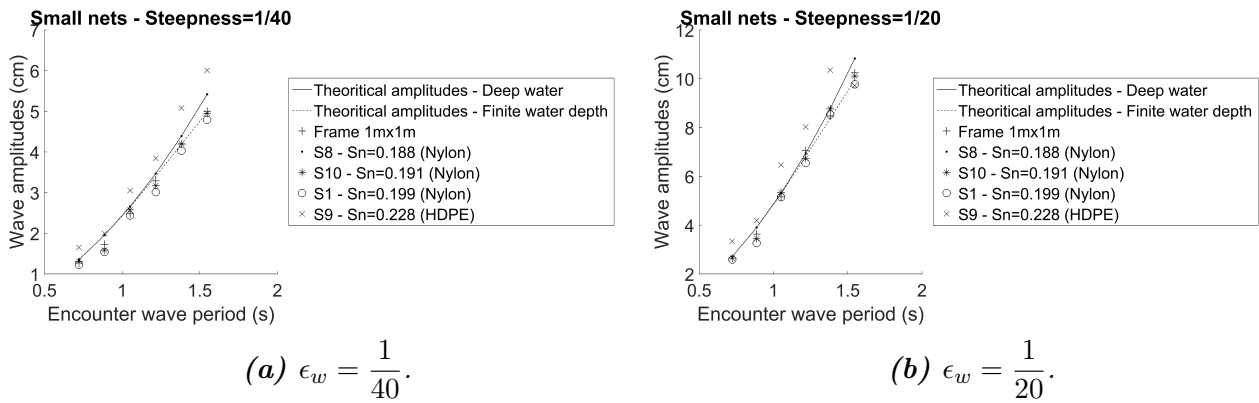
Figure C.46: *Wave amplitudes measured from the carriage in front of the net (WP1) - 1m×1m net panels, $U_0 = 0.2m/s$.*

(a) $\epsilon_w = \dfrac{1}{40}$.

(b) $\epsilon_w = \dfrac{1}{20}$.
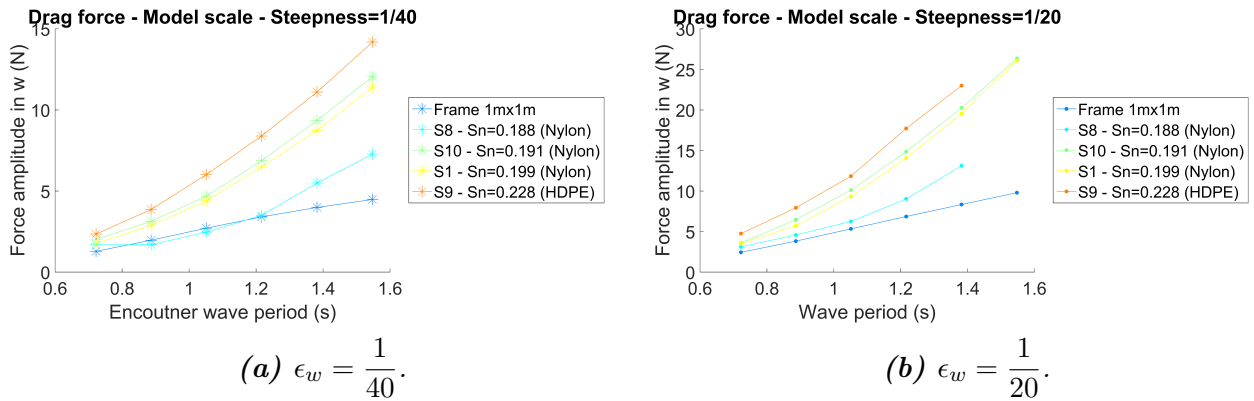
Figure C.47: *Force amplitudes (in ω) - 1m×1m net panels, $U_0 = 0.2m/s$.*

(a) $\epsilon_w = \dfrac{1}{40}$.

(b) $\epsilon_w = \dfrac{1}{20}$.
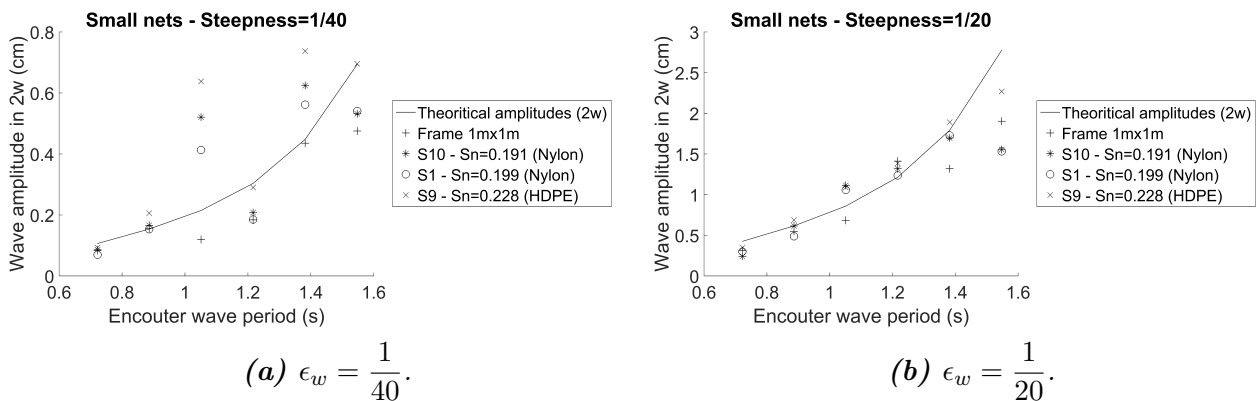
Figure C.48: *Wave amplitudes in 2ω measured from the carriage in front of the net (WP1) - 1m×1m net panels, $U_0 = 0.2m/s$.*

(a) $\epsilon_w = \dfrac{1}{40}$.

(b) $\epsilon_w = \dfrac{1}{20}$.

Figure C.49: *Force amplitudes in 2ω - $1m \times 1m$ net panels, $U_0 = 0.2m/s$.*

C.3.2   2.5m×1m net panels

(a) $\epsilon_w = \dfrac{1}{40}$.

(b) $\epsilon_w = \dfrac{1}{20}$.
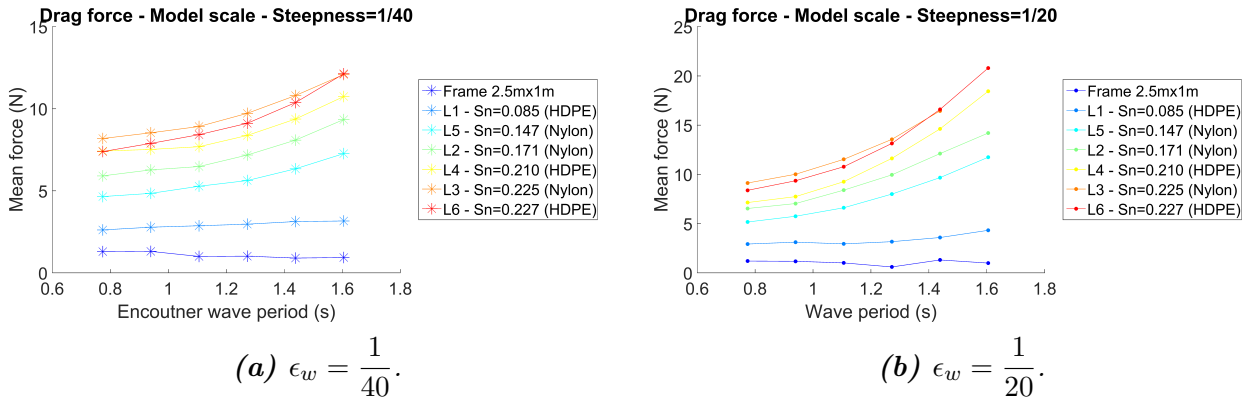
Figure C.50: *Mean drag force - 2.5m×1m net panels, $U_0 = 0.1m/s$.*

(a) $\epsilon_w = \dfrac{1}{40}$.

(b) $\epsilon_w = \dfrac{1}{20}$.

Figure C.51: *Wave amplitudes measured from the carriage in front of the net (WP1) - 2.5m×1m net panels, $U_0 = 0.1m/s$.*
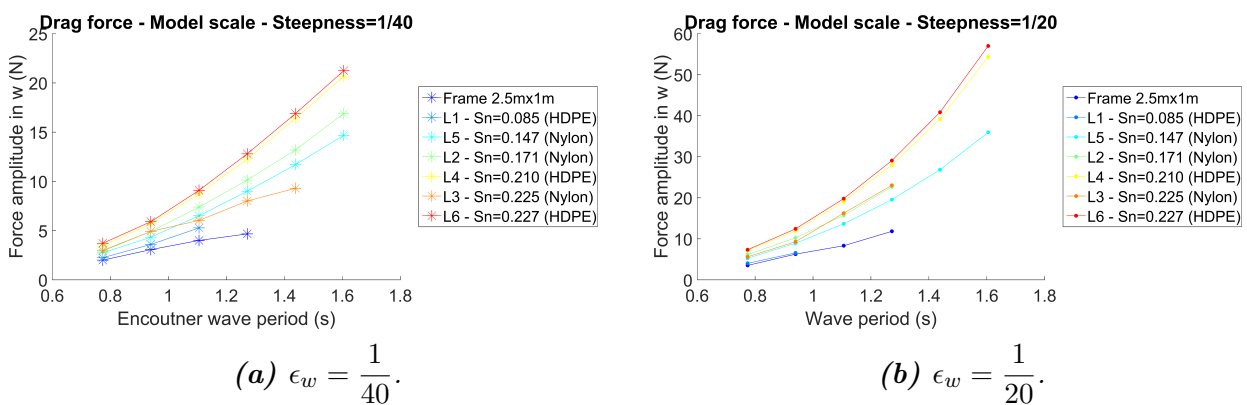
(a) $\epsilon_w = \dfrac{1}{40}$.

(b) $\epsilon_w = \dfrac{1}{20}$.

Figure C.52: *Force amplitudes (in ω) - 2.5m×1m net panels, $U_0 = 0.1m/s$.*
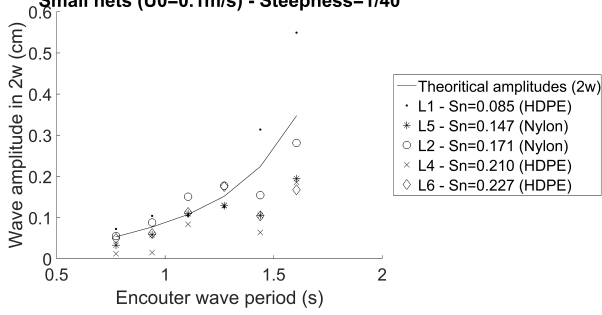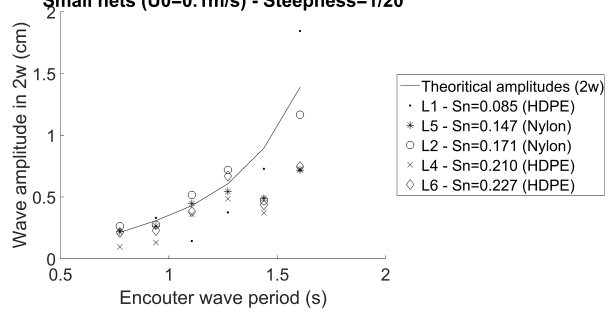
(a) $\epsilon_w = \dfrac{1}{40}$.

(b) $\epsilon_w = \dfrac{1}{20}$.

Figure C.53: *Wave amplitudes in 2ω measured from the carriage in front of the net (WP1) - 2.5m×1m net panels, $U_0 = 0.1m/s$.*
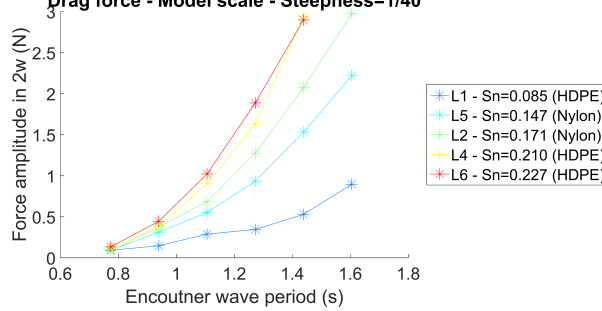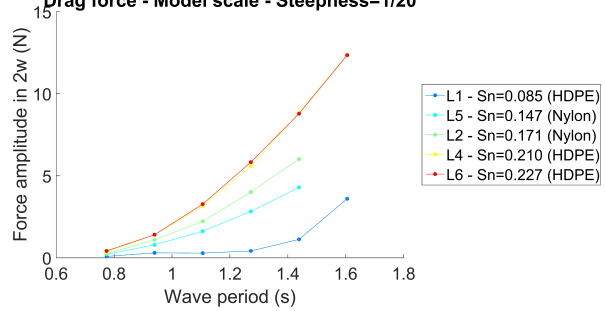
(a) $\epsilon_w = \dfrac{1}{40}$.

(b) $\epsilon_w = \dfrac{1}{20}$.

Figure C.54: *Force amplitudes in 2ω - 2.5m×1m net panels, $U_0 = 0.1m/s$.*
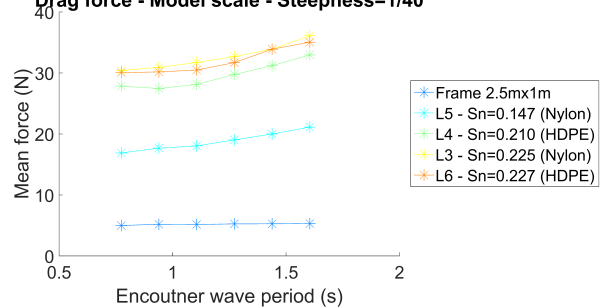
(a) $\epsilon_w = \dfrac{1}{40}$.
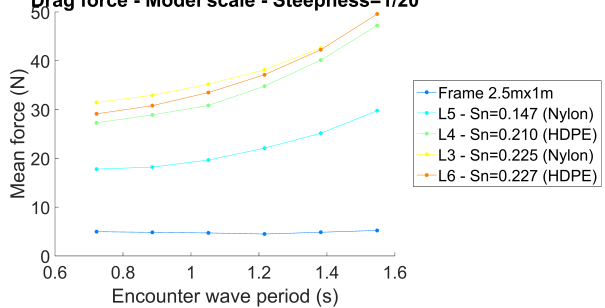
(b) $\epsilon_w = \dfrac{1}{20}$.

Figure C.55: *Mean drag force - 2.5m×1m net panels, $U_0 = 0.2m/s$.*

(a) $\epsilon_w = \dfrac{1}{40}$.

(b) $\epsilon_w = \dfrac{1}{20}$.

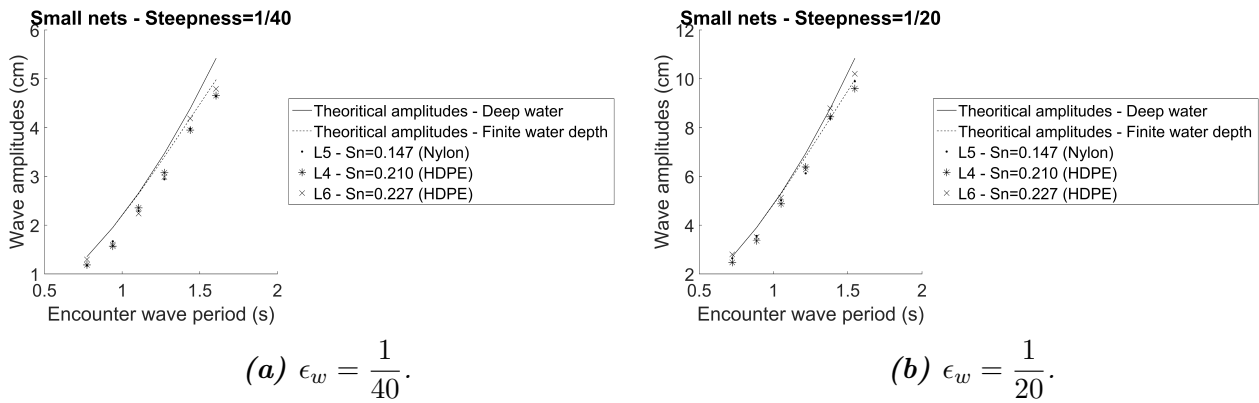**Figure C.56:** *Wave amplitudes measured from the carriage in front of the net (WP1) - 2.5m×1m net panels, $U_0 = 0.2m/s$.*
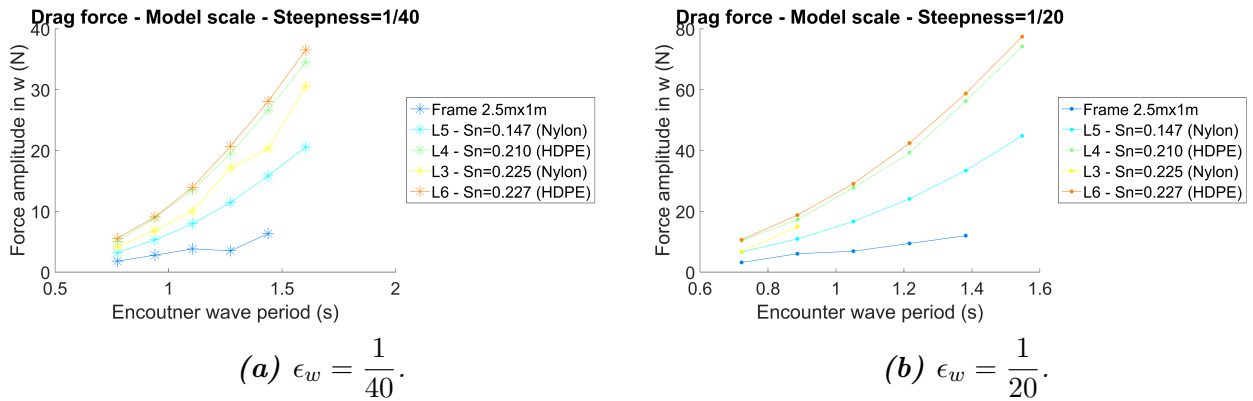

(a) $\epsilon_w = \dfrac{1}{40}$.

(b) $\epsilon_w = \dfrac{1}{20}$.

Figure C.57: *Force amplitudes (in ω) - 2.5m×1m net panels, $U_0 = 0.2m/s$.*

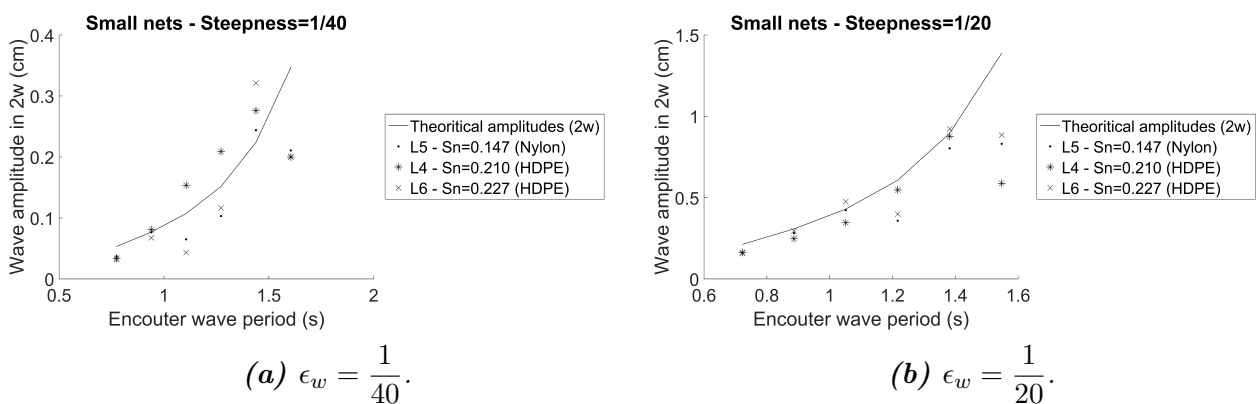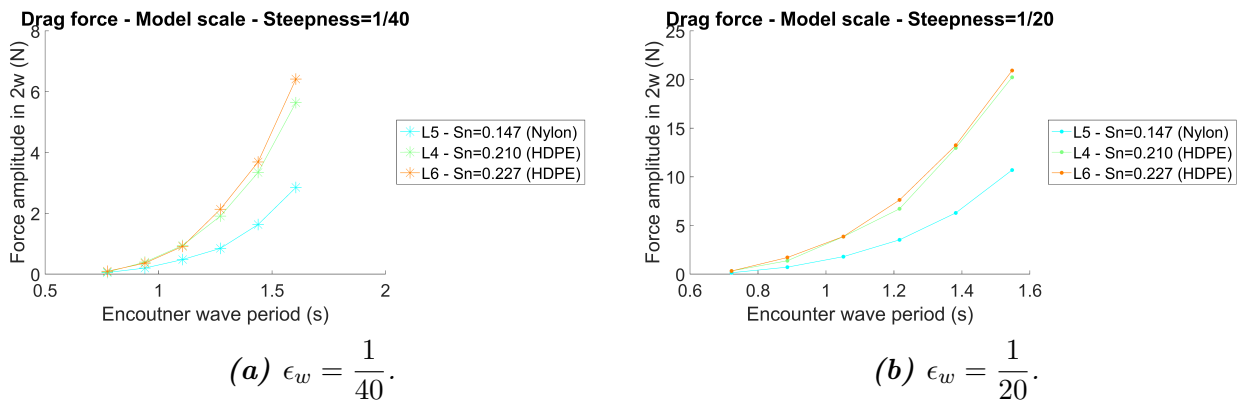**(a)** $\epsilon_w = \dfrac{1}{40}$.

(b) $\epsilon_w = \dfrac{1}{20}$.

Figure C.58: *Wave amplitudes in 2ω measured from the carriage in front of the net (WP1) - 2.5m×1m net panels, $U_0 = 0.2m/s$.*

(a) $\epsilon_w = \dfrac{1}{40}$.

(b) $\epsilon_w = \dfrac{1}{20}$.

Figure C.59: *Force amplitudes in 2ω - 2.5m×1m net panels, $U_0 = 0.2m/s$.*